M M M M M M M M M M M M
M M M M M M M M M M M M
M M M M M M M M M M M M

::: UPC

UNIVERSITAT POLITÈCNICA
DE CATALUNYA

E.T.S.E.I.B.

Departament
d'Enginyeria
Química

SIMULACIÓN DE ESTRUCTURAS Y PROPIEDADES

DE POLIAMIDAS HELICOIDALES

Memoria presentada por David Zanuy Gómara
para optar al grado de Doctor en Ciencias
Químicas.

Trabajo realizado en el Departament
D'Enginyeria Química de la UPC, bajo la
dirección del Dr. Carlos Alemán Llansó.

Barcelona, Marzo de 2001

T
01/120

Crystal Structure of Poly(α-benzyl-γ-glutamate) of Microbial Origin

José Melis, David Zanuy, Carlos Alemán,

Montserrat García-Alvarez and Sebastián Muñoz-Guerra*

Departament d'Enginyería Química, Universitat Politécnica de

Catalunya

ETS d'Enginyers Industrials de Barcelona

Diagonal 647, 08028 Barcelona, Spain

1

Corresponding author: E-mail: munoz@eq.upc.es

ABSTRACT

The conformation and crystal structure of the benzyl ester of microbial poly(γ-glutamic acid) with a nearly racemic composition was investigated by X-ray diffraction, polarized infrared spectroscopy and molecular modeling simulations. Two crystal forms differing in both chain conformation and crystal packing were characterized. Form I was found to be a layered structure made of nearly extended chains with features similar to the well-known γ-form of nylons. Form II consisted of a pseudohexagonal packing of 5/2 helices stabilized by intramolecular hydrogen bonds. These crystal forms were found to be essentially identical to those previously described for optically pure poly(α-benzyl-γ,L-glutamate) prepared by chemical synthesis. Energy calculations combined with diffraction pattern simulations indicated that a statistical structure made of D and L-stereoblocks is the most appropriate to describe the crystal forms of the racemic polypeptide.

INTRODUCTION

Poly(γ-glutamic acid) (PGGA) is a naturally occurring poly(γ-peptide) that is produced by several species of bacteria, mainly by those of the genus *Bacillus*. The biological occurrence of PGGA was accounted in the early twenties[1] although the majority of the related scientific literature was published between 1950 and 1970. An increasing number of publications dealing with the biosynthesis, solution properties and chemical modifications of this fascinating biopolymer has been appearing along the nineties, after almost two decades of apparent forgiveness. The biodegradable character of PGGA and its well proved bioassimilation seem to be the reasons for the current reappraisal of this material for environmental and biomedical applications. Several reviews on PGGA have been published along the second half of this century covering the up-to-date available knowledge.[2-4]

The biosynthesis of PGGA may be carried out in the laboratory without special difficulties. High molecular weight polymers containing variable amounts of D and L-enantiomers are usually obtained in good yields.[5-7] The microstructure of the PGGA chain is not known although there are certain evidences favoring the occurrence of stereoblocks.[8] The ability of unionized PGGA to adopt regular conformations in water was first revealed by spectroscopy measurements[9] and later confirmed by computational methods.[10] Esterification appears to be the preferred procedure to modify the properties of microbial PGGA and to render non-water soluble products. Although the preparation and properties of a variety of poly(γ-glutamate)s of natural origin have been reported,[11-13] the structure of these compounds in the solid state has not been investigated yet.

PGGA is made of glutamic acid units linked between the γ-carboxylic and

the α-amino functionalities. PGGA esters can be regarded therefore as nylon 4

derivatives with an alkoxy or aryloxycarbonyl group pending from the fourth carbon

poly(γ-glutamate)s   poly(α-glutamate)s
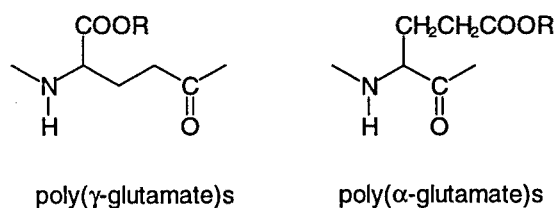
of the main chain repeating unit. A structural study carried out some years ago on

the benzyl and methyl esters of poly(γ,L-glutamic acid) obtained by chemical

synthesis revealed for the first time that these compounds display a structural

behavior comparable to poly(α-glutamate)s.[14] This finding followed those obtained

with poly(β-L-aspartate)s, a family of nylon 3 derivatives which has in common the

ability to adopt helical conformations of α-helix type.[15,16] In these last years,

considerable attention has been addressed to the investigation of the crystal

structure of unconventional oligopeptides as oligo(β-amino acid)s and oligo(γ-amino

acid)s.[17,18] Regular folded structures of α-helix type have been found in both cases

confirming previous results reported for polymers.

A preliminary account on the structural behavior of poly(γ-glutamate)s of

natural origin has been recently issued by the own authors.[19] In the present paper

we wish to report in detail on the conformation and crystal structure of poly(α-

benzyl-γ,DL-glutamate) obtained by esterification of microbial PGGA. It is known

that optically pure poly(α-benzyl-γ,L-glutamate) obtained by chemical synthesis adopts two crystal forms, one consisting of 5/2 helices packed in a hexagonal array and the other made of hydrogen bonded sheets stacked in a layered structure with chains in almost extended conformation.[14] In such case the polymer investigated entirely consisted of L-enantiomeric units and had a molecular weight of about 30,000. In the present case we are concerned with a much higher molecular weight polymer that is composed of mixtures of approximately equal amounts of D- and L-enantiomers. Our aim is to see how the structure of microbial poly(γ-glutamate)s compares to that reported for their synthetic analogues. X-ray diffraction and infrared dichroism are the techniques used for such purpose. Energy calculations and molecular modeling simulations have been used also in this work in order to provide a description of the structure in higher detail than done so far.

MATERIALS AND METHODS

Materials. The sample of poly(α-benzyl-γ,DL-glutamate), abbreviated PAB(DL)G, was a gift of Dr. Kubota from Meiji Co. The polymer was obtained by esterification of bacterially produced poly(γ-glutamic acid) and has an ester content higher than 98% as proved by ^{1}H NMR. The molecular weight of this sample was estimated to be about 480,000 by intrinsic viscosity measurements ($[\eta] = 2.43$ dL g^{-1}) using the viscosity equation reported for poly(γ-benzyl-α,L-glutamate).[20] The enantiomeric composition of the polymer is D:L = 56:44 as determined by HPLC using the Marphey's reagent based method as reported elsewhere.[21]

Measurements. Densities were measured by the flotation method using water-KBr aqueous solution mixtures. Both unoriented and oriented poly(γ-glutamate) films were examined in this work. Isotropic thin films were obtained by casting at room temperature. Uniaxial oriented films were prepared by mechanical stretching under heating at the appropriate temperatures. The degree of orientation achieved was qualitatively estimated under the polarizing optical microscope. Dichroic infrared spectra were recorded on a Perkin-Elmer 2000 instrument provided with an external gold polarizer. Thermal measurements were performed on a Perkin-Elmer equipment consisting of a DSC Pyris-I and a thermobalance TGA-6. Both DSC and TGA traces were recorded under a nitrogen atmosphere at a heating rate of 20 °C min^{-1} using 3-6 mg sample weights. X-ray diffraction patterns were recorded on flat films in a modified Statton camera (W. Warhus, Wilmington, DE) using nickel-filtered copper radiation of wavelength 0.1542 nm and calibrated with molybdenum sulfide ($d_{002} = 0.6147$ nm).

Energy Calculations and Modeling Simulations. A preliminary search for the helical conformations compatible with experimental X-ray diffraction data was performed using the GEMOX (GEneration of polymer molecular MOdels for X-rays) computer program.[22] This is a computational method based on a corrected grid searching algorithm designed to generate all the molecular arrangements sterically feasible for a system with a given helical symmetry and a definite chain repeat length.

Energy calculations were performed with the Amber 4.1[23] and PCSP[24] (Prediction of Crystal Structure of Polymers) computer programs. The latter method

6

is able to generate the atomic coordinates of a polymer in a given crystal lattice and to evaluate the energy of the resulting structure using periodic continuation conditions. Force-field parameters were taken from the Amber's set[25] with exception of the atomic charges, which were explicitly derived for PABG by fitting the quantum mechanics molecular electrostatic potential computed at the *ab initio* HF/6-31G(d) level to the Coulombic one.[26] Crystal modelling was made for the most favorable packing arrangements using the Cerius[2] program.[27] X-ray diffraction patterns were simulated for these models for sample textures similar to those used in the collection of experimental data. All the calculations were performed on SGI Indigo[2] workstations at our laboratory.

RESULTS AND DISCUSSION

Experimental results. Two types of X-ray diffraction patterns were recorded for PAB(DL)G depending on the conditions that were used for the preparation of the sample. They are made to correspond to the crystal forms I and II previously reported for synthetic poly(α-benzyl-γ,L-glutamate).[14]

PAB(DL)G precipitated from a solution in trifluoroacetic acid by adding methanol was found to be in form I, while films prepared by casting from a variety of solvents like dimethyl sulfoxide, hexafluoroisopropanol or $CHCl_3$-TFE were in form II. Form I also appeared in films originally in form II upon heating at temperatures above 200 °C. The powder diffraction patterns of the two forms are compared in Figure 1 illustrating the differences existing between them. The diffraction pattern

7

obtained from a film stretched at high temperature is displayed in Figure 2a. The spacings observed in this diagram reveal that it corresponds to form I. Conversely, a film of PAB(DL)G stretched at temperatures below 90 °C produced the diffraction pattern shown in Figure 2b which contains exclusively the spacings characteristic of form II.

TGA results revealed that no significant decomposition of PAB(DL)G takes place below 300 °C whereas weight loss suddenly increases at temperatures in the 320-370 °C range (Figure 3a). These data allowed us to discard the occurrence of degradation in the samples subjected to thermal treatment previous to X-ray diffraction. DSC heating traces of PAB(DL)G with different initial contents in form I and II are compared in Figure 3b. The trace obtained from a sample originally being in form I showed only one endothermic peak at 250 °C corresponding to the melting of the polymer in such form. A more complex thermogram was obtained for a sample of PAB(DL)G in form II, which may be interpreted by assuming that form II is partially converted into form I at nearly 180 °C. The broad exothermic peak observed in the 200-230 °C region is thought to be due to the melting of the polymer still remaining in form II.

Form I. This form is interpreted as a layered structure of hydrogen-bonded sheets with chains arranged in almost extended conformation. The occurrence of an intermolecular network of hydrogen bonds running approximately normal to the polymer main chain, which is a distinctive feature of this structure, is strongly supported by polarized infrared spectroscopy. The IR spectra registered from an oriented film of PAB(DL)G in form I showed perpendicular dichroism for both the

amide A and amide I bands and parallel dichroism for the amide II band (Figure 4a). Such a dichroic behavior is that should be expected for a structure with the C=O and N-H bonds oriented approximately normal to the chain axis.

The most remarkable features displayed by the fiber diagram of PAB(DL)G in form I (Figure 2a) are the presence on the equator of two strong reflections with spacings at 1.05 and 0.47 nm and the existence of a second layer line revealing an axial spacing in the structure of about 0.60 nm. The 0.47 nm spacing clearly corresponds to the typical distance between hydrogen-bonded polyamide chains and is taken as a firm evidence that sheets are side-by-side packed in an orthogonal array with an intersheet distance of 1.05 nm. The spacing and intensity distribution along the first and second layer lines indicates that the c dimension of the structure, i.e. the axial repeat length, is about 1.20 nm and involves two chemical residues. This implies that PAB(DL)G is crystallized with the chain contracted about 0.03 nm per repeating unit with respect to the all-*trans* conformation. It should be remarked that such a contraction is similar to that taking place in the γ-form[28] of nylons with respect to the fully extended α-form.[29] Both powder and fiber diagrams can be satisfactorily indexed on the basis of a lattice with orthorhombic geometry and parameters a_0 = 0.931 nm, b_0 = .1.044 nm and c_0 = 1.198 nm (Table 1). The unit cell is therefore described as containing two chains in antiparallel arrangement. The density calculated for this structure is 1.26 g mL^{-1}, in excellent agreement with the experimental value of 1.25 g mL^{-1}.

Form II. The diffraction patterns recorded from PAB(DL)G films stretched at low temperature correspond to form II and they are similar also to that reported for the

polymer obtained by chemical synthesis for which a 5/2 helix was put forward.[14] In fact, layer lines appearing at about 1.0 and 0.5 nm with weak and strong intensity, respectively, are in accordance with a helical arrangement that repeats every two turns. The 5/2 helix appeared favored with respect to both the 3/2 and 7/2 helices when the selection rules of Cohran and Crick were applied[30] and it was found to be also the most adequate to match experimental density data. On the other hand, polarized infrared spectra from this form revealed dichroic ratios of bands associated to the amide group of opposite sign to those observed for form I (Figure 4b). Such a dichroic behavior is characteristic of polyamide helices fixed by intramolecular hydrogen bonds so that the C=O and N-H dipoles become aligned nearly parallel to the helix axis.

On the analogy of PAB(L)G,[14] the strong equatorial reflection with a spacing of 1.12 nm may be initially related to the 100 planes of a hexagonal lattice of $a_0 = 1.3$ nm. However, some reflections observed in the X-ray diffraction pattern can not be explained by considering such a simple structure but rather on the basis of pseudohexagonal array of 5/2 helices arranged in antiparallel. The resulting lattice is formally orthorhombic with parameters $a_0 = 1.276$ nm, $b_0 = 2.210$ nm and $c_0 = 0.995$ nm and contains two chain in the unit cell (Table 2). The experimental density of PAB(DL) in form II is 1.27 g mL^{-1}, in very good agreement with the value calculated for the proposed structure which is 1.30 g mL^{-1}.

Modeling and Refinement. The modeling study was developed in three successive steps. Firstly, the molecular conformations for either the 2/1 or 5/2 helices of forms I and II, respectively, were modeled considering an isolated enantiomerically pure D-

polymer chain. Secondly, the helices obtained in the preceding step were used for building up the crystal lattices of forms I and II. Finally the crystal structures of forms I and II were modeled for a statistically mixture of D and L-chains. Form I was solved using a combination of energy calculations and simulations of the diffraction patterns, the latter being directly compared with the experimental diagrams. On the other hand, the crystal structure of form II was modeled using only energy calculations due to the poor quality of the experimental X-ray diffraction patterns produced by this form.

Molecular Conformations. X-ray diffraction data revealed that the 2/1 helix of form I is contracted about 0.03 nm per amide group with respect to the all-*trans* conformation. Such compression may be reached if some backbone torsional angles deviate slightly from 180º. By analogy to the γ-form of nylons,[28] such distortions would affect the torsional angles adjacent to the amide groups, *i.e.* φ and ψ. A chain repeat length of 1.198 nm was attained for a deviation of about 40º of these two angles with respect to the *trans* conformation ($\varphi=-\psi=139.6º$). Such a distortion entails a rotation of 35.5º between the amide plane and the plane containing the all-*trans* backbone carbon atoms. Energy calculations carried out on an isolated chain revealed that this contracted conformation is only 0.3 kcal mol^{-1} residue^{-1} less stable than the all-*trans* one.

On the other hand, a complete survey of molecular models of PAB(D)G compatible with a 5/2 helix having a repeat distance of about 1 nm was carried out with the GEMOX program.[22] The most stable conformation for PAB(D)G was found to correspond to a right-handed helix with intramolecular hydrogen bonds set

between the C=O of the amide *i* and the NH of the amide *i+2*. This 5/2 helix
appeared to be energetically favored with respect to the 2/1 helix of form I by 4.1
kcal mol^{-1} residue^{-1}. The two PAB(D)G helices are schematically represented in
Figure 5.

The Crystal Structure of Form I. Initially, the PAB(D)G 2/1 helix shown in Figure 5
was taken for building up the crystal in form I. The geometry lattice was defined
according to X-ray diffraction data and the conformation of the side phenyl groups
optimized by force-field calculations. The fiber X-ray diffraction pattern arising from
the modeled structure after refining against experimental data is shown in Figure 6a.
Two orthogonal views of the refined PAB(D)G crystal lattice in form I are depicted in
Figure 7 and the conformational parameters and hydrogen bond geometry resulting
for such structure are given in Table 3. Although this model is able to reproduce
satisfactorily the reflections contained in the diagram shown in Figure 2a, a number
of spots other than experimentally observed are present in addition.

The crystal model generated above was then used to construct the
PAB(DL)G crystal. This was performed by considering an occupancy of 50% of
PAB(D)G and PAB(L)G chains at every position of the lattice. The powder pattern
simulated for this racemic structure reproduces satisfactory the experimental
pattern as it is shown in Table 4 where observed and calculated intensities of *hk*0,
*hk*1 and *hk*2 reflections are qualitatively compared. Figure 6b shows the fiber
pattern simulated for this structure, which appears to be in much better agreement
with the experimental one than that calculated for the optically pure crystal model

12

(Figure 6b). Thus, the 110 reflection appearing with strong intensity for PAB(D)G but not found in the experimental diffraction pattern, is removed whereas all others along the equator remain essentially unchanged. Moreover, the $11l$ and $12l$ reflections present in the simulated diffraction pattern of PAB(D)G have also disappeared according to what is experimentally observed.

The Crystal Structure of Form II. Our aim at this point was just to built a model for the form II of poly(γ,DL-glutamate)s compatible with the available experimental data. For this purpose a hexagonal array of 5/2 helices of PAB(D)G was built in antiparallel arrangement corresponding to the orthorhombic lattice established on the basis of X-ray diffraction data. A systematic energy study was performed in order to find the most favorable arrangement for the helices. Starting models for energy minimization were generated by systematic rotation of one chain around its axis at intervals of $15°$ within the range 0-$360°$ while the neighboring chains were held at their initial orientations. The equatorial projection of the lowest energy unit cell displaying the packing of one chain with its six neighbors is depicted in Figure 8. It should be mentioned that the main chain conformational parameters of the 5/2 helix remain essentially unaltered with respect to those obtained for the corresponding isolated chain, indicating that the conformation is barely sensitive to packing effects. This may be attributed to the great stability provided to the 5/2 helix by intramolecular hydrogen bonding. On the other hand, the resulting side chain dihedral angles, which are shown in Table 3, were found to differ considerably from those obtained for form I. Inspection to the position adopted by the benzyl side groups in each form indicated that the stacking interactions tend to favor form II with respect to form I. Thus, the center-to-center distance between phenyl rings is 0.451

nm and 0. 402 nm for forms I and II, respectively, the latter being closer to the distance predicted for a stacked benzene dimer, i.e. 0.377 nm.[31]

Given the configurational heterogeneity of PAB(DL)G, the stability of the crystal structure of form II was examined in relation to the enantiomeric composition. This study was carried out using a polymer chain containing 10 explicit residues and applying periodic boundary conditions along the helix axis. In a first step the energy of a D-chain in the right handed 5/2 helical conformation was evaluated when an increasing number of D-units (1 to 5) were replaced by L-units. It was found that the helix becomes extremely unstable upon substitution, even when the side chain dihedral angles were again reoptimized. These results are incompatible with the occurrence of a D,L-chain consisting of a statistical distribution of the enantiomeric units and give support to a PAB(DL)G polymer composed of homogeneous D and L-stereoblocks. Accordingly, we investigated next the isomorphic substitution of D-chains by L-chains in the pseudohexagonal structure displayed in Figure 8. Calculations were performed using seven explicit chains and applying periodic boundary conditions along the three axes. The conformational parameters used to build the left-handed 5/2 helices made of L-units were those displayed in Table 3 but with opposite sign. It was found that the energy of the mixed structure could increased up to 5.5 kcal mol^{-1} residue[-1] depending on the specific array followed for substitution. Finally, a crystal structure as that depicted in Figure 8 but with an occupancy of 50% of D-chains and L-chains at every position of the lattice was constructed. This structure represents a statistically structure for PAB(DL)G made of either a mixture of D- and L-chains or a mixture of two populations of crystallites entirely made of D- or L-chains, respectively. The later situation should certainly

14

occur in more or less extension since form II has been observed for PAB(DL)G within a wide range of enantiomeric compositions. Unfortunately, the short number of X-ray experimentally observed reflections for form II makes unreliable any further refinement of the structure on the basis of such data. Nevertheless a preliminary analysis showed that the simulated fiber diffraction diagram obtained from the crystal structure in form II for PAB(D)G resembles that obtained for PAB(DL)G provided that D and L-chains are statistically arranged and that both diagrams contain all the reflections experimentally observed for this form. On the contrary, the diffraction pattern simulated for form II with a structure made of an ordered arrangement of D and L-chains displayed a good number of additional spots which is inconsistent with what is experimentally observed.

FINAL CONCLUSIONS

Two crystal forms I and II have been found for the benzyl ester of bacterially produced poly(γ-glutamic acid) with a nearly racemic composition. Form I is a layered structure with chains in almost extended conformation reminiscent of the well-known γ-form of nylons. Form II is a regularly folded structure with chains in 2/5 helical conformation. These two forms are essentially the same as those described for the optically pure low molecular weight poly(α-benzyl-γ,L-glutamate) of synthetic origin. In the present case, building the crystal structures with a polymer made of a mixture of D and L-units creates a formidable structural problem that has been addressed by modeling and energy calculations. The energy analysis of an isolated molecule has shown that the 5/2 helix is incompatible with a chain made of D and L units distributed at random. On the other hand, molecular modeling supported by diffraction pattern simulations has shown that a statistical lattice consisting of D and

15

L chain homogeneous segments arranged at random is the most suitable for representing the crystal forms of PAB(DL)G. These results are consistent with a poly(γ-glutamic acid) having a microstructure in D and L-stereoblocks. The results presented in this work bring out for the first time the structural properties of the esters of naturally occurring poly(γ-glutamic acid) and proved that they adopt essentially the same structures as their synthetic analogs.

ACKNOWLEDGEMENTS

REFERENCES

1. Kramar, E. *Centr. Bakteriol. Parasitenk. Abt. I* **1921**, *88*, 401.

2. Nitecki, D.E.; Goodman, J.W. **1971** in *Chemistry and Biochemistry of Amino Acids, Peptides and Proteins*, Weinstein B. Ed., New York, p 87.

3. Troy F.A. in *Peptide antibiotics biosynthesis and functions*, Walter de Gruyter, New York, p 49.

4. A. Gross, *Bacterial Poly-γ-(glutamic acid)* in *Biopolymers from Renewable Resources*, D.L. Kaplan Ed. Springer, Berlin 1998, p 195.

5. Kubota, H.; Matsunobu, T.; Uotani, K.; Takebe, H.; Satoh, A.; Tanaka, T.; Taniguchi, M. *Biosci. Biotech. Biochem.* **1993**, *57*, 1212.

6. Cromwick, A-M.; Gross, R.A. *Int. J. Biol. Macromol.* **1995**, *17*, 259.

7. Goto, A.; Kunioka, M. *Biosci. Biotech. Biochem.* **1992**, *56*, 1031.

8. Tanaka, T.; Fujita, K-I.; Takenishi, S.; Taniguchi, M. *J. Ferm. Bioeng.* **1997**, *84*, 361.

9. a) Rydon, H.N. *J. Chem. Soc.* **1964**, 1328. b) Marlborough, D.L. *Biopolymers* **1973**, *12*, 1083.

10. Zanuy, D.; Alemán, C.; Muñoz-Guerra, S. *Int. J. Biol. Macromol.* **1998**, *23*, 175.

11. Borbély, M; Nagasaki, Y; Borbély, J., Fan, K., Bhogle, A.; Sevoian, M. *Polym. Bull.* **1994**, *32*, 127.

12. Kubota, H.; Fukuda, Y.; Takebe, H.; Endo, T. *USA Patent* 5,118,784, (1994)

13. Gross, R.A.; McCarthy, S.P.; Shah, D.T. *USA Patent* 5.378, 807, (1995)

14. Puiggalí, J.; Muñoz-Guerra, S.; Rodríguez-Galán, A.; Alegre, C.; Subirana, J.A. *Makromol. Chem. Macromol. Symp.* **1988**, *20/21*, 167.

15. Fernández-Santín, J.M., Aymamí, J.; Rodríguez-Galán, A.; Muñoz-Guerra, S.; Subirana, J.A. *Nature* (London) **1984**, *311*, 53.

16. Muñoz-Guerra, S.; Fernández-Santín, J.M.; López-Carrasquero, F.; Subirana, J.A. in *Enciclopedia of Polymeric Materials Encyclopedia*, Salamone, J.C. Ed. CRC Press, Boca Raton, Fl, 1996, p4694.

17. a) Seebach, D.; Abele, S.; Gadermann, K.; Guichard, G.; Hintermann, T.; Jaun, B.; Mathews, J.L.; Schreiber, J.; V.Oberer, L.; Hemmel, U.; Wichmer, H. *Helv. Chim. Acta* **1998**, *81*, 932. b) Hintermann, T., Gademann, K.; Jaun, B.; Seebach, D. *Helv. Chim. Acta* **1998**, *81*, 983.

18. Apella, D.H.; Christianson, L.A.; Karle, I.L.; Powell, D.R.; Gellman, S.H. *J. Am. Chem. Soc.* **1996**, *118*, 13071.

19. Muñoz- Guerra, S.; Melis, J.; Pérez-Camero, G. *Polymer. Preprints; ACS* **1999**, *81*, 244. .

20. Doty, P.; Bradbury, J.A.; Haltzer, A.M. *J. Am. Chem. Soc.* **1956**, *78*, 947.

21. Pérez-Camero, G.; Congregado, F.; Bou, J.J.; Muñoz-Guerra, S. *Biotech. Bioeng.* **1999**, *63*, 110.

22. Navas, J.J.; Alemán, C.; Muñoz-Guerra, S. *Polymer* 1996, *37*, 2589.

23. Pearlman, D.A.; Case, D.A.; Caldwell, J.W.; Ross, W.S.; Cheatham III, T.E.; Ferguson, D.M.; Seibel, G.L.; Singh, U.C.; Weiner, P.K.; Kollman, P.A. *Amber 4.1*, University of California, San Francisco, 1995.

24. León, S.; Navas, J.J.; Alemán, C. *Polymer* 1999, *40*, 7351.

25. Weiner, S.J.; Kollman, P.A.; Nguyen, D.T.; Case, D.A. *J. Comput. Chem.* 1990, *7*, 230.

26. Alemán, C.; Luque, F.J.; Orozco, M. *J. Comput. Aided Mol. Design*, 1993, *7*, 721.

27. Cerius^2 1.6, Molecular Simulations Inc. Burlington, MA.

28. Kinoshita, Y. *Makromol. Chem.* 1959, *33*, 1.

29. Bunn, C.W.; Garner, E.V. *Proc. R. Soc. London, Ser. A* 1947, *189*, 39.

30. Cohran, W.; Crick, F. *Nature* 1952, *169*, 234.

31. Jorgensen, W.L.; Severance, D.L. *J. Am. Chem. Soc.* 1990, *112*, 4768.

Table 1. Observed and calculated X-ray diffraction spacings (nm) of form I of PAB(DL)G.

layer line	d_{obs}[a]		d_{calc}[b]	$h\,k\,l$[b]
	powder	fiber		
$l = 0$	1.034	1.048	1.044	0 1 0
	0.463	0.472	0.466	2 0 0
	0.342	0.339	0.347, 0.348	2 2 0, 0 3 0
	0.250	0.262	0.261	0 4 0
$l = 1$	0.727	0.722	0.735	1 0 1
	0.439	0.434	0.434	2 0 1
	0.393	0.406	0.401	2 1 1
$l = 2$	0.598	0.601	0.599	0 0 2
	0.500	0.502	0.504, 0.519	1 0 2, 0 1 2
	0.463	0.450	0.454	1 1 2
$l = 3$	0.377	0.388	0.373, 0.367,	0 1 3, 1 0 3, 0 0 3
$l = 4$	0.280	0.280	0.285, 0.288	0 1 4, 1 0 4
$l = 5$	0.232	0.234	0.233	0 1 5

[a]Spacings observed in X-ray diffraction patterns of unoriented and oriented films.

[b]Spacings calculated and indexed on the basis of an orthorhombic unit cell with

a_O = 0.931 nm, b_O = 1.044 nm and c_O = 1.198 nm

Table 2. Measured and calculated X-ray diffraction spacings of form II of PAB(DL)G.

layer	d_{obd} [a]		d_{calc} [b]	$h\ k\ l$ [b]
	powder	fiber		
l= 0	1.120	1.119	1.105	0 2 0
	0.567		0.552	0 4 0, 2 2 0
	0.475	0.459	0.483	2 3 0
	0.421	0.406	0.418	2 4 0, 3 1 0
l= 1	0.567	0.555	0.537	2 0 1, 1 3 1
l= 2	0.502	0.50 - 0.40	0.498	0 0 2
	0.475	0.50 - 0.40	0.464	1 0 2
		0.50 - 0.40	0.454	0 2 2
	0.421	0.50 - 0.40	0.4.27	1 2 2
		0.396	0.392	2 0 2
l= 3	0.324	0.321	0.321	1 0 3
l= 4	0.252	0.251	0.249	0 0 4

[a]Spacings observed in X-ray diffraction patterns of unoriented and oriented films.

[b]Spacings calculated and indexed on the basis of an orthorhombic unit cell with

a_O= 1.276 nm, b_O= 2.210 nm and c_O= 0.995 nm.

Table 3. Conformational angles and hydrogen bonding geometries for forms I and II of PAB(D)G.

	Form I	Form II
helix	2/1	5/2
torsional angles[a]		
φ	-139.6	-137.9
ξ_1	180.0	53.0
ξ_2	180.0	75.6
ψ	139.6	-143.8
χ_1	60.0	-140
χ_2	180.0	180.0
χ_3	130.0	180
χ_4	-105.0	170
hydrogen bond[b]	intermolecular	intramolecular
d(H...O)	0.1888	0.1816
<N-H...O	175.8	164.8

[a]In degrees. The side chain of the 5/2 helix was not refined against X-ray data.

[b]Distances in nm and angles in degrees.

22
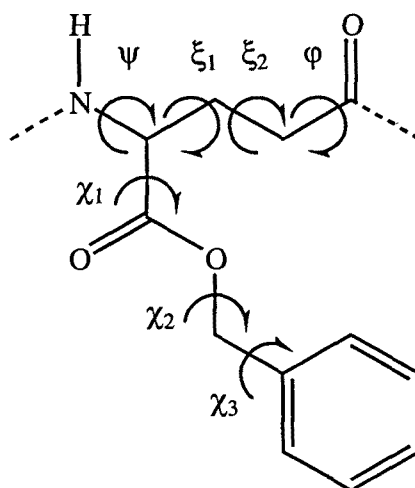
Table 4. Observed and calculated intensities for the Form I of PAB(DL)G.

hkl	I_{obs}	I_{calc} (%)
010	vs	100
101	vw	1.0
002	m	5.3
102/012	m	3.7
	s	19.8
200/112	s	9.9
	m	4.8
211		
220/030		

CAPTIONS TO FIGURES

Figure 1. Compared powder X-ray diffraction patterns of PAB(DL)G in form and in form II.

Figure 2. X-ray diffraction patterns of a stretched film of PAB(DL)G in form I (a) and in form II (b).

Figure 3. a) TGA trace of PAB(DL)G and its derivative curve. b) DSC traces of PAB(DL)G in form I (botton) and in form II (top).

Figure 4. Polarized infrared spectra of PAB(DL)G in form I (a) and in form II (b). The solid and dotted lines correspond to the parallel and perpendicular orientation of the film axis to the polarized infrared vector.

Figure 5. Equatorial and axial views of the helical models for PAB(D)G in form I (2/1 helix) and in form II (right handed 5/2 helix).

Figure 6. Simulated X-ray diffraction patterns produced by the structure modeled for form I made of PAB(D)G chains (a) and PAB(DL)G chains (b).

Figure 7. Form I of PAB(D)G. a) View of the projection down the *c*-axis. (b) View of the plane normal to the *b*-axis).

Figure 8. View of the structure of PA(D)G in form II when projected down the *c*-axis.

0.34 nm
1.03 nm
1.12 nm
0.46 nm
0.50 nm

Fig. 1. Melis et al.

0.60nm

1.05nm

0.47nm

a

0.5 – 0.4nm

1.12nm

b
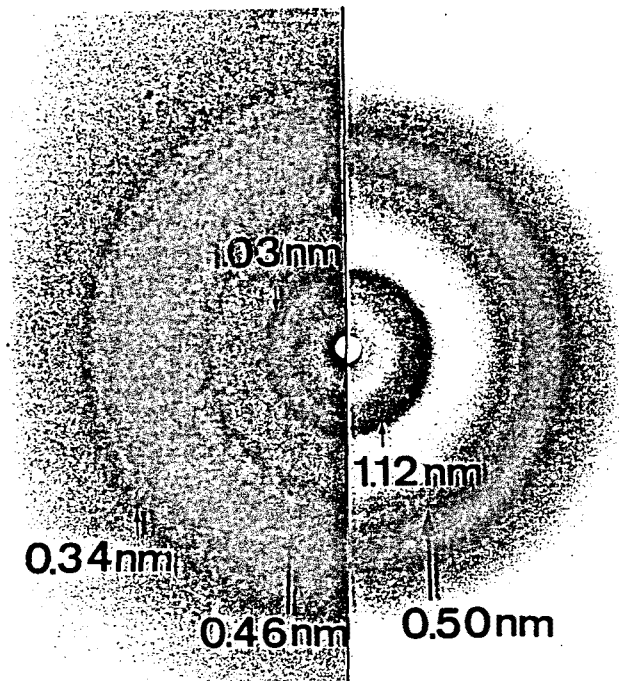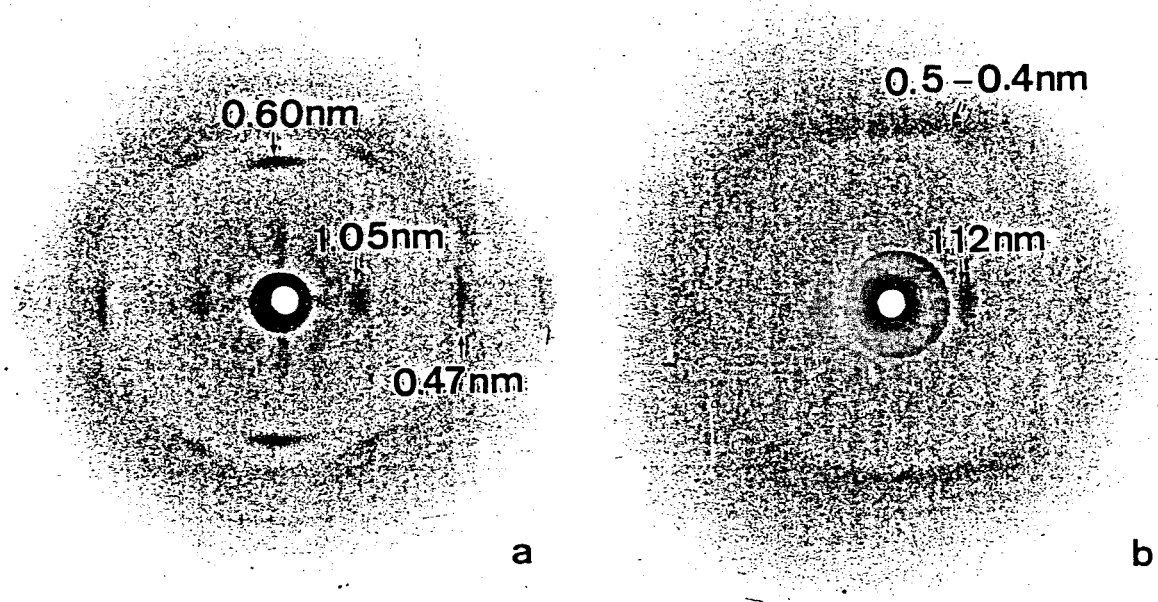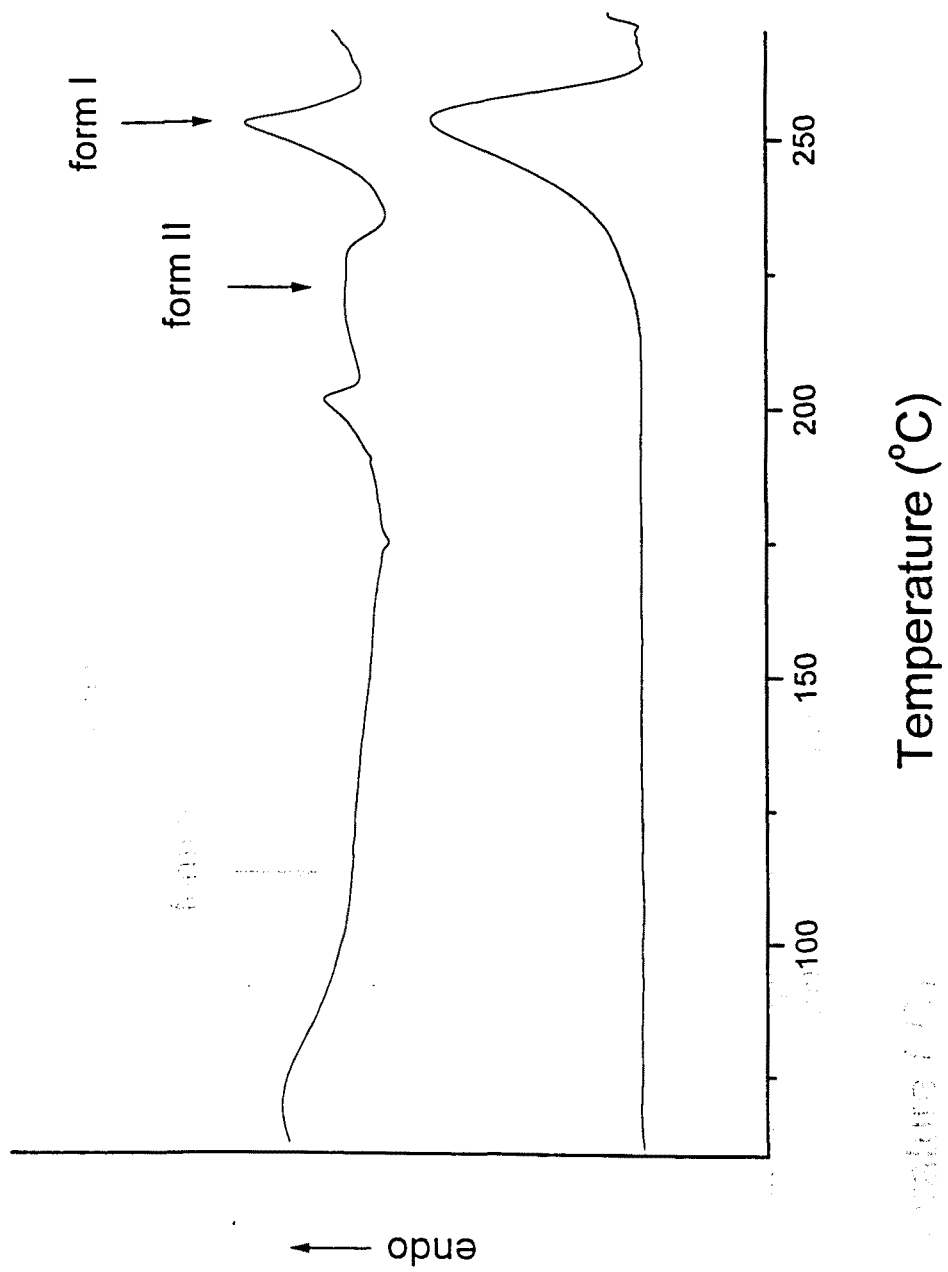
Fig. 2. Melis et al.

Fig. 3. Melis et al.
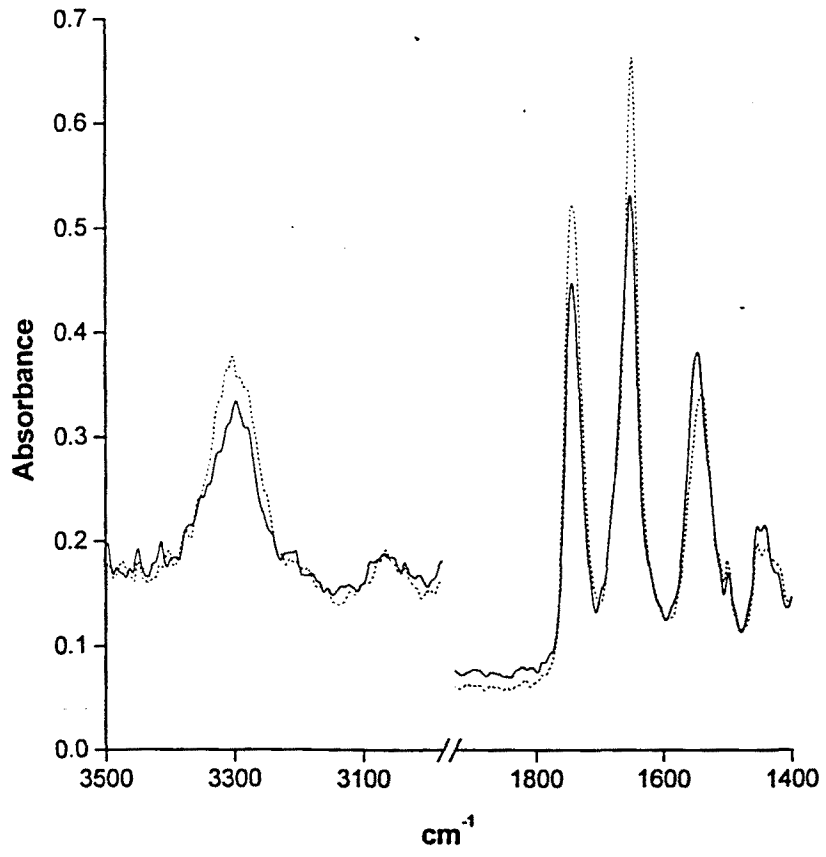
a)

b)

Fig. 4. Melis et al.
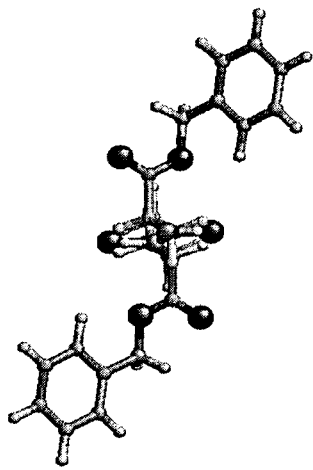
2/1 Helix

5/2 Helix

Fig. 5. Melis et al.

(a)

1 1̄ 0

(b)

h k 4

h k 2

002

102, 012

200

040

010

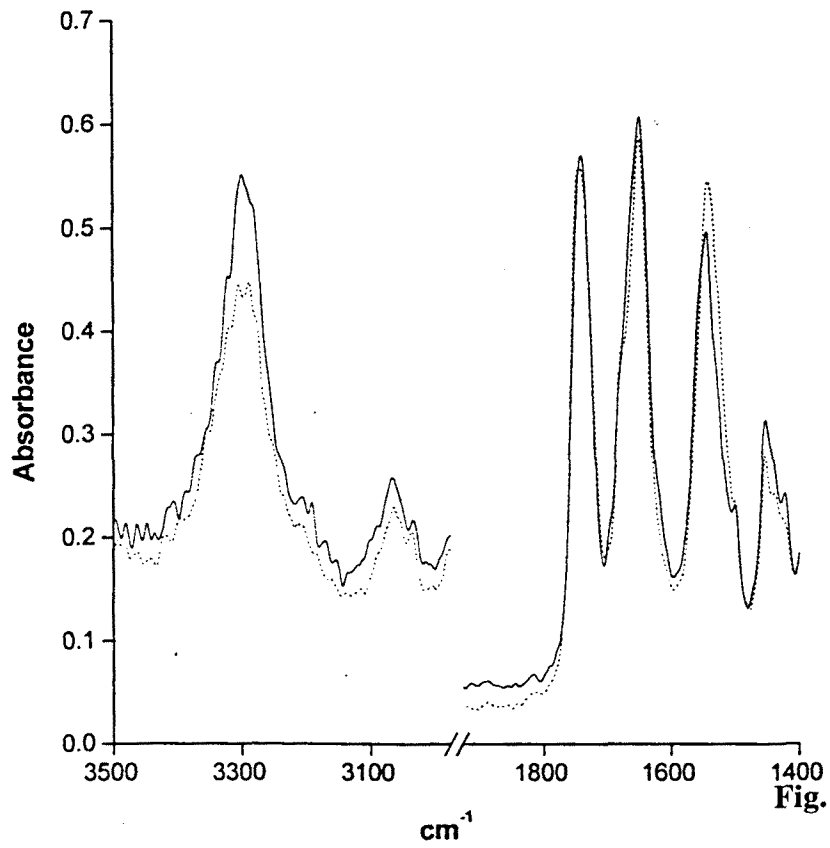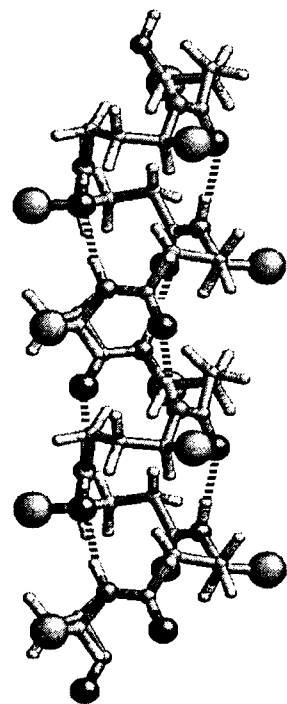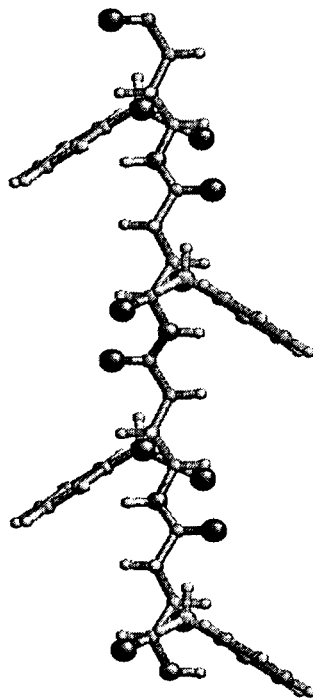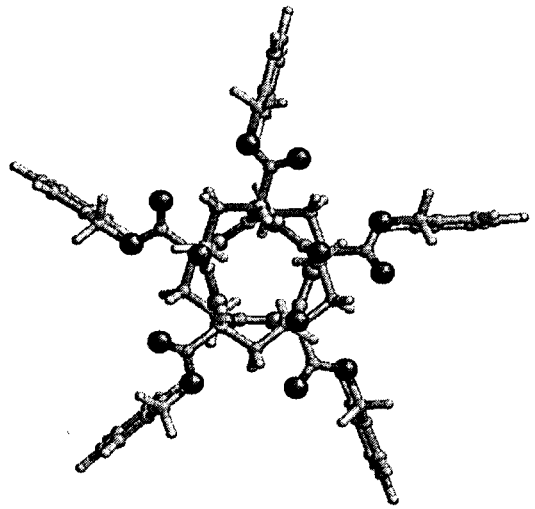030,
200
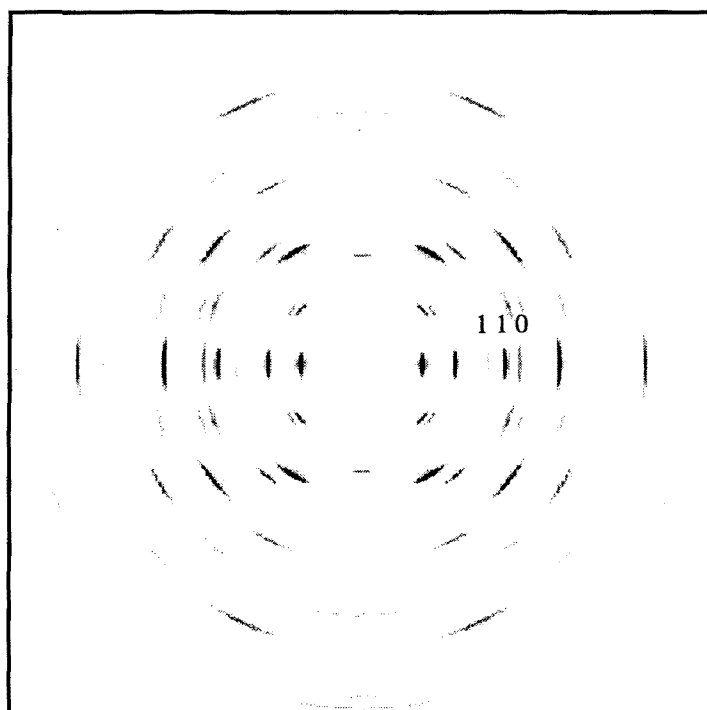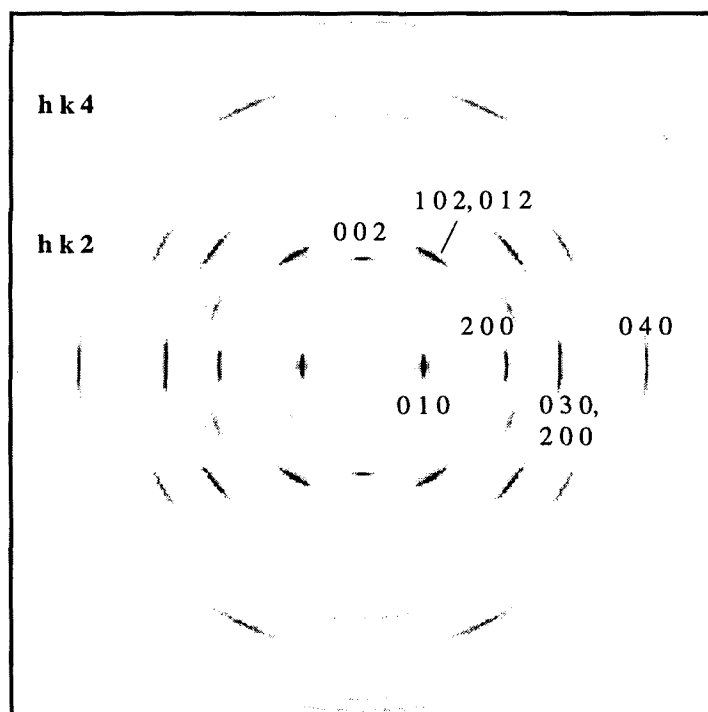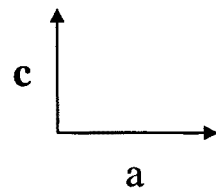
Fig.6. Melis et al.

Fig.7. Melis et al.

Fig.8. Melis et al.

V.5. La forma II del poli(α-etil-γ-glutamato)

La forma II es, de todas las formas cristalinas de los poli(α-alquil-γ-glutamato)s, la única que se ha detectado en todos los compuestos que presentan un grupo alquilo con menos de 6 átomos de carbono.
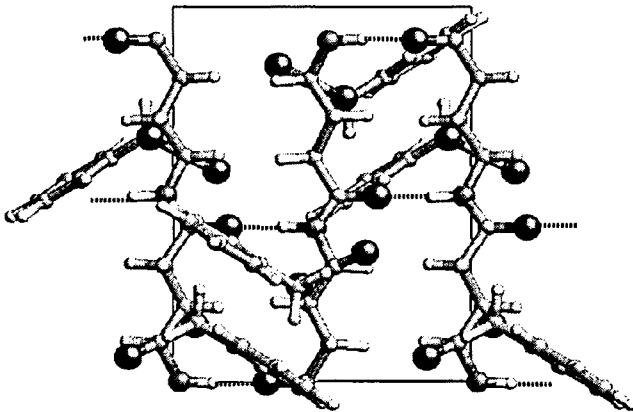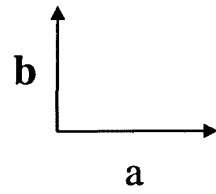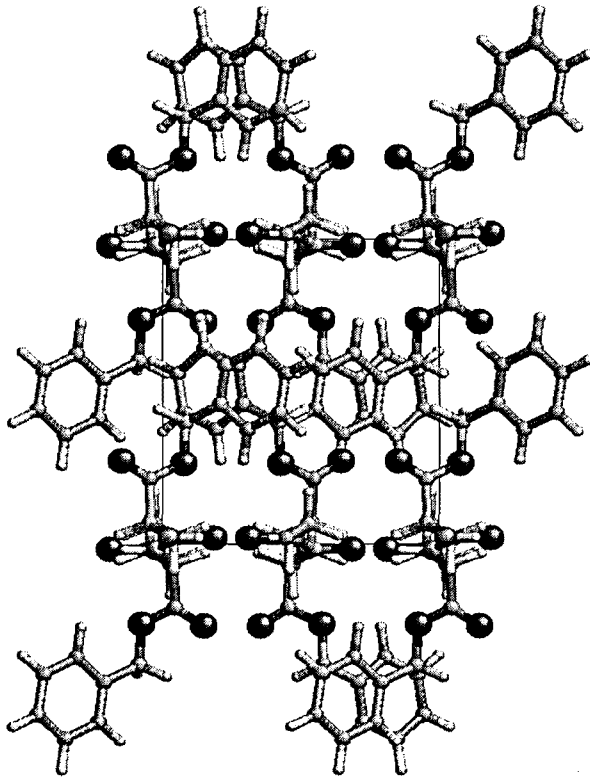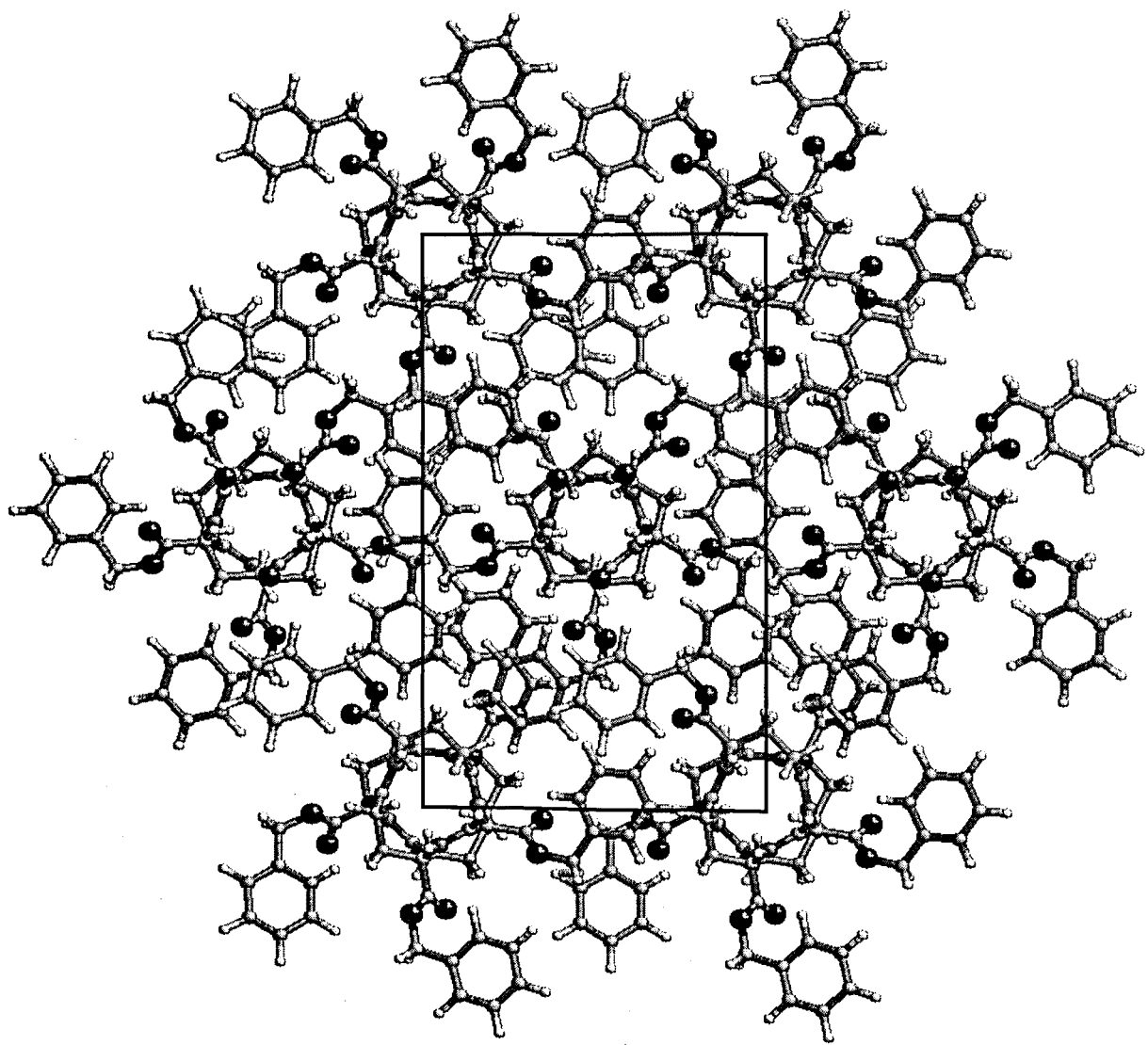
Tal como ya ha sido introducido en el apartado anterior, esta forma cristalina presenta una celdilla pseudo - hexagonal donde las cadenas de polímero adoptan una conformación helicoidal de simetría 5/2. Dichas hélices se caracterizan por estar estabilizadas por puentes de hidrógeno intramoleculares, entre el NH del grupo amida *i* y el C=O del grupo amida *i+2*. Además, los datos de difracción de rayos X indican que las hélices de láminas adyacentes se empaquetan en disposición antiparalela.

La celdilla unitaria empleada para el modelado de la forma II del PAAG-2 ha sido la determinada mediante difracción de rayos X (Melis, 1999): a_0=11.54 Å, b_0=19.9 Å, c_0= 10.01 Å y α= β= γ= 90°. Debido a que los datos de difracción experimentales no muestran cambios aparentes en función de la proporción de enantiómero L, el modelado de la estructura de la forma II se ha realizado partiendo de un modelo de polímero constituido únicamente por enantiómero D (PAADG-2).

V.5.1. Métodos

La conformación helicoidal 5/2 modelada para el PABG (sección **V.4**) fue utilizada como punto de partida para la generación del empaquetamiento cristalino. Mediante el programa PCSP se realizaron cálculos energéticos para optimizar la conformación de la cadena lateral y la posición relativa entre cadenas del cristal. Todos los cálculos energéticos se llevaron a cabo usando los parámetros del campo de fuerzas Amber 4.1 (Cornell et al., 1995) a excepción de las cargas atómicas. Éstas se derivaron mediante el ajuste del MEP obtenido a partir de cálculos AM1 (Dewar et al., 1982) al MEP clásico.

Se simularon los patrones de difracción de rayos X para las estructuras cristalinas más favorecidas energéticamente mediante el programa Cerius[2] (1994).

V.5.2. Resultados

Para determinar el empaquetamiento más favorable de las cadenas de polímero se realizaron cálculos energéticos en función los siguientes parámetros:

- Conformación de la cadena lateral
- Posición relativa entre hélices de una misma lámina (*setting angle*, θ)
- Posición relativa entre hélices de diferentes láminas.

En primer lugar se optimizó la conformación de la cadena lateral. Para ello se realizó en primer lugar una exploración sistemática del ángulo diedro χ_1 (figura **V.7**) considerándose una hélice 5/2 aislada. El ángulo fue variado de 0 a 360° con incrementos de 5°, mientras que los ángulos diedros χ_2 y χ_3 se mantuvieron fijos a 180°. Las conformaciones más favorecidas para χ_1 se muestran en la tabla **V.2**.
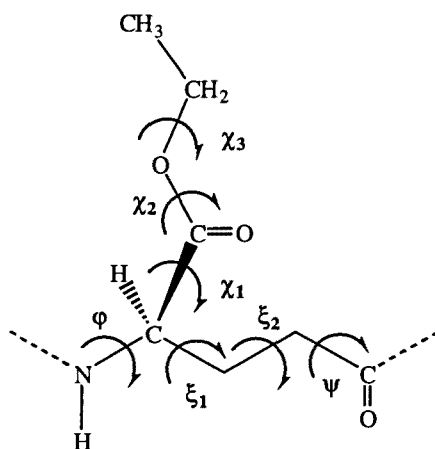
Figura V.7. Representación esquemática de la unidad constitucional del PAADG-2. En el esquema se muestran los ángulos de torsión que definen la conformación del polímero.

Una vez establecidos los valores de χ_1, se realizó una exploración para el ángulo χ_3. Para la obtención de este parámetro debe tenerse en cuenta el efecto del entorno cristalino, puesto que el diedro χ_3 determina la posición del extremo de la cadena lateral. Por este motivo la optimización de este ángulo diedro se realizó de forma concertada con la exploración del empaquetamiento entre las hélices de una misma lámina. Para ello se construyó un sistema de 3 hélices paralelas, situadas a lo largo del

eje x y separadas por 11.54 Å (distancia a_0). El sistema empleado se representa esquemáticamente en la figura **V.8**.

Tabla V.2. Valores del ángulo χ_1 para las conformaciones más favorecidas. Los ángulos se dan en grados y las diferencias de energía entre conformaciones (ΔE) en kcal mol^{-1} res^{-1}.

Conformación	χ_1	ΔE
I	340	0.0
II	0	+0.05
III	170	+0.21
IV	60	+1.31

Se realizaron cuatro exploraciones diferentes, partiendo de cada una de las 4 conformaciones de χ_1 obtenidas anteriormente. En cada exploración se empleó un paso de variación de 5°, en el mismo rango de valores que en el diedro anterior. Así mismo, la exploración del empaquetamiento dentro de la lámina se realizó variado el *setting angle* desde 0 a 360° (con incrementos de 5°). Es decir, en total se realizaron 4x72x72 cálculos de la energía del sistema, obteniéndose 71 empaquetamientos posibles de hélices 5/2 paralelas con una energía relativa inferior a 20 kcal mol^{-1} res^{-1}.
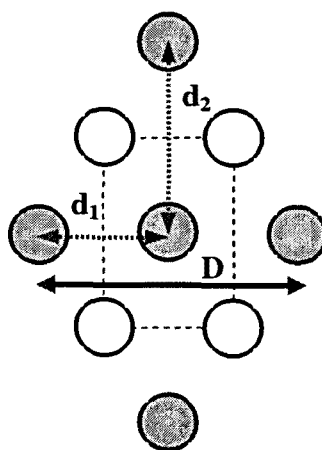
Figura V.8. Representación esquemática de los modelos empleados para la optimización del empaquetamiento de la forma II. Para explorar la estructura de una lámina se empleó un sistema modelo constituido por tres cadenas paralelas, que en el dibujo corresponden a los círculos grises señalados mediante una doble flecha continua, siendo D dos veces el parámetro a_0. El modelo de lámina es el punto de partida para el modelo utilizado en la optimización del empaquetamiento mediante la inclusión de las cadenas antiparalelas (representadas mediante círculos blancos), donde d_1 y d_2 son iguales a los parámetros a_0 y b_0 respectivamente.

Una vez establecidos los mejores parámetros estructurales para una lámina se pasó a la optimización del empaquetamiento de las cadenas antiparalelas. Para ello se usó un sistema modelo de 9 cadenas de polímero explícitas (según el esquema explicado en la figura V.8). En este punto, se exploró la mejor ubicación de las cadenas antiparalelas respecto de las láminas modeladas en el paso anterior. Además se optimizó la posición relativa de las cadenas antiparalelas mediante rotaciones entorno al eje helicoidal.

De los 71 empaquetamientos considerados para la lámina de hélices paralelas, solo 4 de ellos proporcionaron estructuras energéticamente favorecidas, las cuales se muestran en la tabla V.3. Es destacable que cuando el ángulo χ_1 se encuentra en *gauche* (conformación IV en la tabla V.2) el empaquetamiento se ve especialmente estabilizado, contrastando con el hecho que esta conformación fuese el mínimo menos favorecido para la hélice aislada.

Tabla V.3. Resumen de los parámetros estructurales optimizados para de la forma II PAADG-2. Los valores de los ángulos diedros de la cadena lateral y los ángulos que definen la posición relativa entre cadenas (θ y θ') se dan en grados. Las diferencias de energía entre estructuras (ΔE) se expresan en kcal mol^{-1} res^{-1}.

Estructura	ΔE	χ_1	χ_2	χ_3	θ^a	θ'^b
1	0.0	60	180	130	100	185
2	+0.35	60	180	120	30	35
3	+11.6	340	180	210	150	110
4	+12.7	170	180	200	80	35

[a] orientación relativa de los ejes de rotación de dos hélices en disposición paralela.
[b] orientación relativa de los ejes de rotación de dos hélices en disposición antiparalela.

Para los cuatro empaquetamientos resultantes se simuló el patrón de difracción de rayos X mediante el programa Cerius^2. En la tabla V.4 se muestran los resultados obtenidos donde se comparan, para las diferentes reflexiones observadas, los espaciados y las intensidades calculadas con los valores estimados experimentalmente.

Tabla V.4. Comparación entre los espaciados e intensidades observadas (**d obs** y **I obs**, respectivamente) en el diagrama de difracción de rayos X en fibras del PAADG-2 y los valores calculados (**d calc** y **d obs**) para cada uno de los modelos obtenidos mediante cálculos de energía.

h k l[a]	d obs[b,c]	I obs[b]	d calc[c]	I calc[c]			
				1	2	3	4
0 2 0/1 1 0	10.00	mf	9.995	100	100	100	100
2 0 0/1 3 0	5.70	md	5.77	6.75	9.66	12.8	3.55
0 4 0	4.96	md	5.00	1.54	5.52	8.89	4.62
0 3 1	5.50	d	5.56	2.29	2.33	3.7	9.44
0 0 2	5.00	f	5.000	20.4	14.6	30.1	24.7
1 2 2	4.20	mf	4.17	47.8	20.2	65.87	64.01
1 0 3	3.21	d	3.21	4.20	4.33	0.23	9.75
0 0 4	2.48	d	2.5	0.0	0.0	0.0	0.0

[a] Indexado sobre la base de una red ortogonal de parámetros $a_0=11.54$ Å, $b_0=19.9$ Å y $c_0=10.01$ Å
[b] Melis, 1999
[c] Valores de los espaciados en Å
[d] Intensidades en %

A pesar de las pocas reflexiones que presenta el diagrama de difracción de rayos X y de la estimación cualitativa de las intensidades (tanto para el polímero puro como para el racémico), las cuatro estructuras modeladas permiten explicar a grandes rasgos el diagrama de fibra experimental. Únicamente la estructura 2 presenta una desviación importante en las intensidades de las reflexiones del segundo estrato, especialmente en la (1 2 2). Sin embargo, las tres estructuras restantes permiten explicar correctamente las dos características principales del diagrama de difracción experimental: una reflexión muy intensa ecuatorial a 10.0 Å (0 2 0) y las dos reflexiones típicas de la forma II, la meridional de 5.0 Å (0 0 2) y la reflexión del segundo estrato a 4.17 Å (1 2 2).

Finalmente, teniendo en cuenta los resultados obtenidos mediante cálculos energéticos y de simulación de rayos X la estructura más probable para la forma II corresponde a la número 1, la cual se muestra en la figura **V.9**.
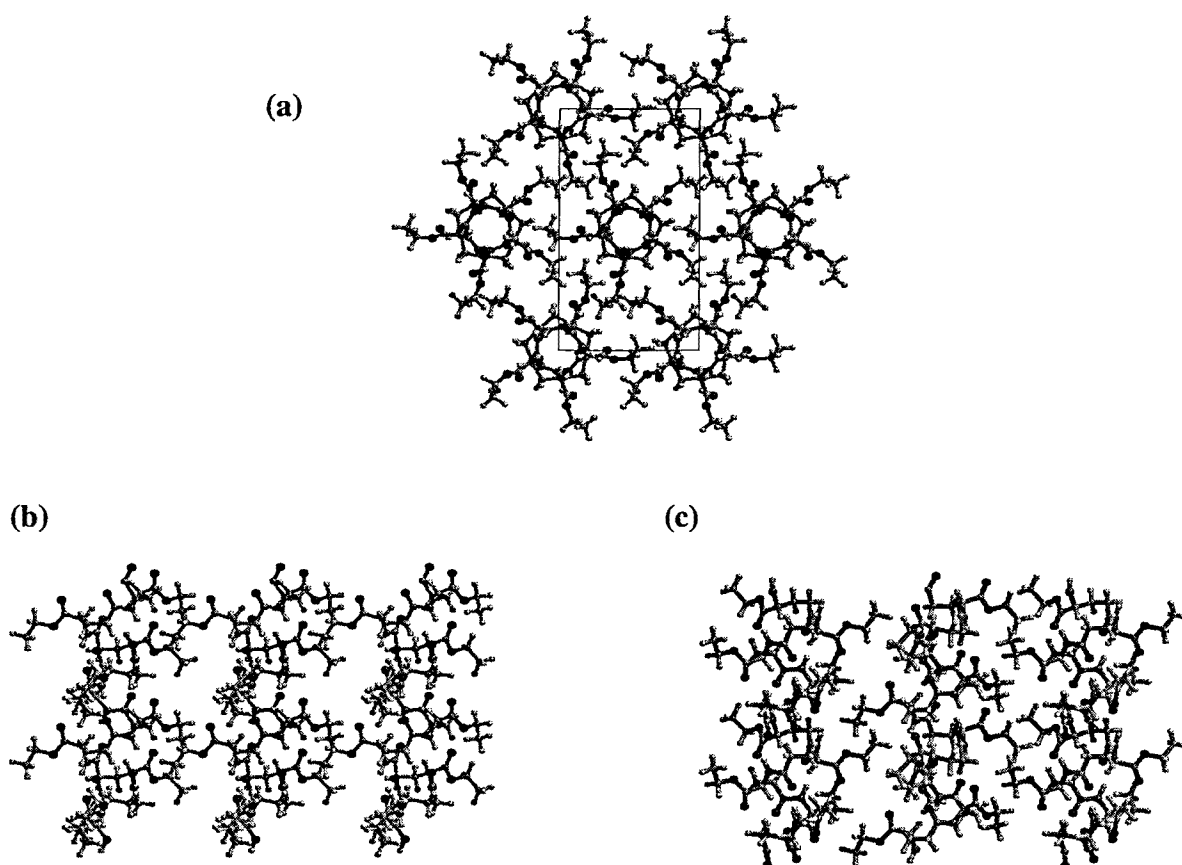

Figura V.9. Proyecciones ecuatorial **(a)**, a lo largo del plano (1 0 0) **(b)** y del plano (1 1 1) **(c)** de la estructura cristalina del PAADG-2.

V.6. "A computation study of poly(α-ethyl-γ-glutamate): Application of force-field calculations to determine the crystal structure of form III"

Zanuy, D.; Ferro, D.R.; Alemán, C.; Muñoz-Guerra, S.

A computation study of poly(α-ethyl-γ-glutamate): Application of force-field calculations to determine the crystal structure of form III

David Zanuy,[1] Dino R. Ferro,[2] Carlos Alemán[1] and Sebastián Muñoz-Guerra[1]

1.- Departamen d'Enginyeria Química, ETSEIB, Universitat Politècnica de Catalunya, Diagonal 647, Barcelona E-08028, Spain

2.- Istituto di Chimica delle Macromolecole del CNR, Via E. Bassini 15, I-20133 Milano, Italy

ABSTRACT

Poly(α-ethyl-γ-glutamate), a poly(γ-peptides) with an alkoxy group attached to the γ-carbon, present two crystal forms which are denoted II and III. We have applied different computational approaches based on molecular mechanics to determine the crystal structure of form III. For this purpose, experimental information derived from X-ray diffraction and IR dichroism has been used to discriminate among the different minimum energy structures obtained. Results indicate that form III of poly(α-ethyl-γ-glutamate) consists of an orthorhombic unit cell with two helices of symmetry 2/1 stabilized by intermolecular hydrogen bonds, which are arranged in antiparallel along b-axis.

INTRODUCTION

Poly(α-alkyl-γ-glutamate)s, are a class of poly(γ-peptide)s, *i.e.* polymers derived from γ-amino acids, that have attracted great interest because of their capability to take up conformations similar to those of poly(α-peptide)s. In fact, poly(α-alkyl-γ-glutamate)s are nylon 4 derivatives with an alkoxy group attached to the γ-carbon of the repeating unit:
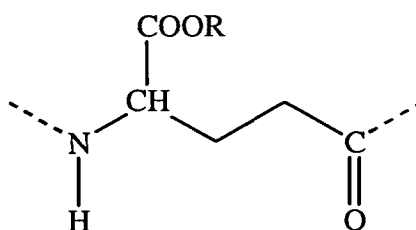
Scheme I

The structure of poly(α-alkyl-γ-glutamate)s was initially investigated by one of us thirteen years ago.[1] In such work a preliminary study about the structure of poly(α-benzyl-γ-L-glutamate) and poly(α-methyl-γ-L-glutamate) obtained by chemical synthesis was performed using both X-ray and electron diffraction. More recently, we have reported in detail the conformation and crystal structure of poly(α-benzyl-γ-DL-glutamate).[2] This polymer presents a nearly racemic composition and is easily obtained by esterification of microbial poly(γ-glutamic acid). Two crystal forms were found for the benzyl esters of bacterial and synthetic origin. Form I consists of a layered structure with chains in almost extended conformation, while

3

form II exists as a pesudohexagonal lattice made of up-and-down helices with 5 residues per two turns.

In a very recent work, we present a study about the crystal structure of the methyl, ethyl and isopropyl esters of poly(γ-glutamic acid).[3] Both optically pure (D) and nearly racemic polymers were considered. All the compounds again displayed two crystal polymorphs. Form II was very similar to that of the benzyl derivative. Indeed, the only difference among them was the packing of the side chains. On the other hand, a new crystal form, denoted form III, was also detected. The infrared dichroism data and the X-ray diffraction pattern (Figure 1) provided some information about both the molecular conformation and the packing of the chains. However, no atomistic model has been proposed for the form III of poly(α-alkyl-γ-glutamate)s at the present time. In this work, an analysis of the crystal structure of form III have been carried out for poly(α-ethyl-γ-D-glutamate), denoted PAAG-2 henceforth, with computational tools.

METHODS

In our aim for solving the crystal form III of PAAG-2, we used different theoretical methodologies to make the widest structure exploration. The conformational search of the helix, *i.e.* the exploration of the main chain dihedral angles (Figure 2), was performed using the GEMOX[4] computer program. On the other hand, all the energy minimizations were performed with the CHAMP/93[5] program and single point energy calculations were done using the PCSP program.[6] Furthermore, X-ray diffraction patterns

4

were simulated with the Cerius^2 program.[7] The strategy followed to find an atomistic model for the investigated crystal structure is summarized in Figure 3, where we depict a flowchart of the procedure used.

Generation of polymer conformation. A preliminary search for the helix conformation compatible with the X-ray diffraction data was performed using the GEMOX program.[4] This computational method was especially designed to generate all the molecular arrangements sterically feasible for a system with a given helical symmetry and a chain repeat length. The van der Waals parameters were taken from AMBER libraries.[8]

For all the helical conformations generated by GEMOX, energy minimizations were performed with the CHAMP/93 system,[5] which is a molecular mechanics program developed for crystal structure calculations (see below).

Generation of crystal lattice. All the crystal structures were built using the CHAMP/93 program,[5] which is the latest version of the molecular mechanics program developed at the ICM laboratory of Milan. A feature of this method particularly useful for the present work is that the input is structured as series of commands, controlled by a simple but efficient meta-language, which allows for automatic repetition of previous commands with a wide possibility of changing parameters and files. Furthermore, this meta-language allows building periodical structures just by defining basic

5

symmetry operations. Both characteristics make possible the systematic search of different packings with little effort.

An important consequence of this particular working procedure is the possibility of performing energy minimizations in the cartesian space taking into account only the effect of the atoms which are not equivalent in the defined symmetry relationships. At the same time, it allows to include geometrical restraints by the symmetry operations themselves. In the present work we kept the cell parameters dimensions and the helical symmetry fixed. Each minimized structure was an energy minimum for a given group of symmetry operations, *i.e.* pseudo-space group (see text below).

Energy Calculations. All energy minimizations were performed using Allinger′s MM2 force field,[9] which is implemented in CHAMP/93. The reliability of such force-field for many energy calculations of crystalline polymers have been tested for many years.[10-13] For this study, we updated the amide parameters in order to reproduce the molecular geometry of polypeptides.[14] Furthermore, we used the last version of the parameters developed to simulate hydrogen bonds formed by amide and carbyxilic groups.[15] In all these calculations the cutoff applied was 12.0 Å.

Single point calculations were performed with the PCSP program,[6] which is able to generate atomic coordinates of a polymer in a given crystal lattice and to evaluate the energy of the resulting structure using periodic continuation conditions. PCSP calculations were made using AMBER force

field parameters[8] with exception of the atomic charges. These parameters were explicitly derived for PAAG-2 (Figure 2) by fitting the quantum mechanics molecular electrostatic potential to the Coulombic one[16].

Crystal modeling was made for the most favorable packing arrangements using Cerius^2 program.[7] X-ray diffraction patterns were simulated for these models for sample textures similar to those ones used in the collection of experimental data.

Calculations were performed on Sun 20, SGI Origin 128 and SGI Indigo^2 workstations at Milan and Barcelona.

RESULTS

Main Chain Conformation. Combination of X-ray diffraction and infrared dichroism data suggested[3] a pseudo-extended conformation similar to the β-sheet of poly(α–peptides). This fact was supported by two evidences: i) PAAG-2 displayed perpendicular dichroism indicating that hydrogen bonds between amide groups are arranged perpendicular to the fiber direction; and ii) the meridian reflection found in the X-ray diagram at 0.92 nm reflects an important contraction with respect to the all-*trans* conformation (about 0.17 nm per amide group). We assumed the simplest helical symmetry, 2/1 helix, for joining both criteria.

A complete exploration of all the possible conformations compatible with both 2/1 symmetry and a helical period at 0.92 nm was performed using the program package GEMOX[4] (Figure 2). We enlarged our research spectra by smoothing the geometric restriction on the helical period to the experimental error, *i.e.* 0.92 ± 0.05 nm. A set of 74 different conformations was obtained, which differ among them by at least more than 20° in one dihedral angle. All these conformations were minimized using CHAMP/93[5] program. We made this process with geometry restrains, by fixing the helical symmetry and the chain repeat length at the experimental value.

Only twelve different minimum energy conformations were obtained, which are displayed in Table 1. One of these conformations, labeled as **3** in Table 1, presents a weak intramolecular hydrogen bond between two consecutive

amide groups. We discard such conformation for further investigations since it is not consequent with IR dichroism data. All the other conformations were considered for packing calculations because their amide groups were arranged perpendicular to the helical axis.

Results displayed in Table 1 indicate that for reaching the experimentally observed helical pitch at least two dihedral angles of the main chain must adopt a *gauche* conformation. This is an expected result since the contraction with respect to the all-*trans* conformation is as much as 0.17 nm per residue. An extreme case is that obtained for conformation **12** in which the four dihedral angles present a *gauche* conformation.

Another interesting feature concerns to the distribution of the backbone dihedral angles. Table 1 shows that for the more favored helical structures the folding usually involves to the central dihedral. By analogy with the conventional γ-form of nylons,[17] *i.e.* non substituted polyamides, it could be expected a contraction on the main chain conformation induced by the folding of the dihedral angles adjacent to the amide groups, while the central ones remain in *trans*. Indeed, conformation **8** presents such structural pattern. However, this conformation is 5.1 kcal·mol^{-1}·residue^{-1} destabilized with respect to the lowest energy one. Thus, these results suggest that substitution at the γ-carbon induce a dramatic change in the conformational preferences of polyamides.

9

Generation of Crystal Lattice. The X-ray diffraction data obtained from a stretched film in form III (Figure 1) were used to build the crystal lattice. The assignment of the Miller´s indexes had some degree of indetermination since there were only a few strong reflections. This experimental evidence can be due to the high degree of symmetry achieved in the organization of the molecules, *i.e.* a lot of systematic extintions, and/or to a very efficient crystal packing, *i.e.*, a dense structure. According to these criteria, we started assuming a simple orthorhombic cell by assigning the strongest equatorial reflection to the distance between chains linked by intermolecular hydrogen bonds (a_0=0.462 nm). Thus, by imposing the parameter a_0 the only value of b_0 able to explain the remaining spots was 0.1848 nm. The density provided by these parameters assuming two chains per unit cell (1.32 gr/cm^3) is in agreement with the experimental value (1.28 gr/cm^3).

In order to explore all the possible arrangements of 2/1 helices on this initial lattice we built eight crystal lattices, which are depicted in Figure 4, using the CHAMP/93 program. By this way, we were able to consider all the chain packings compatible with the experimental lattice using simple symmetry relationships. Thus, we define eight different pseudo-space groups (Figure 4), as the sum of different elemental symmetry operations. These groups contained all the information of both the molecular chain and the packing and, therefore, the effects of the conformation and the crystal environment were simultaneously taken into account with a very low computational cost.

10

As can be seen in Figure 4, we have considered the packing of both parallel and antiparallel chains along the b-axis. It should be mentioned that this point could not be consequent with the crystallographic data in some cases. However, our main aim was to avoid forgetting any possibility such, for instance, to have two independent chains due to small conformation disorders.

Complete energy minimizations were done of the eight lattices displayed in Figure 4 considering each one of the 11 selected main chain conformations (see Table 1). The all-*trans* conformation was initially considered in all cases. These 88 possible crystal lattices led to 27 different structures with favorable energy, *i.e.* structures without steric clashes (data not shown). Table 2 lists the number of favorable energy structures for each pseudo-space group. It is worth noting the most populated pseudo-space groups are those with an antiparallel arrangement (about 65%), while structures with a parallel packing are less common (about 36%).

Single point calculations of the more stable structures were performed with the AMBER[8] force field using the PCSP program.[6] Results provided by both MM2 and AMBER force fields are shown in Table 3. It is worth noting only five different conformations are able to provide low energy packings. These are labelled as **1, 5, 6, 7** and **11** in Table 1. On the other hand, the geometric parameters for the intermolecular hydrogen bonds range from 0.168 to 0.211 nm (H...O distances) and from 141.6° to 160° (<N-H...O angles).

11

It is especially remarkable that the two force fields predicted more favorable energies for the structures with the chains packing in antiparallel than for the parallel arrangements. Indeed, only one of the structures listed in Table 3 (structure V) presents a parallel arrangement of the chains. Another interesting feature is that many of the structures listed in Table 3 belong to the BI* or FI* pseudo-space group, i.e. with the second chain shifted 1/2 along the a-axis. Indeed, only structures IV and VIII present a different organization of the molecules in the pseudo-cell, i.e. PI* and ZI*, respectively.

These results provide a different picture of the structural preferences of PAAG-2 with respect to that displayed in Table 2. In spite of having briefly the same quantity of structures with and without shifting along a-axis, the first ones are more favored in MM2 force field. However, this trend is inverted when the energy is evaluted using the AMBER force field. Thus the relative energy order of the different structures is not the same for the two force fields. Furthermore, the energy differences predicted by MM2 are smaller than those provided by the AMBER force field. These discrepancies can be explained by considering the expressions used by the two force fields to evaluate the van der Waals and electrostatic interactions. Thus, MM2 describes the hydrogen atoms bonded to carbon with hybridization sp^3 with a hardness larger than that employed by AMBER, leading to greater intermolecular distance between the packed chains in the former case. However, the largest difference between the two force fields is related with

the treatment of the electrostatic effects. In this case, atomic charges explicitly derived for PAAG-2 were used in AMBER calculations and, therefore, a better description of the electrostatic interactions is expected with this force field.

Refinement. Finally, the X-ray diffraction pattern was simulated for each minimum energy structure using the Cerius[2] package program[7] . Results were compared with experimental data.

In a first screening, all the structures that briefly reproduce the main spots of the experimental pattern were selected, *i.e.* R-factor = $\Sigma \mid I_o\text{-}I_c \mid$ / $\Sigma \; I_o \leq$ 90%. Only eight structures of the 27 minimum energy packing obtained in the last section were able to explain the observed spots. This include all the structures showed in Table 3 with exception of the one belonging to the pseudo-space F1*, *i.e.* structure V. Thus, it is worth noting that only the structures with an antiparallel arrangement are able to explain satisfactorily the experimental diffraction pattern.

A complete exploration of the conformational space of the side chain was made for the eight selected structures in order to obtain the best agreement between the theoretical and experimental diffraction patterns. These calculations were performed by rotating the dihedral angles of the side chain in steps of 30 degrees. A complete energy minimization was performed for each new conformation. In all cases calculations were carried out into the

crystal lattice, *i.e.* using the pseudo-space group generation of CHAMP/93 program.

A total of 93 new structures were characterized as energy minima, the X-ray diffraction pattern being simulated for all of them. A selection of these structures was initially done just making a visual examination of the X ray diffraction pattern. By this way we discarded 42 structures. The remaining structures were analyzed in terms of R-factor. The resulting values for the R-factor ranged from 87 to 25%. The best fitting between the theoretical and the experimental values was obtained for the models described in Table 4.

The structure with the lowest R-factor (25.3%) corresponds to a pseudo-space ZI*. Figure 5 shows the fibber pattern simulated for this structure. Figure 6 shows the three projections of the resulting unit cell. This is in an orthorhombic cell with two chains arranged in antiparallel along b-axis, which provide a layered structure of 2/1 helices stabilized by intermolecular hydrogen bonds. This structure is in good agreement with both X-ray diffraction and IR dichroism data. Furthermore, it is worth noting that it corresponds to the lowest energy packing, even although the backbone conformation (labelled as 5 in Table 1) had a relative energy of 3.6 kcal/mol residue.

REFERENCES

1. Puiggalí, J.; Muñoz-Guerra, S.; Rodríguez-Galán, A.; Alegre, C.; Subirana, J. A. *Makromol. Chem., Macromol. Symp.* **1988**, *20/21*, 167.

2. Melis, J.; Zanuy, D.; Alemán, C.; García-Alvarez, M.; Muñoz-Guerra, S. **2001**, submitted.

3. ?????

4. Navas, J.J.; Alemán, C.; Muñoz-Guerra, S. *Polymer* **1996**, *37*, 2589.

5. Ferro, D.R. Ragazzi, M. *Conformational (Hyper) Analysis Milan Package,* Instituto di Chimica delle Macromolecole del CNR: Milano, Italy, 1993.

6. León, S.; Navas, J.J.; Alemán, C. *Polymer,* **1999**, *40*, 7351

7. Cerius^2 1.6, Molecular Simulations Inc. Burlington, MA.

8. Weiner, S.J.; Kollman, P.A.; Nguyen, D.T.; Case, D.A. *J. Comput. Chem.* **1990**, *7*, 230

9. Allinger, N.; Yuh, Y.H. *QCPE,* **1980**, *12*, 395.

10. Ferro, D.R.; Brückner, S.; Mielle, S.V.; Ragazzi, M. *Macromolecules,* **1990**, *23*, 1676

11. Ferro, D.R.; Brückner, S.; Mielle, S.V.; Ragazzi, M. *Macromolecules,* **1990**, *24*, 1156

12. Ferro, D.R.; Brückner, S.; Mielle, S.V.; Ragazzi, M. *Macromolecules,* **1991**, *25*, 5231

13. Ferro, D.R.; Mielle, S.V.; Brückner, S., *Macromolecules,* **1998**, *31*, 6926

14. Lii, J-H.; Gallion, S.; Bender, C.; Wikström, H.; Allinger, N.; Flurchick, M.F.; Teeter, M.M *J. Comput. Chem.*, **1989**, *10*, 503.

15. Allinger N.L.; Randall A.K.; Imam, M.R. *J. Comput. Chem.*, **1988**, *9*, 591

16. Alemán, C.; Luque, F.J.; Orozco, M.J. *J. Comput. Aided Mol. Design* **1993**, *7*, 721

17. Kinoshita, Y. *Makromol. Chem.* **1959**, *33*,1.

CAPTIONS TO FIGURES

Figure 1. X-ray diffraction patterns of a stretched film of PAAG-2 in form III.

Figure 2. Flow chart showing the various steps followed to arrive at the crystal structure of the form III of PAAG-2.

Figure 3. Chemical formula for the structural unit of PGGA-2. The torsional angles and the atomic charges are displayed.

Figure 4. Schematic representation of the different chain packings considered for the form III of PGGA-2. Each packing corresponds to a pseudo-space group.

Figure 5. Simulated X-ray diffraction pattern produced by the structure modeled for form III of PAAG-2.

Figure 6.

Table 1.- Relative energies (ΔE in kcal/mol residue) and main chain dihedral angles[a] (in degrees) for the 12 structures found by combining GEMOX and CHAMP/93 calculations.

#	ΔE^b	φ	ξ_1	ξ_2	ψ
1	0.0	106.59	-179.37	-39.04	94.71
2	1.9	171.36	-55.99	-134.81	67.38
3[c]	2.7	171.68	-79.09	71.02	-154.23
4	3.3	59.37	54.70	168.46	72.15
5	3.6	57.27	127.05	54.52	71.94
6	3.7	-158.88	69.92	-179.44	-97.52
7	4.2	-81.06	49.05	178.91	-142.16
8	5.1	-84.19	156.51	-136.34	58.04
9	5.7	-176.57	172.75	-72.11	75.54
10	5.7	-82.79	-46.20	-170.81	-56.89
11	7.1	-143.13	150.4	67.62	-94.52
12	7.5	-62.31	-81.85	-83.93	-57.31

[a] See Figure 1.

[b] Energies computed using the MM2 force field implemented in CHAMP/93.

[c] This conformation presents an intermolecular interaction between two consecutive amide groups, the geometric parameters being d(H...O) = 0.182 nm and < N-H...O = 142°.

Table 2. Number of structures with a favorable energy for each pseudo-space group considered in this study.

Pseudo-Space Group	n^a	
	1	**Ī**
Zn*	4	5
Pn*	1	3
Bn*	1	4
Fn*	4	5
	Parallel arrangement	*Antiparallel arrangement*
	10	17

[a] See Figure 4

Table 3.- Relevant structural parameters for the more favored crystal lattice. Relative energies (ΔE, in kcal/mol residue) computed with both MM2 and AMBER force fields, and geometrical parameters for the intermolecular hydroben bonds (distances in Å and angles in degrees) are listed.

#	Pseudo-space group[a]	ΔE MM2	ΔE AMBER	Conformation[b]	d(H...O)	<N-H...O
I	BI*	0.0	2.5	7	0.174	153.5
II	FI*	1.8	2.3	5	0.169	158.3
III	BI*	1.8	5.5	5	0.170	169.0
IV	PI*	1.9	0.0	6	0.168	159.0
V	F1*	2.2	2.1	5	0.210	145.0
VI	FI*	3.2	5.0	1	0.182	158.0
VII	BI*	4.0	6.7	11	0.170	141.6
VIII	ZI*	4.9	6.3	5	0.181	155.3

[a] See Figure 4.

[b] See Table 1.

Table 4. Refined structural parameters for the form III of PAAG-2. The relative energies (ΔE in kcal/mol residue) provided by the MM2 and AMBER force fields are listed.

Conformation[a]	Pseudo-Space group[b]	ΔE	Side chain Conformation[c]			R-factor (%)
			χ_1	χ_2	χ_3	
5	ZI*	0.0 *0.0*	-110.7	-150.1	-177.9	25.3
5	ZI*	+4.551 *+0.9*	-136.9	-174.3	64.7	39.0
5	ZI*	+10.62 *+3.25*	-171.7	168.2	87.5	59.6
5	FI*	+2.309 *+3.15*	-154.5	172.4	82.8	61.1

[a] See table 1

[b] See figure 1

[c] In degrees

Fig. 1. Zanuy et al., 2001

```
┌─────────────────────┐              ┌──────────────┐
│ Experimental        │              │   GEMOX      │
│ Information          │─────────────▶│ Generation   │
│ c₀= 0.92 nm          │              │ of Helical   │
│ 2/1 Helix Symmetry   │              │ Conformations│
└─────────────────────┘              └──────────────┘
```

Experimental Information
c_0= 0.92 nm
2/1 Helix Symmetry

GEMOX
Generation
of Helical
Conformations

CHAMP/93
Energy
Minimization

Intramolecular
Hydrogen
Bond ?

Yes → Helical Model
Rejected

No

Helical Model
Accepted

Experimental information
a_0= 9.24 nm
b_0= 18.48 nm

CHAMP/93
Generation Crystal
Lattices

Cerius^2
Simulation
of X-Ray Pattern

Exploration of the
Side Chain
Conformational Space

R factor≤ r % → No → Rejected Structure

Yes

Refinement

Fig. 2. Zanuy et al., 2001

0.266

H

0.071

H H

-0.529

O

-0.560 N   ψ   ξ₁   ξ₂   φ   C 0.680

0.039 C   -0.065   C

- 0.368

0.106 H   C 0.832

- 0.568 O   χ₁   O - 0.508

χ₂

H₁₁₁₁₁₁ C 0.131

0.067 H   χ₃   C   H   0.089

- 0.242   H

H

0.122 H

Fig. 3. Zanuy et al., 2001

$Zn*$

$Pn*$

$1/2\ c$

$1/2\ a$

$Bn*$

$Fn*$

$1/2\ a$

$1/2\ c$

$n=1 \rightarrow 2ond$ Chain Parallel

$n=I \rightarrow 2ond$ Chain AntiParallel

Fig. 4. Zanuy et al., 2001
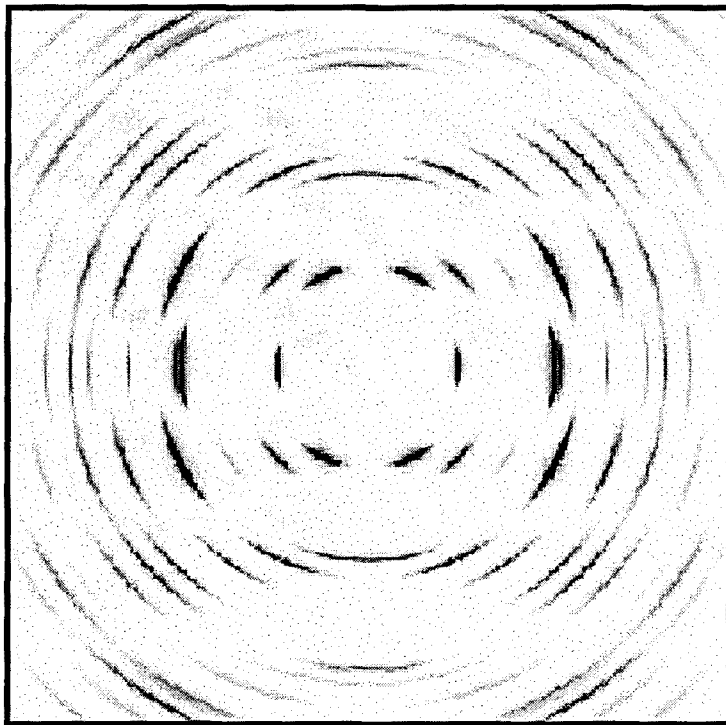
Fig. 5. Zanuy et al., 2001
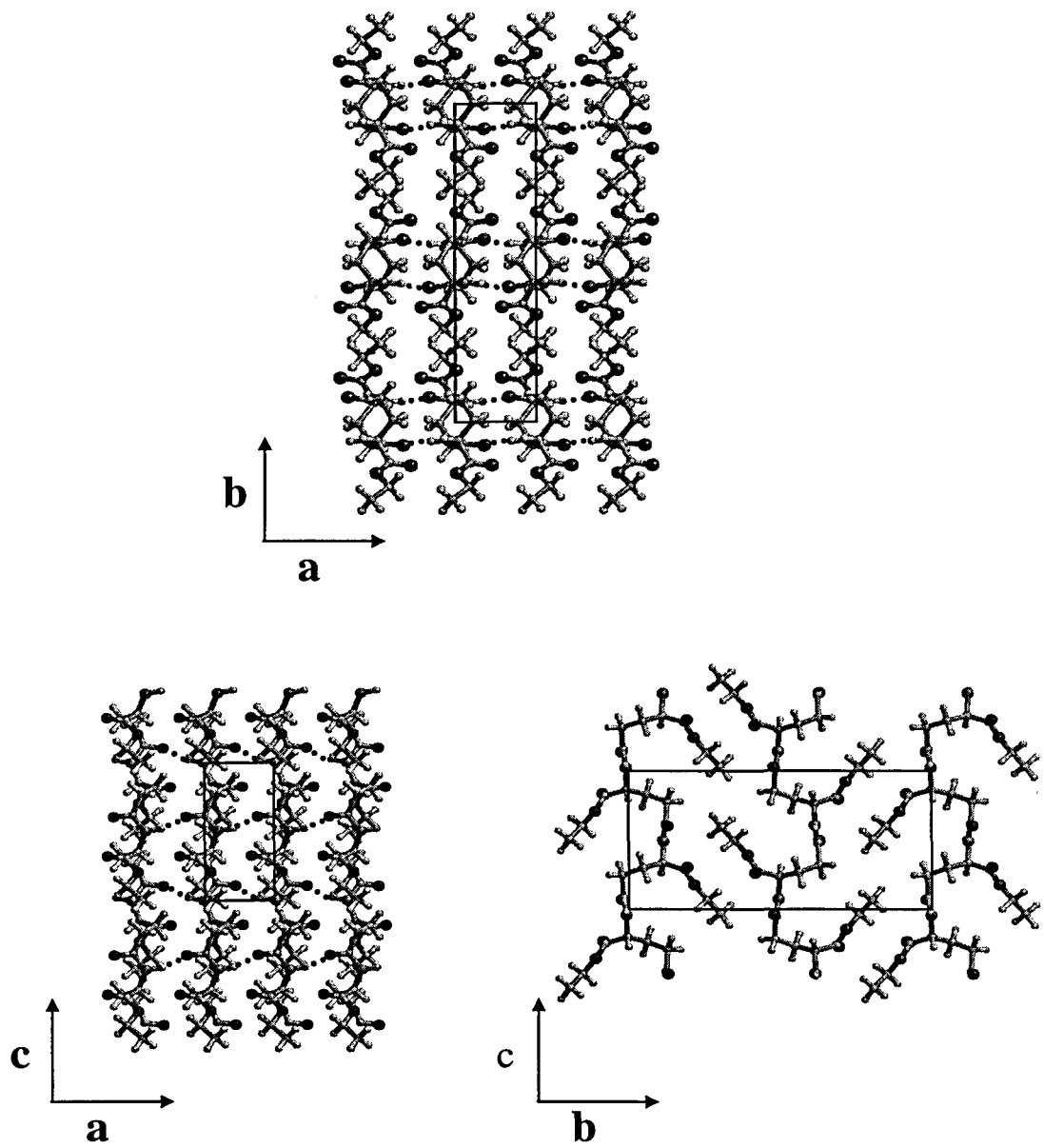
Fig. 6. Zanuy et al., 2001

V.7. Conclusiones parciales

1) Se ha obtenido un modelo a nivel atomístico de la forma I del poli(α-bencil-γ-glutamato). En esta forma cristalina las cadenas de polímero adoptan una conformación casi extendida de simetría 2/1, empaquetándose en disposición antiparalela en una celdilla cristalina ortorrómbica, de manera que se forman puentes de hidrógeno entre cadenas adyacentes. Las cadenas laterales del polímero se disponen perpendiculares a la dirección del eje helicoidal, optimizando las interacciones de apilamiento de los grupos aromáticos. El modelo obtenido, no solo reproduce los datos de difracción de rayos X para el polímero homoquiral, sino que reproduce la mayoría de las extinciones que diferencian las muestras obtenidas con diferentes proporciones enantiómero L. Dichas extinciones son compatibles con una constitución formada por bloques homoquirales que cristalizan en dominios independientes.

2) Se ha examinado mediante cálculos energéticos la forma II del PAB(D)G. Para ello se ha considerado un empaquetamiento de hélices 5/2 dextrorsas en disposición antiparalela. Los grupos bencilo laterales se disponen a 0.402 nm de forma que las interacciones de apilamiento proporcionan gran estabilidad a la estructura. Por otro lado, la hélice 5/2 ha resultado ser extremadamente inestable frente a la substitución de unidades D por unidades L, lo que indica que es incompatible con una distribución estadística de unidades enantioméricas en la cadena de PAB(DL)G. El modelo propuesto para dicho polímero está constituido por una mezcla de cadenas D y L que se distribuyen estadísticamente o formando microdominios cristalinos.

3) Se ha modelado el empaquetamiento cristalino para la forma II del PGGA-2 a partir de cálculos energéticos. Esta forma cristalina se caracteriza por presentar un empaquetamiento antiparalelo de hélices 5/2 estabilizadas por puentes de hidrógeno intramoleculares. Las cadenas de láminas adyacentes se encuentran giradas 185°, lo que equivale a decir que están desplazas respecto al eje c_0 aproximadamente el período de repetición de la hélice. La estructura obtenida reproduce satisfactoriamente los datos de difracción de rayos X disponibles.

4) Se ha resuelto la estructura cristalina de la forma III del PGGA-2. El modelo propuesto consiste en una celdilla ortorrómbica, con dos cadenas por celdilla, que da lugar a un empaquetamiento laminar de hélices 2/1. Las hélices se disponen paralelamente a lo largo del eje a_0 y la estructura está estabilizada por puentes de hidrógeno intermoleculares que se establecen entre cadenas de una misma lámina. A lo largo del eje b_0 las cadenas de láminas adyacentes se estructuran en disposición antiparalela. Las cadenas laterales adoptan una conformación plegada la cual resulta estabilizada por las interacciones de van der Waals.

VI. RESULTADOS:

ESTUDIO DE LAS INTERACCIONES Y LAS
PROPIEDADES CONFORMACIONALES DE LOS
COMPLEJOS POLIELECTROLITO-
TENSIOACTIVO DERIVADOS DE POLIPÉPTIDOS

VI. ESTUDIO DE LAS INTERACCIONES Y LAS PROPIEDADES CONFORMACIONALES DE LOS COMPLEJOS POLIELECTROLITO - TENSIOACTIVO DERIVADOS DE POLIPÉPTIDOS

VI.1. Autoasociación

La generación de estructuras químicas no se limita únicamente a la unión de átomos o moléculas mediante enlaces covalentes. Existe un gran número de materiales cuya obtención se basa únicamente en la capacidad que presentan sus componentes moleculares para dar asociaciones estables. Estos sistemas se denominan de forma general complejos "autoasociados" (*self-assembled complexes*).

En la naturaleza existen ejemplos muy conocidos de sistemas químicos que, de forma espontanea, se asocian para dar estructuras estables. Buenos ejemplos son las bicapas lipídicas que dan lugar a las membranas celulares o la doble hélice en los ácidos nucleicos (Whitesides et al., 1991).

Los complejos autoasociados se caracterizan por el tipo de interacción que permite su formación. Así, la asociación de sus componentes se da mediante interacciones no covalentes, como puentes de hidrógeno, interacciones hidrofóbicas o interacciones electrostáticas. La naturaleza de estas interacciones permite a dichos complejos reorganizar su estructura como respuesta a cambios en las condiciones ambientales (temperatura, tipo de disolvente, etc.). Por último, y en contraste con los materiales que se preparan mediante vías sintéticas tradicionales, los complejos autoasociados pueden obtenerse de forma simple y rápida (Stupp et al., 1993).

A nivel industrial, como ya ha sido ampliamente comentado, se requieren materiales cuyas propiedades estén bajo un control muy preciso. Los complejos autoasociados, en este contexto, presentan un gran potencial tecnológico, puesto que su estructura puede ser controlada variando las condiciones que modulan la interacción entre sus componentes y, en consecuencia, muchas de sus propiedades.

VI.1.1. Complejos polielectrolito – tensioactivo

De todos los materiales formados por autoasociación, los más extensamente estudiados son aquellos que están constituidos por cadenas poliméricas cargadas (polielectrolitos) y iones moleculares anfifílicos (tensioactivos). Los tensioactivos más usados están formados por pequeñas "cabezas" polares y una "cola" hidrofóbica. El proceso de asociación se da mediante una reacción de intercambio iónico, guiada por la atracción electrostática entre los componentes del complejo.

Los complejos polielectrolito - tensioactivo pueden ser clasificados en función del procedimiento de obtención que se siga y de las propiedades que se derivan como consecuencia de la formación del complejo:

- *Obtención en interfase aire/agua*: dan lugar a estructuras laminares mucho más estables que las estructuras formadas únicamente por la asociación de moléculas de tensioactivo (Royappa y Rubner, 1992).

- *Obtención por absorción en fase sólida*: en este grupo de complejos los tensioactivos generalmente presentan dos grupos cargados, obteniéndose el complejo por absorción de tensioactivo en la matriz de polielectrolito (Mao et al., 1993).

- *Mezcla de disoluciones:* tensioactivos y polielectrolito se ponen en contacto mediante una mezcla de las disoluciones donde se tienen los reactivos. Los complejos resultantes pueden presentar propiedades de cristal líquido como consecuencia de la estructuración de las "colas" hidrofóbicas, mientras que las cadenas de polímero incrementan la estabilidad térmica de las fases ordenadas (Ujiie y Iimura, 1992).

VI.1.2. Estequiometría de los complejos

Del último grupo comentado, se pueden obtener diferentes tipos de complejos en función de la concentración relativa polielectrolito/tensioactivo. Si existe un exceso de polielectrolito se obtienen micelas solubles en agua (Figura **VI.1a**), que están organizadas por pequeñas agrupaciones de tensioactivo (asociados mediante las "colas

hidrofóbicas) rodeadas de polímero polielectolito. El exceso de carga del sistema queda entonces en contacto con el medio acuoso (Ibraginova et al., 1986).
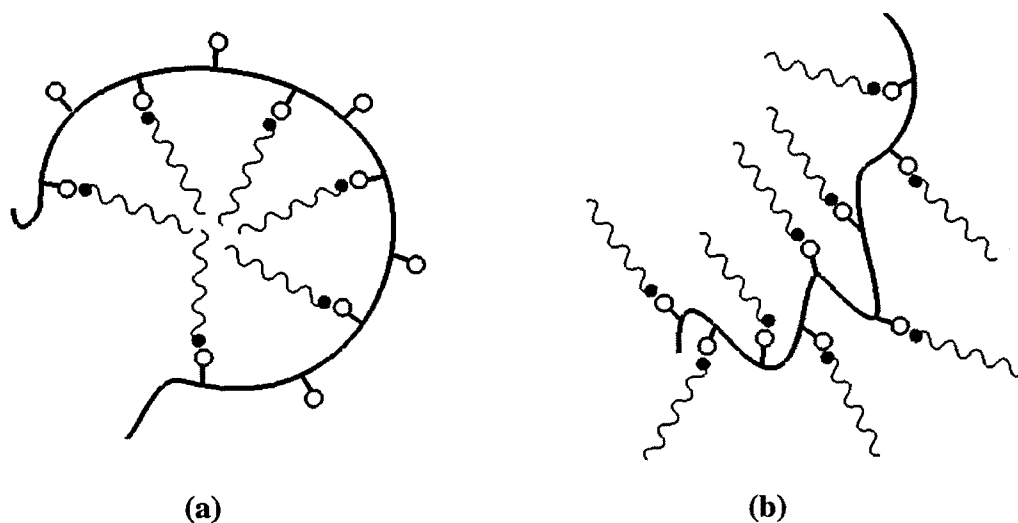

(a)   **(b)**

Figura VI.1. Representación esquemática de la organización de los complejos polielectrolito - tensioactivo no estequiométricos **(a)** y de los complejos estequiométricos **(b)** cuando se mezclan sus constituyentes en medio acuoso. Las moléculas de tensioactivo se representan en rojo y los polielectrolitos en azul.

Si por el contrario, se mezclan cantidades equimolares en agua se forman espontáneamente los complejos estequiométricos (Figura **VI.1b**), los cuales son insolubles en agua y precipitan. Es decir, en función de la estequiometría de los complejos la solubilidad en medio acuoso varía. Sin embargo, estos compuestos son solubles en disolventes orgánicos de baja polaridad, dónde la unión polielectrolito - tensioactivo se mantiene estable (Antonietti et al., 1994).

Los complejos estequiométricos presentan la peculiaridad de combinar las propiedades de cada uno de sus componentes. Las cadenas de polímero dan flexibilidad y estabilidad térmica al sistema, mientras que las colas hidrofóbicas de las moléculas de tensioactivo mantienen su capacidad para ordenarse en estructuras laminares. Así, la constitución que se obtiene es semejante a la de los polímeros tipo peine. En este caso, las cadenas laterales corresponden a las moléculas de tensioactivo asociadas a los grupos cargados del polielectrolito.

VI.2. Complejos polielectrolito - tensioactivo derivados de polipéptidos

De todos los polielectrolitos poliméricos usados para la obtención de complejos estequiométricos los polipéptidos han sido los que más interés han despertado. La razón es la capacidad intrínseca que presentan estos polímeros para adoptar conformaciones regulares. Éste punto es especialmente importante puesto que dicha capacidad no se ve alterada cuando se forman los complejos, lo cual permite controlar las propiedades del nuevo material en relación directa a la estructura molecular (Ponomarenko et al., 1996a).

Los complejos polipéptido - tensioactivo más ampliamente estudiados han sido aquellos que están constituidos por ácido PAGA con tensioactivos del tipo alquiltrimetilamonio (Figura **VI.2a**) y por poli(α-L-Lisina) con tensioactivos del tipo sulfato de alquilo (Figura **VI.2b**)

(a)   (b)
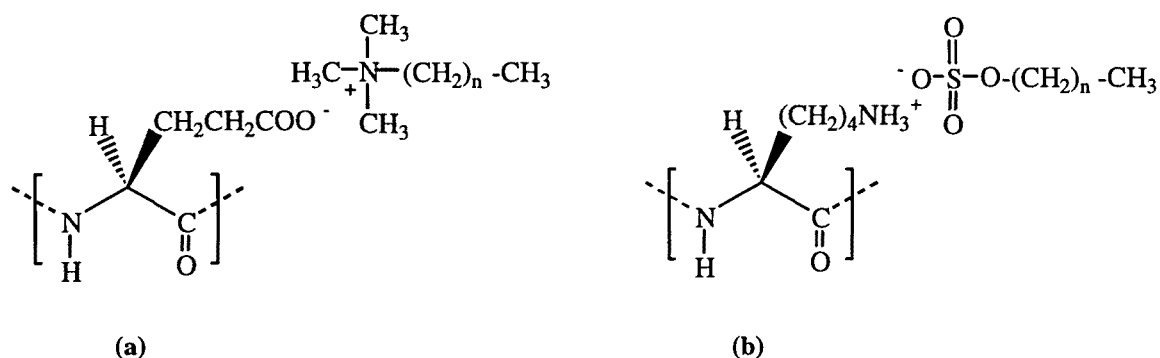
Figura VI.2. Representación esquemática de los complejos polipéptido - tensioactivo constituidos (a) por ácido PAGA (Ponomarenko et al., 1996a y 1996b). y (b) poli(α-L-lisina) (Ponomarenko et al., 1996c).

Estos complejos, tal como se describirá a continuación, presentan grandes analogías conformacionales y estructurales con los polímeros tipo peine derivados del PAGA y de la poli(α-L-lisina) constituidos por cadenas alquílicas unidas covalentemente.

VI.2.1. Conformación en disolución

El carácter anfifílico de estos complejos y la presencia de los grupos iónicos en especial, hace que el rango de disolventes orgánicos en que son solubles sea muy

reducido. Los complejos estequiométricos constituidos por PAGA y por poli(α-L-lisina) son solubles únicamente en algunos disolventes orgánicos polares, como por ejemplo el cloroformo.

Los estudios realizados por Ponomarenko et al. (1996b y 1996c) en disolución de cloroformo mediante RMN de protón indican una presencia predominante conformaciones tipo hélice α para las cadenas de polipéptido, tanto en complejos derivados del PAGA como de la poli(α-L-lisina). Si se añaden agentes desnaturalizantes a la disolución, como el TFA, se induce una transición hélice - ovillo sin que ello conlleve la ruptura de los complejos. Dicha transición se da por un aumento de la movilidad de la cadena polipeptídica, mientras que no se observa un cambio marcado en la conformación en los iones moleculares de tensioactivo (Figura VI.3).
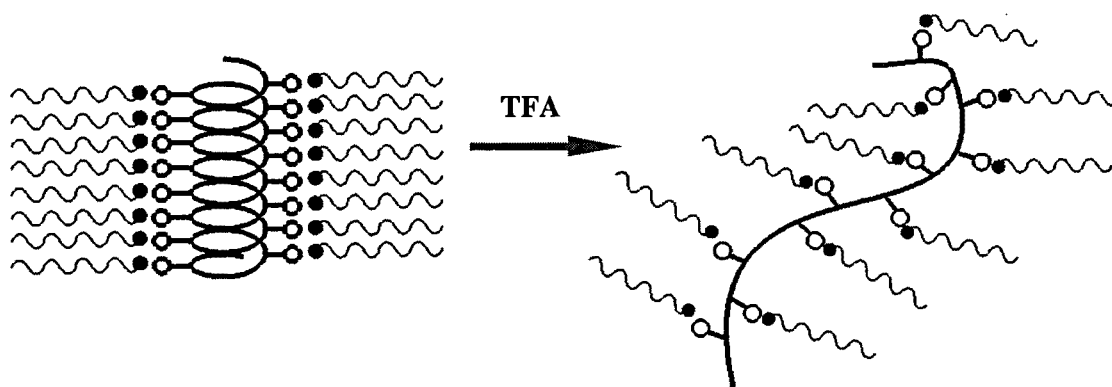
Figura VI.3. Representación esquemática de la transición hélice - ovillo para los complejos polipéptido - tensioactivo en cloroformo. Nótese como las cadenas de tensioactivo (en rojo) tienden siempre a estar en contacto con el entorno orgánico. El polipéptido (en azul) y los grupos cargados (bolas) quedan alejados del medio por efecto las cadenas alifáticas del tensioactivo.

Hay que destacar que, a pesar del cambio conformacional, la interacción con el disolvente sigue siendo la misma: las cadenas alquílicas en contacto con en el medio orgánico y las cadenas de polipéptido y los grupos polares alejados del medio.

VI.2.2. Estado sólido. Conformación y estructura

De forma general, y tal como ha sido apuntado anteriormente, la estructuración de los complejos estequiométricos tiende a ser laminar. Dicha tendencia es consecuencia de la estructuración de las cadenas alifáticas que induce a todo el sistema

a dar un empaquetamiento de láminas de polielectrolitos separadas por las zonas donde se estructuran las cadenas hidrofóbicas. Sólo cuando la longitud de las cadenas alquílicas de los tensioactivos es demasiado corta los complejos resultantes dan estructuras desordenadas.

VI.2.2.1 Conformación de las cadenas de polipéptido

En los complejos derivados del PAGA, las cadenas polipeptídicas adoptan una conformación de hélice α tal como mostraron los estudios de CD y FTIR realizados por Ponomarenko et al. (1996b). Un incremento de la temperatura del sistema induce una transición hélice - ovillo reversible por enfriamiento.

Los ésteres de alquílico del PAGA en estado sólido también presentan una conformación de hélice α para la cadena de polipéptido (Watanabe et al., 1985). Sin embargo, Ponomarenko et al. vieron que la estabilidad conformacional de la cadena polipeptídica frente a la temperatura era inferior para los complejos que para los ésteres de alquilo. Este punto parecía mantener una estrecha relación con las repulsiones electrostáticas que existen entre los grupos carboxilato cercanos en el espacio.

Por último, los complejos constituidos por poli(α-L-Lisina) tienden a presentar conformaciones de hoja β en estado sólido en contraste con los polímeros análogos formados por cadenas alquílicas unidas covalentemente, que presentan conformaciones de hélice α (Sasaki y Iwanami, 1986).

VI.2.2.2 Conformación de las cadenas laterales del tensioactivo

Independientemente de la conformación de la cadena de polipéptido y de la longitud del segmento alifático, las cadenas laterales del tensioactivo tienden a adoptar conformaciones totalmente extendidas a temperatura ambiente. Este hecho es consecuencia de la organización supramolecular del complejo, que se discutirá a continuación.

VI.2.2.3. *Estructura supramolecular. Organización bifásica*

Los complejos basados en polipéptidos, y de hecho la mayoría de los complejos estequiométricos, tienden a formar estructuras laminares. Estudios realizados por Ponomarenko et al. (1996b y 1996c) mediante difracción de rayos X a bajo ángulo (SAXD) muestran claramente esta organización. Se observa como el período más largo de las láminas es independiente de la conformación que adopten las cadenas de polielectrolito, mientras que la orientación relativa de las láminas sí depende de dicha conformación. En los complejos derivados del PAGA, cuyas cadenas polipeptídicas adoptan una conformación de hélice α, las láminas se orientan perpendicularmente a la dirección del eje helicoidal. Por el contrario, en los complejos derivados de la poli(α-L-lisina) la orientación relativa de las cadenas de polipéptido depende de las condiciones en que se obtengan los complejos. Si la cadena polipeptídica adopta una conformación de hoja β, dicha orientación es perpendicular a la dirección del eje de la cadena. Sin embargo, si se fuerza al polipéptido a perder su conformación (en condiciones desnaturalizantes) se observa como las cadenas de polímero pierden su estructuración laminar, orientándose al azar.

La manera en que se estructuran los cationes moleculares de tensioactivo únicamente ha sido estudiada en detalle para los complejos derivados del ácido PAGA. La organización de sus cadenas alifáticas es muy parecida a la descrita para las cadenas hidrofóbicas de los ésteres de alquilo del PAGA. Es decir, las cadenas alquílicas se estructuran en una fase distinta a la de las cadenas polipeptídicas, en dirección perpendicular a la superficie de la lámina e interdigitadas (Figura **VI.4**). En función de su longitud, las cadenas alifáticas pueden llegar a cristalizar en una red hexagonal (a partir de 16 átomos de carbono).
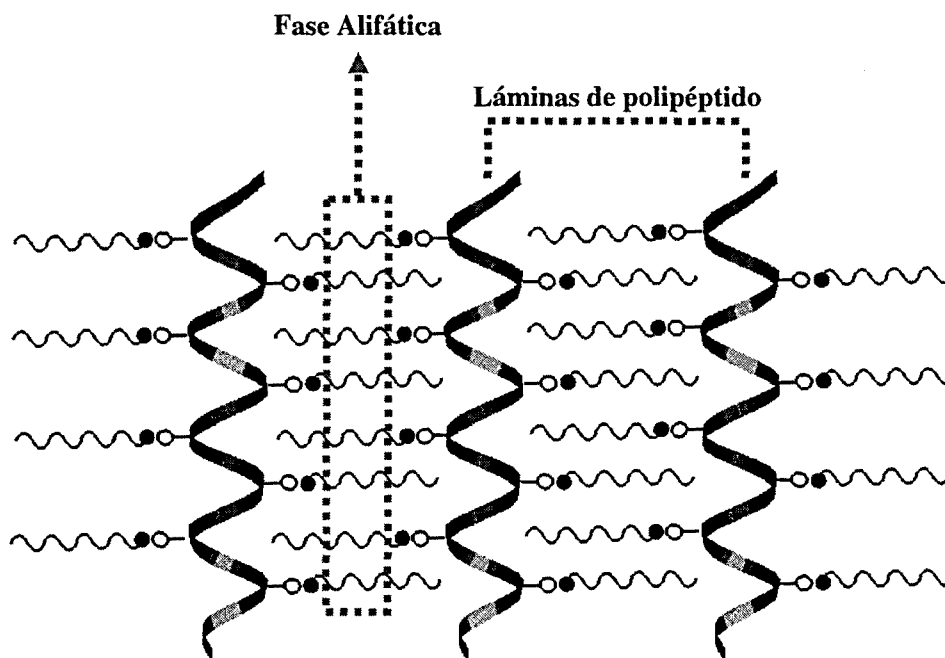
Figura VI.4. Representación esquemática e idealizada de la organización supramolecular de los complejos polielectrolito – tensioactivo en estado sólido. Véase la interdijitación de las cadenas alifáticas (en rojo) y la organización laminar de las cadenas de polipéptido (en azul).

VI.3. Nuevos complejos estequiométricos basados en el ácido poli(γ-glutámico) de biosíntesis

Dentro de este contexto, muy recientemente, y continuando la línea marcada en nuestro laboratorio de desarrollar nuevos materiales biocompatibles, se han obtenido complejos estequiométricos a partir de PGGA y bromuro de alquiltrimetilamonio (Pérez-Camero et al., 1999b).

La obtención de estos complejos, abreviados nATMA·PGGA dónde n denota el número de carbonos de la cadena lateral alifática del tensioactivo, es tan simple y rápida (Figura **VI.5**) como la de los complejos basados en el PAGA anteriormente expuestos. Únicamente se deben mezclar las disoluciones acuosas de poli(γ-glutamato) de sodio y de bromuro de alquiltrimetilamonio. La temperatura de formación de los complejos oscila entre 25 y 70 grados, en función de la longitud de la cadena alquílica del tensioactivo (Tabla **VI.1**).

$$n = 12, 14, 16, 18, 20, 22$$
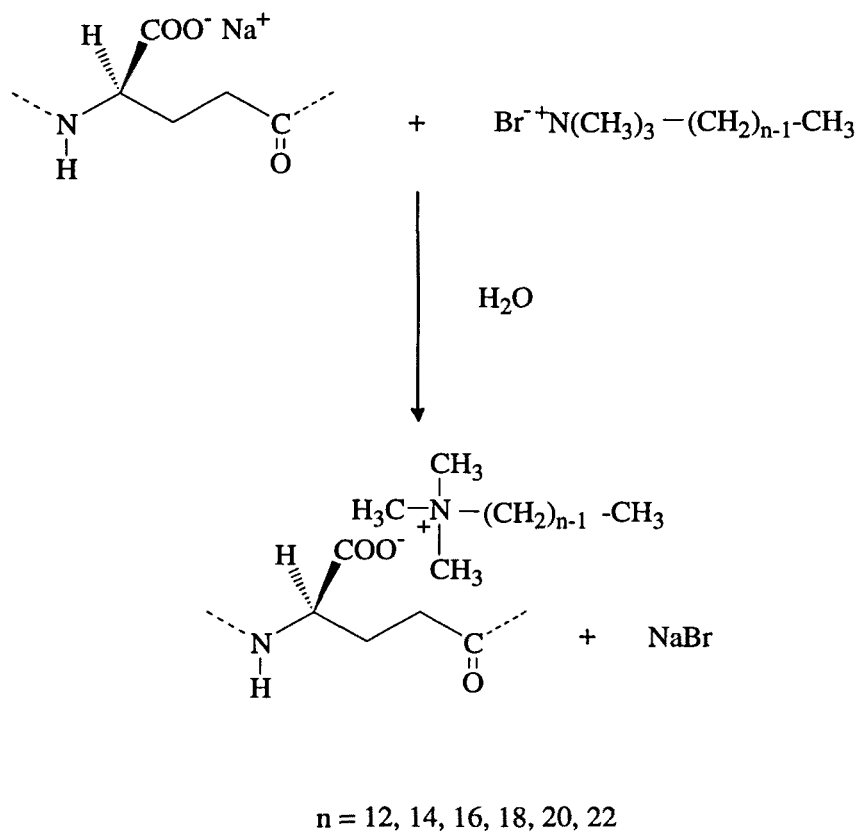
Figura VI.5. Esquema del procedimiento de obtención de los complejos estequiométricos nATMA·PGGA.

Los complejos nATMA·PGGA presentan las siguientes características:

- Son solubles en disolventes orgánicos de baja polaridad.

- Precipitan durante el procedimiento de obtención en medio acuoso.

- En estado sólido son capaces de formar películas transparentes, resistentes y térmicamente estables hasta temperaturas superiores a de 240° C.

Tabla VI.1. Proporción relativa polielectrolito - tensioactivo, temperatura y rendimientos del proceso de obtención de los complejos nATMA·PGGA (Muñoz et al., en prensa)

Complejo	Relación NaPGGA/nATMABr	Temperatura (°C)	Rendimiento
12ATMA·PGGA·	1/2	ambiente	56 %
14 ATMA·PGGA	1/2	ambiente	62 %
16 ATMA·PGGA	1/2	ambiente	67 %
18 ATMA·PGGA	1	50	57 %
20 ATMA·PGGA	1	60	89 %
22 ATMA·PGGA	2/1	70	54 %

VI.3.1. Estructura de los complejos nATMA·PGGA en estado sólido

Los complejos nATMA·PGGA han sido caracterizados mediante FTIR, difracción de rayos X y DSC, respectivamente (Pérez-Camero et al., 1999b). Los datos obtenidos mediante FITR y CD no aportan ninguna información concluyente sobre la conformación de las cadenas de polielectrolito en estado sólido. Sin embargo, parece apuntarse la presencia de algún tipo de estructura secundaria en las cadenas polipeptídicas. Estos resultados no son definitivos puesto que las señales obtenidas por FITR son de una intensidad muy baja y para los datos de CD no existen sistemas de referencia con los que comparar los resultados.

La estructura en estado sólido de los complejos nATMA·PGGA ha sido caracterizada mediante difracción de rayos X (SAXD). Sin embargo, la información obtenida únicamente está relacionada con la estructuración de los cationes moleculares de tensioactivo. Estos presentan una organización de tipo laminar y, cuando el número de carbonos en la cadena lateral del nATMA es igual o superior a 18, las cadenas parafínicas cristalizan en una red hexagonal.

A pesar de que la difracción de rayos X no ha proporcionado ningún dato acerca de la estructuración de las cadenas polipeptídicas, se ha postulado una organización laminar bifásica, por analogía con los complejos derivados PAGA. Es decir, se ha

aceptado una conformación regular para las cadenas de PGGA y una estructuración de tipo laminar para las mismas (Pérez-Camero, 2000).

VI.4. Objetivos

El objetivo general de este capítulo es estudiar y comprender las claves físico - químicas que determinan la formación de los complejos autoasociados. Puesto que no existe ningún precedente publicado en que se estudie este tipo de sistemas, podemos dividir dicho objetivo en dos bloques distintos:

1) *Estudio de la interacción electrostática en complejos polielectrolito - tensioactivo derivados de polipéptidos*: mediante el uso de compuestos modelo, se abordará el estudio de las interacciones que caracterizan este tipo de complejos. De este estudio genérico se intentará obtener información sobre los siguientes aspectos:

    i) Efecto de la naturaleza química de los aniones moleculares en la estabilidad de los complejos formados.

    ii) Efecto del número de iones en la disposición geométrica de los complejos y en los efectos cooperativos.

2) *Estudios conformacionales de complejos polielectrolito - tensioactivo derivados de polipéptidos*: Se caracterizarán mediante dinámica molecular los complejos derivados del PAGA y del PGGA en disolución de cloroformo. Más concretamente se investigarán en detalle los siguientes aspectos:

    i) Conformación del polipéptido y de los tensioactivos, así como la geometría de la interacción electrostática, en complejos estequiométricos derivados del PAGA y tensioactivos del tipo *n*ATMA.

    ii) Conformación del polielectrolito molecular y del tensioactivo en los complejos estequiométricos *n*ATMA·PGGA.

VI.5. "A quantum mechanical study of the ionic interactions in model compounds of poly-electrolite-surfactant complexes derived from polypeptides"

Alemán C.; Zanuy, D. *Chem. Phys. Lett.*, **2000**, *319*, 318-326.

A quantum mechanical study of the ionic interactions in model compounds of polyelectrolite–surfactant complexes derived from polypeptides

Carlos Alemán *, David Zanuy

Departament d'Enginyeria Química, E.T.S. d'Enginyers Industrials de Barcelona, Universitat Politècnica de Catalunya, Diagonal 647, E-08028 Barcelona, Spain

Received 13 September 1999; in final form 29 December 1999

Abstract

A quantum mechanical study on the interactions of alkyltrimethylammonium–acetate (with alkyl = methyl, ethyl, propyl and butyl), methylammonium–methyl sulfate and methylammonium–acetate ion pairs in the gas phase and in solution is presented. These are model complexes for the ionic interactions of self-assembled polyelectrolite–surfactant complexes derived from polypeptides. Two different solvents (water and chloroform) were used to analyze the effects of varying the dielectric constant of the surrounding media on the ionic interactions. The stability of the methylammonium–methyl sulfate and methylammonium–acetate ion pairs was compared to that of the corresponding non-ionic hydrogen-bonded forms. © 2000 Published by Elsevier Science B.V. All rights reserved.

1. Introduction

Salt bridges are among the more thoroughly investigated interactions in biological chemistry. Such interactions are due to the important and often quite specific functions played by ion pairs [1]. They act as binding sites in enzymes [2], mediate molecular recognition [3] and modulate the allosteric behavior of proteins [4]. Their role in determining the stability of secondary-structural elements has been also considered [5]. Indeed, several studies on model peptides

have shown that the character and position of salt-bridging groups affect helix formation [6]. Salt bridges are also involved in connecting different subunits of proteins [7] or in the control of the equilibrium between various conformational states [8]. As a consequence a number of theoretical studies about the energetic of salt bridges [9–12] and the contribution of this interaction to protein stability has been reported for the last years.

For the last decade ion-pair interactions have also attracted considerable interest in polymer science. They have been used to design materials consisting of polyelectrolytes and oppositely charged surfactants [13–19]. Such complexes assemble in aqueous

* Corresponding author. Fax: +34-93401-6600/7150; e-mail: aleman@eq.upc.es

solutions through the electrostatic interactions be-
tween polyion chain units and oppositely charged
surfactant ions, being stabilized by hydrophobic in-
teractions of the surfactant alkyl side chains in water.
Stoichiometric polyelectrolite–surfactant complexes
are insoluble in water but can be dissolved in some
common organic solvents of low polarity without
dissociation [13,17]. Complexation of polymers with
oppositely charged low-molecular-weight com-
pounds may result in stiffening leading to the forma-
tion of main chain liquid crystals in organic solvents
[20].

Most work in this area has involved biopolymers,
which can form a variety of highly ordered sec-
ondary structures, offering polymer–surfactant com-
plexes with useful properties. Complexes formed by
the synthetic sodium poly(α,L-glutamate) and the
oppositely charged alkyltrimethylammonium surfac-
tants [13,18] have been reported. In these complexes
the polymer chains adopt an α-helix conformation in
the solid state. Conversely, the alkyl chains of sur-
factant are extended but positionally disordered if
contains 16 or less carbon atoms in the alkyl groups
while those with 18 carbon atoms crystallize in a
hexagonal lattice. This behavior is similar to that
observed in poly(γ-alkyl-α,L-glutamate)s, which
have been widely investigated as liquid crystals [21].
On the other hand, complexes formed by poly
(L-lysine) hydrobromide and alkyl sulfate anions have
been also reported [19]. Polypeptide chains in the
solid complex can adopt either β-helix of β-sheet
conformations whereas the surfactants present an
extended conformation forming a layer with tail-to-
tail arrangements.

Here we present a theoretical study on the stabil-
ity of the ionic interactions involved in self-assem-
bled complexes derived from polypeptides. A num-
ber of small model complexes have been used to
mimic the interactions between charged polypeptides
and the oppositely charged surfactants. Binding free
energies were computed in the gas phase using
high-level ab initio calculations. Calculations in solu-
tion were performed using a self-consistent reac-
tion-field (SCRF) method allowing to get insight into
the effect of the bulk solvent on the ionic interac-
tions. Two different solvents (water and chloroform)
were used to analyze the effect of varying the dielec-
tric constant of the surrounding media.

2. Methods

2.1. Gas-phase calculations

Full geometry optimizations were performed at
the HF, MP2 and DFT levels of theory using the
6-31 + G(d) [22] basis set. All the DFT calculations
were carried out using the Becke's three-parameter
hybrid functional with gradient corrections provided
by the LYP functional (B3LYP) [23,24]. Force con-
stant analyses were performed to verify the mini-
mum energy state of the optimized geometries. Sin-
gle-point calculations were performed using the 6-31
+ G(d) and 6-311 + G(d, p) [22] basis sets. The ba-
sis set superposition error (BSSE) was corrected
following Boys and Bernardi [25]. The binding ener-
gies were corrected by the addition of the thermal
and entropic (298 K) effects using the standard
procedures in GAUSSIAN-94 [26] program in order to
obtain the Gibbs free energy. Thus, to conduct the
thermodynamical analysis we confined ourselves to
the harmonic approximation.

2.2. Solvation calculations

SCRF calculations were performed to incorporate
the solvent effects on the stability of the complexes
investigated. These methods have been successfully
used to investigate related topics [27]. In order to
examine the influence of the permittivity of the
medium on the stability of the complexes investi-
gated, calculations were performed in water and
chloroform. The semiempirical AM1 version [28,29]
of the polarizable continuum model formulated by
Miertus, Scrocco and Tomasi [30] (MST) was used
to determine the electrostatic component of the free
energy of solvation (ΔG_{sol}). The cavitation contribu-
tion was introduced following Pierotti's scaled parti-
cle theory [28,29], and the van der Waals component
was calculated by using an optimized linear relation-
ship with the atomic surface area. The solute cavity
was built up using the standard procedure [29], but it
was reduced by a factor of 0.92 for calculations
involving charged species [28]. In these calculations
ab initio gas-phase geometries were used. It should
be emphasized that because of the semiempirical
formulation of the method, the root mean square
deviation between the experimental and MST/AM1

ΔG_{sol} values is only 1.0 and 0.4 kcal/mol for aqueous and chloroform solutions, respectively [28,29]. Calculations were performed with an adapted version of MOPAC93 Revision 2 program [31].

3. Results and discussion

3.1. Ion-pair complexes in the gas phase

The complexes constituted by the acetate anion and the alkyltrimethylammonium cation (complexes I) with alkyl = methyl (Ia), ethyl (Ib), propyl (Ic) and butyl (Id) have been calculated to model the interactions that appear in the self-assembled complexes formed by poly(α,L-glutamate) and alkyltrimethylammonium ions.

Ia: R=-H
Ib: R=-CH₃
Ic: R=-CH₂-CH₃
Id: R=-CH₂-CH₂-CH₃
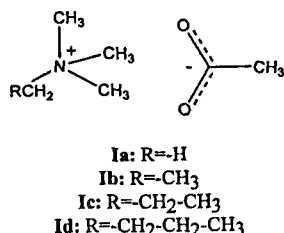
Fig. 1 shows the most relevant intermolecular parameters for the complexes **Ia**, **Ib**, **Ic** and **Id** optimized at the HF/6-31 + G(d) level. Intermolecular distances obtained for these complexes are very similar, the largest difference being 0.040 Å. However, a detailed inspection to Fig. 1 reveals that intermolecular distances present a systematic variation. Thus, they increase with the size of the alkyl group in the alkyltrimethylammonium cation suggesting a reduction in the strength of the binding. Table 1 reports the gas-phase binding energies (ΔE), which were corrected for BSSE, obtained for the four complexes at both HF/6-31 + G(d) and MP2/6-31 + G(d) levels of theory. The results provided by the two computational levels are in excellent agreement, the differences between them being ~ 2–3 kcal/mol, i.e. lower than 3%.

Table 1 shows the gas-phase binding enthalpies (ΔH^{298}), which were obtained by adding the differ-
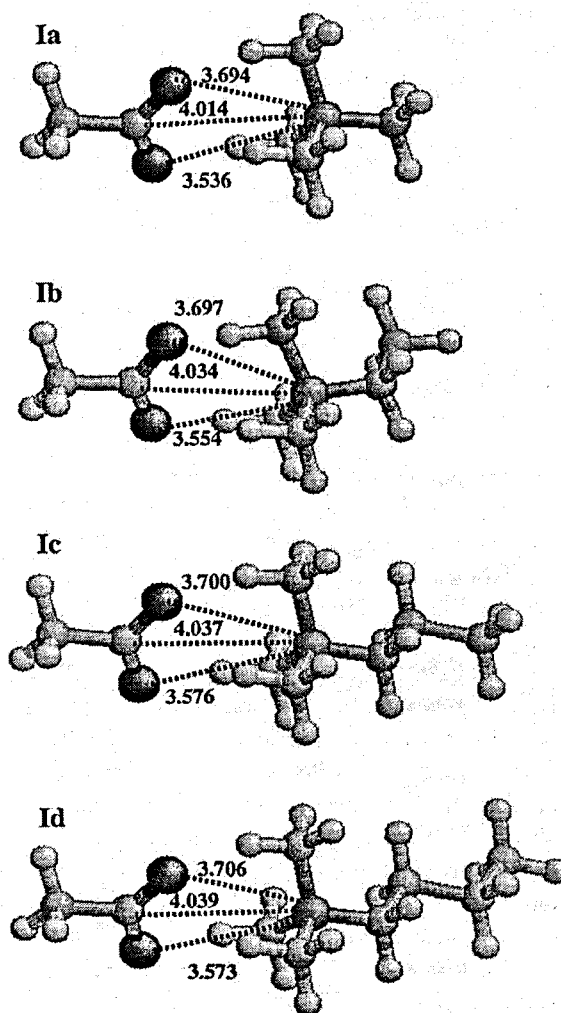
Fig. 1. Optimized geometries for the tetramethylammonium–acetate (Ia), ethyltrimethylammonium–acetate (Ib), propyltrimethylammonium–acetate (Ic) and butyltrimethylammonium–acetate (Id) ion pairs. Selected intermolecular parameters are displayed.

ences between the values of zero-point energy and thermal corrections of the complex and the ions to the ΔE computed at the MP2/6-31 + G(d) level, and the entropic corrections ($-T\Delta S$) for complexes I. As it can be seen, the zero − point energies and thermal corrections upon binding lead to a destabilization of ~ 10.7–11.2 kcal/mol. On the other hand, the unfavorable contribution arising from the entropic term ranges from 9.0 to 9.7 kcal/mol. As a result, the binding free energy ($\Delta G^{298} = \Delta H^{298}$ −

Table 1

Energy[a] (E; in a.u.), number of imaginary frequencies (v_i), binding energy[a,b] (ΔE; in kcal/mol), binding enthalpy[a,b,c] (ΔH^{298}; in kcal/mol), entropic contribution ($-T\Delta S$; in kcal/mol) and binding free energy (ΔG^{298}; in kcal/mol) calculated in the gas phase for the investigated ion pairs

Complex	E HF/6-31 + G(d)	v_i	E MP2/6-31 + G(d)	ΔE HF/6-31 + G(d)	ΔE^a MP2/6-31 + G(d)	ΔH^{298}	$-T\Delta S$	ΔG^{298}
Ia	−440.086779	0	−441.419566	−95.6	−97.4	−86.7	9.0	−77.7
Ib	−479.120325	0	−480.587564	−94.2	−96.9	−86.2	9.1	−77.1
Ic	−518.155215	0	−519.755127	−93.5	−95.4	−84.7	9.1	−75.6
Id	−557.190396	0	−558.922629	−93.1	−95.0	−83.8	9.7	−74.1
II	−757.463900	0	−758.597757	−114.8	−116.5	−105.4	10.0	−95.4
III[d]	−323.022624	1	−323.952754	−127.6	−128.2	−114.2	14.0	−100.2

[a] Geometries calculated at the HF/6-31 + G(d) level.

[b] Thermodynamical contributions at 298 K calculated at the HF/6-31 + G(d) level.

[c] The differences between the values of zero-point energy and thermal corrections of the complex and the separated ions were added to the ΔE computed at the MP2/6-31 + G(d) level.

[d] The imaginary frequency obtained in complex III (see text) was not considered for the calculation of thermodynamic contributions.

$T\Delta S$) between alkyltrimethylammonium and acetate ions varies from −77.7 to −74.1 kcal/mol.

An interesting feature can be extracted from the results obtained for these four complexes. This is that the gas-phase binding free energy of the complexes varies as follows: Ia > Ib > Ic > Id. Thus, the binding free energy drops 3.6 kcal/mol when the alkyl group changes from methyl to butyl. The reduction in the binding free energy is consistent with the variation observed for the intermolecular parameters confirming that the strength of this ionic interaction decreases when the size of the alkyl group in the alkyltrimethylammonium cation increases. This feature clearly illustrates the electron leasing associated to the alkyl chains in classical organic chemistry. It is worth noting that the difference in the binding free energies for Ic and Id is 1.5 kcal/mol, suggesting that the ionic interaction for complexes with an alkyl group larger than butyl should provide a lower stabilization than that obtained for Id.

The effects of both the computational procedure and the basis set in the ionic interactions subject of

Table 2

Selected intermolecular parameters[a] determined from geometry optimizations of complex Ia at different levels of theory
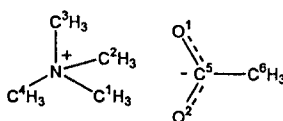
Parameter	HF/6-31 + G(d)	MP2/6-31 + G(d)	B3LYP/6-31 + G(d)
d(N ··· C5)	4.014	3.958	3.996
d(N ··· O1)	3.536	3.466	3.434
d(N ··· O2)	4.014	3.643	3.755
d(C1 ··· C5)	3.681	3.590	3.777
d(C2 ··· C5)	3.781	3.722	3.714
d(C3 ··· C5)	3.870	3.863	3.776
∠N ··· C5–C6	175.8	175.3	171.9
∠C4–N ··· C5–C6	110.4	99.8	177.1

[a] Distances and angles in ångströms and degrees, respectively.

study have been determined for **Ia**. Table 2 summarizes selected intermolecular parameters for **Ia** of the geometries optimized at the HF, MP2 and B3LYP levels of theory. All these structures were optimized using the 6-31 + G(d) basis set. The intermolecular distances determined from both HF and B3LYP calculations are in good agreement with those predicted at the MP2 level. Thus, the values obtained at the latter level of theory are the smallest ones but the differences with respect to the values predicted at the HF and B3LYP levels can be considered acceptable. However, inspection to the dihedral angle defined by the atoms $\angle$C4–N $\cdots$ C5–C6 (see Table 2) reveals that the arrangement of the acetate anion with respect to the tetramethylammonium cation provided by the HF and MP2 methods differs from that predicted at the B3LYP level. Thus, HF and MP2 geometry optimizations lead to a geometry where the oxygen atoms of the acetate alternate with respect to the methyl groups of the tetramethylammonium (**case A**). Conversely, the B3LYP minimum presents an eclipsed arrangement between one oxygen atom of the acetate and one methyl group of the tetramethylammonium (**case B**) suggesting a failure of this functional. These two arrangements, i.e. **cases A** and **B**, are illustrated in the following scheme where the

hydrogen atoms have been neglected to make clearer the representation.

Case A   **Case B**
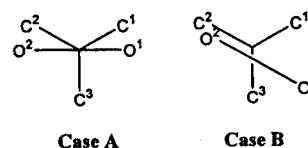
Table 3 shows the binding energies computed at the HF/6-31 + G(d), HF/6-311 + G(d, p), MP2/6-31 + G(d), MP2/6-311 + G(d, p), B3LYP/6-31 + G(d) and B3LYP/6-311 + G(d, p) levels using the geometries of **Ia** optimized at the HF/6-31 + G(d), MP2/6-31 + G(d) and B3LYP/6-31 + G(d) levels. The calculated binding energy is not dependent on the basis set. Thus, the largest difference between the 6-31 + G(d) and 6-311 + G(d, p) results is 0.1, 0.5 and 0.6 kcal/mol at the HF, MP2 and B3LYP levels of theory. On the other hand, a larger dependence may be traced with the level of theory. Thus, comparison of the HF/6-311 + G(d, p) and B3LYP/6-311 + G(d, p) binding energies with the MP2/6-311 + G(d, p) ones shows that the largest difference is 2.5 and 0.8 kcal/mol, respectively. The overall of

Table 3

Energies (E; in a.u.) and binding energies (ΔE; in kcal/mol) calculated in the gas phase for the complex **Ia** at different levels of theory[a]

Level of theory	E	ΔE
HF/6-31 + G(d)//HF/6-31 + G(d)	−440.086779	−95.6
HF/6-311 + G(d, p)//HF/6-31 + G(d)	−440.201746	−95.7
MP2/6-31 + G(d)//HF/6-31 + G(d)	−441.419566	−97.4
MP2/6-311 + G(d, p)//HF/6-31 + G(d)	−441.700611	−97.8
B3LYP/6-31 + G(d)//HF/6-31 + G(d)	−442.858179	−97.5
B3LYP/6-311 + G(d, p)//HF/6-31 + G(d)	−442.978946	−98.0
HF/6-31 + G(d)//MP2/6-31 + G(d)	−440.081461	−96.2
HF/6-311 + G(d, p)//MP2/6-31 + G(d)	−440.195900	−96.2
MP2/6-31 + G(d)//MP2/6-31 + G(d)	−441.424500	−98.3
MP2/6-311 + G(d, p)//MP2/6-31 + G(d)	−441.704088	−98.7
B3LYP/6-31 + G(d)//MP2/6-31 + G(d)	−442.861898	−98.6
B3LYP/6-311 + G(d, p)//MP2/6-31 + G(d)	−442.981152	−99.2
HF/6-31 + G(d)//B3LYP/6-31 + G(d)	−440.082027	−95.9
HF/6-311 + G(d, p)//B3LYP/6-31 + G(d)	−440.196591	−96.0
MP2/6-31 + G(d)//B3LYP/6-31 + G(d)	−441.423852	−98.0
MP2/6-311 + G(d, p)//B3LYP/6-31 + G(d)	−441.703817	−98.5
B3LYP/6-31 + G(d)//B3LYP/6-31 + G(d)	−442.862843	−98.7
B3LYP/6-311 + G(d, p)//B3LYP/6-31 + G(d)	−442.982149	−99.3

[a] Level of energy calculation//level of geometry optimization.

the results clearly indicate that correlation contributions to the binding energy are non-negligible and that the MP2/6-31 + G(d)//HF/6-31 + G(d) level of theory is suitable to investigate the ionic interactions under study.

The interaction between poly(L-lysine) cation and the oppositely charged surfactant alkyl sulfate has been modeled by a complex formed by methylammonium and methyl sulfate ions (complex II). The ion-pair constituted by methylamonium cation and acetate anion (complex III) has been also considered for comparison.

The ion-pair complex III is not a 'true' energy minimum on the potential energy surface, but in order to be able to characterize this complex without having a hydrogen transfer, HF/6-31 + G(d) geometry optimization was performed by imposing the necessary constraint. Fig. 2 shows the optimized geometries for II and III. As it can be seen, the distance between the two ions is shorter in II and III than in I, suggesting a stronger binding in the former complexes. Table 1 includes the binding energy, binding enthalpy and binding free energy values for these ion pairs. It should be noted that for III, the imaginary frequency associated to the constraint imposed during geometry optimization was not taken to compute the thermodynamic corrections. It is expected that the uncertainties introduced from this procedure will be small.

The binding energies of complexes II and III estimated at the MP2/6-31 + G(d) levels are − 116.5 and − 128.2 kcal/mol, respectively. On the other hand, the binding free energies are − 95.4 and − 100.2 kcal/mol, respectively. It should be emphasized that both the binding enthalpy and binding free energy values listed in Table 1 for III are slightly

Fig. 2. Optimized geometries for the methylammonium–methyl sulfate (II) and methylammonium–acetate (III) ion pairs. Selected intermolecular parameters are displayed.

overestimated due to the apparition of two imaginary frequencies. The interaction of methylammonium with acetate is preferred by ~ 4.8 kcal/mol with respect to the interaction with the methyl sulfate. Moreover, the binding in complexes with alkyltrimethylammonium is ~ 18–26 kcal/mol less stabilized than in complexes with methylammonium. This feature is probably due to the larger concentration of the positive charge in the latter cation as revealed the analysis of the atomic charges.

3.2. Relative stability between ion-pair and hydrogen-bonded complexes in the gas phase

Another interesting point concerning ion-pair complexes is the difference in stability between ion-pair and non-ionic hydrogen-bonded forms. In order to get insight into this point the complexes IV and V,

which are the hydrogen-bonded forms of **II** and **III**, respectively, were investigated.
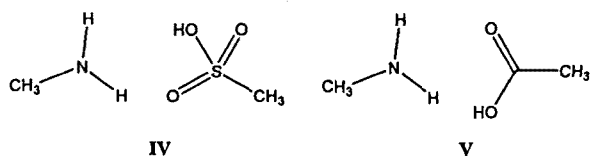

IV   V

Fig. 3 shows the geometries optimized at the HF/6-31 + G(d) level, where selected geometrical data are included. Table 4 lists the free energy difference between the ion-pair and hydrogen-bonded complexes. It is worth noting that the hydrogen-bonded forms are lower in energy than the corresponding ion-pair complexes. Moreover, **V** is significantly more stabilized with respect to **III** than **IV** with respect to **II**.

These results obtained for methylammonium–acetate and methylamine–acetic acid complexes are in satisfactory agreement with the values reported in the literature for related systems, even although our free energy difference is slightly overestimated due to the constraints imposed in the geometry optimiza-
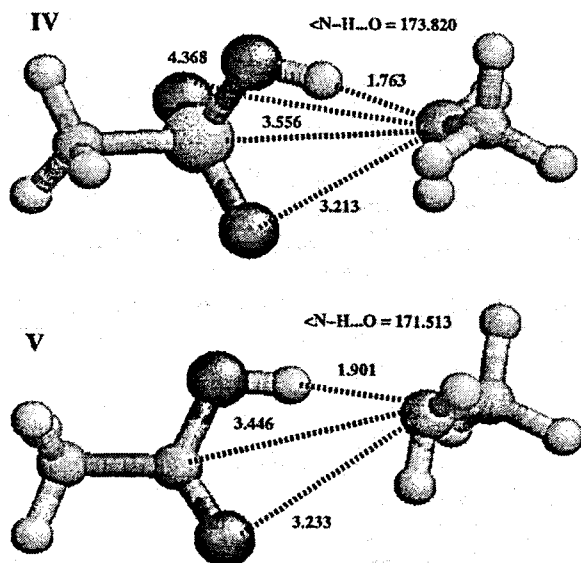
Fig. 3. Optimized geometries for the methylamine methylsulfuric acid (IV) and methylamine acetic acid (V) hydrogen-bonded complexes. Selected intermolecular parameters are displayed.

Table 4
Free energy differences (in kcal/mol) between the ion-pair and hydrogen-bonded complexes in the gas phase, aqueous solution and chloroform solution

Environment	II–IV	III–V
Gas phase[a]	1.0	17.6
Aqueous solution[b]	−21.8	−2.2
Chloroform solution[b]	−0.9	11.1

[a] The free energy difference in the gas phase was computed using the energies obtained at the MP2/6-31 + G(d) level and the thermodynamical corrections estimated at the HF/6-31 + G(d) level.

[b] The free energy difference in solution is obtained by adding the binding free energy difference in the gas phase to the difference between the free energies of solvation of the ion-pair and the non-ionic hydrogen-bonded complexes.

tion of **III**. Thus, the neutral formic acid–ammonia [9] and formic acid–trimethylamine [10] non-ionic complexes were estimated to be 11.3 and 7.0 kcal/mol favored with respect to the formate–ammonium and formate–trimethylammonium ion pairs, respectively, using very high levels of theory (up to QCISD(T)/6-311 + G(d,p) and MP4SDQ/6-311 + G(3df,2p), respectively). On the other hand, the methylguanidinium–acetate ion pair was predicted to be 1.7–8.3 kcal/mol less stable than the corresponding hydrogen-bonded complex at the MP2/6-31 + G(d) level [13].

3.3. Ion-pair complexes in aqueous and chloroform solutions

The free energies of solvation and the binding free energies in aqueous and chloroform solution for the ion pairs investigated are reported in Table 5. As expected, in all cases complexes are less solvated than isolated ions. This effect is mainly due to the partial annihilation of the net charges upon complexation. The formation of ion-pair complexes is strongly destabilized by the solvent in all cases, the destabilization being larger in water than in chloroform. Thus, the solvation of the isolated ions in bulk water is very favorable due to the strong electrostatic interactions between the solute and the solvent. The strength of these electrostatic interactions decreases with the dielectric constant of the solvent.

Table 5
Free energies of solvation (ΔG_{sol}; in kcal/mol) and binding free energies[a] (ΔG_{bind}; in kcal/mol) for the complexes investigated in aqueous and chloroform solutions

Complex	Aqueous solution		Chloroform solution	
	ΔG_{sol}	ΔG_{bind}	ΔG_{sol}	ΔG_{bind}
Ia	−31.2	26.0	−19.5	−3.4
Ib	−31.5	23.7	−19.9	−3.9
Ic	−31.6	23.1	−20.3	−3.4
Id	−32.0	25.8	−21.1	−2.3
II	−38.0	33.3	−19.2	−9.4
III	−25.5	41.1	−14.1	−6.7

[a] The binding free energy in solution was obtained by adding the binding free energy in the gas phase to the difference between the free energy of solvation of the complex and the separated ions.

The results indicate that the environment plays a crucial role to the binding free energy of ion-pair complexes. The complexation process is destabilized in aqueous solution for all the ion pairs investigated. Thus, the large energy penalty arising upon desolvation of the interacting ions is not counterbalanced by the gas-phase binding free energy. The binding free energy in aqueous solution of II and III is ~ 7–18 kcal/mol less favored than those of complexes I. Thus, the free energies of solvation of the ions are more favored for the former complexes since there are more polar groups accessible to the solvent. The destabilizing effect of chloroform, although less important than that of water, is still significant. Thus, the change in the free energy of solvation between the complex and the separated ions amounts to ~ 72–74, 86 and 93 kcal/mol for I, II and III, respectively. As a consequence, the binding of the ion-pair species in chloroform solution is stabilized by ~ 2–9 kcal/mol due to the favorable gas-phase contribution.

3.4. Relative stability between ion-pair and hydrogen-bonded complexes in aqueous and chloroform solutions

The free energy difference in aqueous and chloroform solutions between the ion-pair and non-ionic hydrogen-bonded complexes are displayed in Table 4. As it can be seen, the environment makes a decisive contribution to the relative stability of ionic

and hydrogen-bonded complexes. In the gas phase, the complexation process is greatly favored, and the hydrogen-bonded complex is more stable than the ion pair. However, water destabilizes the hydrogen-bonded complexes with respect to the ion pairs. However, as was discussed before the binding in aqueous solution is strongly unfavored (see Table 5). Accordingly, it can be concluded that water does not stabilize neither the ionic nor hydrogen-bonded complexes owing to the large energy penalty arising upon desolvation of the interacting monomers. The situation, nevertheless, is quite different in chloroform, where the binding of ionic species occurs. Moreover, the preference of the neutral complex over the ion pair is largely reduced or even reversed. Thus, the ion pair II is 0.9 kcal/mol favored with respect to IV whereas the neutral form V is ~ 11.1 kcal/mol more stable than III, the latter free energy difference being 5.5 kcal/mol lower than in the gas phase.

4. Summary

Gas-phase ab initio calculations show that the binding free energy of complexes formed by acetate anion and alkyltrimethylammonium cation ranges from −74.1 to −77.7 kcal/mol, depending on the size of the alkyl group. On the other hand, the binding free energy in the gas phase of methylammonium–methyl sulfate and methylammonium–acetate ion pairs is −95.4 and −100.2 kcal/mol, respectively. Accordingly, the strength of this stabilizing interaction decreases when the number and size of the alkyl groups increase. Calculations in aqueous solution reveal that the complexation process is unfavored for all the ion pairs investigated due to the large energy cost associated to the desolvation of the separated ions. This energy penalty is lower is chloroform, being partially compensated by the strong interaction between the ions. Accordingly, the assembly of the oppositely charged ions is favored in chloroform solution by ~ 2–9 kcal/mol.

The free energy differences between the ion-pair and the non-ionic hydrogen-bonded forms indicate that the latter are favored in the gas phase whereas the former are most stable in aqueous solution. Thus, a comparison of the results obtained in aqueous and

chloroform solutions shows how the stability of the ion pairs increases with the dielectric constant of the solvent. However, the binding process only occurs in solvents with a relative low dielectric constant due to the large energy penalty arising upon desolvation of the separated ions in polar solvents like water.

Acknowledgements

References

[1] D.J. Barlow, J.M. Thornton, J. Mol. Biol. 168 (1983) 867.

[2] J.F. Riordan, R.D. McElvany, C.L. Borders, Science 195 (1977) 884.

[3] B.E. Raumann, M.A. Rould, C.O. Pabo, R.T. Sauer, Nature (London) 367 (1994) 754.

[4] T.E. Schmirmer, P.R. Evans, Nature (London) 343 (1990) 140.

[5] D. Gandini, L. Gogioso, M. Bolognesi, D. Bordo, Proteins 24 (1996) 439.

[6] S. Marquesse, R.L. Baldwin, Proc. Natl. Acac. Sci. USA 84 (1987) 8898.

[7] O. Dym, M. Mevarech, J.L. Sussman, Science 267 (1995) 1344.

[8] A.R. Fersht, J. Mol. Biol. 64 (1972) 497.

[9] D. Heidrich, N.J.R. van Eikema Hommes, P. von Ragué Schleyer, J. Comput. Chem. 14 (1993) 1149.

[10] T. Liljefors, P.O. Norrby, J. Am. Chem. Soc. 119 (1997) 1052.

[11] X. Barril, C. Alemán, M. Orozco, F.J. Luque, Proteins: Struct. Funct. Genet. 32 (1998) 67.

[12] Z.S. Hendsh, B. Tidor, Prot. Sci. 3 (1994) 211.

[13] K.N. Bakeev, M.S. Yang, W.J. MacKnight, A.B. Zezin, V.A. Kabanov, Macromolcules 27 (1994) 300.

[14] H. Okuzaki, Y. Osada, Macromolecules 28 (1995) 380.

[15] M. Antonietti, J. Conrad, Angew. Chem., Int. Ed. Engl. 33 (1994) 1869.

[16] M. Antonietti, A. Kaul, A. Thünemann, Langmuir 11 (1995) 2633.

[17] A.V. Kabanov, V.G. Sergeev, M. Foster, V.A. Kasaikin, A.V. Levashov, V.A. Kabanov, Macromolecules 28 (1995) 3657.

[18] M. Antonietti, J. Conrad, A. Thünemann, Macromolecules 27 (1994) 6007.

[19] E.A. Ponomarenko, D.A. Tirrell, W.J. MacKnight, Macromolecules 29 (1996) 8751.

[20] G.H. Fredickson, Macromolecules 26 (1993) 2825.

[21] J. Watanabe, H. Ono, I. Uematsu, A. Abe, Macromolecules 18 (1985) 2141.

[22] M.J. Frisch, J.A. Pople, J.S. Binkley, J. Chem. Phys. 80 (1984) 3265.

[23] A.D. Becke, J. Chem. Phys. 98 (1993) 1372.

[24] P.J. Stephens, F.J. Devlin, C.F. Chabalowski, M.J. Frisch, J. Phys. Chem. 98 (1994) 1623.

[25] S.F. Boys, F. Bernardi, Mol. Phys. 19 (1970) 553.

[26] M.J. Frisch, et al., GAUSSIAN-94, Revision B3, Gaussian, Inc., Pittsburgh, PA, 1995.

[27] D. Heidrich, M. Ruckert, H.-J. Köhler, Chem. Phys. Lett. 136 (1987) 13.

[28] M. Orozco, F.J. Luque, Chem. Phys. 182 (1994) 237.

[29] F.J. Luque, Y. Zhang, C. Alemán, M. Bach, J. Gao, M. Orozco, J. Phys. Chem. 100 (1996) 4269.

[30] S. Miertus, E. Scrocco, J. Tomasi, Chem. Phys. 55 (1981) 117.

[31] J.J.P. Stewart, MOPAC93 Revision 2; Fujitsu 1993. Adapted to perform MST calculations by F.J. Luque, M. Orozco.

VI.6. "Binding in Complex Ionic Systems: Anticooperative Effects in Systems Stabilized by Electrostatic Interactions"

Alemán, C.; Zanuy, D. *Chem. Phys. Lett.*

Binding in Complex Ionic Systems:

Anticooperative Effects in Systems

Stabilized by Electrostatic Interactions

Carlos Alemán[*] and David Zanuy

Departament d'Enginyeria Química, E.T.S. d'Enginyers Industrials de
Barcelona, Diagonal 647, Barcelona E-08028, Spain. Fax: 34-93-4016600.
E-mail: aleman@eq.uc.es

1

ABSTRACT

We compute the binding energies of complexes involving more than two molecular ions. More specifically, complexes constituted by acetate anions and either tetramethylammonium or sodium cations have been considered. Calculations have been performed at the ab initio HF and MP2 levels using the 6-31+G(d) basis set. Solvation effects have been represented by a continuum reaction field procedure.

INTRODUCTION

Salt bridges are among the more thoroughly investigated interactions in protein chemistry due to the important and often quite specific functions played by ion pairs [1-4]. For the last decade the interest in ion-pair interactions has been extended to materials science. Thus, remarkable advances in noncovalent chemistry have led to design new materials consisting of charged polymer chains (polyelectrolytes) and oppositely charged small amphiphilic molecules (surfactants) [5-14]. These complexes tend to form self-assembled supramolecular structures that may exhibit interesting properties like formation of liquid crystalline phases, stable porous and selective membranes [10,11].

Most work in this area has been concerned with biopolymers, which can form a variety of highly ordered secondary structures [5,12,13]. Polypeptides offer advantages in the development of polymer-surfactant complexes since the properties of the systems may be manipulated by controlling the polymer chain conformation, i.e. by solvent or temperature. Complexes formed by synthetic sodium poly(α,L-glutamate) and the oppositely charged alkyltrimethylammonium surfactants are among the most well-studied and important polypeptide-surfactant complexes (Scheme I) [5].

Scheme I

3
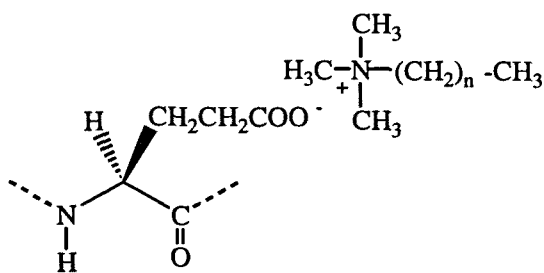
In these materials surfactant chains are electrostatically attached to the polypeptide α-helices, the whole system being organized in a lamellar structure with layers of the polypeptide chains separated by bimolecular layers of surfactant (Scheme II).
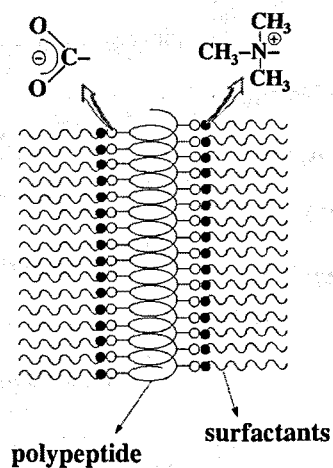
Scheme II

The electrostatic interactions between the carboxylate anions and the alkyltrimethylammonium cations involved in self-assembled complexes derived from polypeptides have been recently investigated using quantum mechanical calculations [15]. Thus, the quantum mechanical binding energy was evaluated at the MP2/6-31+G(d)//HF/6-31+G(d) level for a set of four bimolecular complexes: $CH_3COO^-...^+NR(CH_3)_3$, where R= $-CH_3$, $-CH_2-CH_3$, $-(CH_2)_2-CH_3$ and $-(CH_2)_3-CH_3$. Results indicated that the strength of the electrostatic interaction slowly drops when the size of the alkyl group R increases. However, some aspects concerning the interaction between the polypeptide and the surfactant remain unknown yet.

4

The aim of this letter is to gain more insight into the electrostatic interaction characteristic of polypeptide-surfactant complexes using quantum mechanical calculations. For this purpose, we have examined the strength of this interaction considering complexes constituted by more than two molecular ions. Furthermore, we have investigated the changes introduced in the binding energies when alkyltrimethylammonium cations are replaced by metal cations. A special attention has been given to the analysis of the cooperative effects, the results obtained for the electrostatic interactions being compared with those recently provided by weaker interactions like the hydrogen bond [16]. Finally, we have investigated the influence of the solvent on both the binding energy and cooperative effects. Thus, calculations in both aqueous and chloroform solution have been performed using a self consistent reaction field (SCRF) procedure.

METHODS

All ab initio molecular orbital calculations were carried out using the Gaussian-98 suite of programs [17]. Eight different complexes were considered in the present work to model electrostatic interactions: $CH_3COO^-...^+N(CH_3)_4$ (**Ia**), $CH_3COO^-...^+Na$ (**IIa**), $CH_3COO^-...^+N(CH_3)_4...CH_3COO^-$ (**Ib**), $CH_3COO^-...^+Na...CH_3COO^-$ (**IIb**), $N(CH_3)_4^+...CH_3COO^-...^+N(CH_3)_4$ (**Ic**), $Na^+...CH_3COO^-...^+Na$ (**IIc**), $CH_3COO^-...^+N(CH_3)_4...CH_3COO^-...^+N(CH_3)_4$ (**Id**) and $CH_3COO^-...^+Na...CH_3COO^-...^+Na$ (**IId**). Geometries of all these complexes were fully optimized in the gas-phase at the HF/6-31+G(d) level [18]. The starting points for geometry optimizations are schematically described in Figure 1. As can be seen, three different arrangements were used as starting points for the calculations of complexes involving three molecular ions (**Ib,**

5

IIb, Ic and **IIc**), whereas only one arrangement was considered for complexes with two and four molecular ions (**Ia, IIa, Id** and **IId**). It is worth noting that all these arrangements can be classified as types **A** and **B** (Figure 1). In type **A** the anions are placed at the positions expected for the carboxylate groups in an α-helix of the polypeptide-surfactant complexes and the cations were arranged in front of them (see Scheme II), while in type **B** the ions of opposite sign are aligned. Single point calculations on the HF/6-31+G(d) optimized complexes were performed at the MP2/6-31+G(d) level. Basis set superposition errors (BSSE) were calculated using the counterpoise method [19].

The quantum mechanical binding energy for a given complex, $\Delta E_{b(QM)}$, was computed as the difference between the energy of the complex and the sum of the energies calculated for the molecular ions (eq. 1):

$$\Delta E_{b(QM)} = E(\text{complex}) - \Sigma\, E(\text{monomers})$$

(1)

The cooperative energy, ΔE_{coop}, for the complexes containing three or more molecular ions was estimated as the difference between the quantum mechanical and the expected binding energies (eq 2). The expected binding energy, $\Delta E_{b(E)}$, was supplied by the sum of the quantum mechanical binding energies of all the dimers contained in the complex (eq 3). Accordingly, ΔE_{coop} provides an evaluation of the many-body (nonadditive) effects.

$$\Delta E_{coop} = \Delta E_{b(QM)} - \Delta E_{b(E)}$$

(2)

$$\Delta E_{b(E)} = \Sigma_{dimers}\, \Delta E_{b(QM)}$$

(3)

6

SCRF calculations were performed to incorporate the solvent effects in the complexation process. The free energy of solvation (ΔG_{sol}) in aqueous and chloroform solutions were determined using the AM1 version [20,21] of the polarizable continuum model formulated by Miertus, Scrocco and Tomasi (MST) [22]. In the MST/AM1 method the ΔG_{sol} is given by the addition of electrostatic and steric contributions (eq 4), where the latter term was computed as the sum of cavitation and van der Waals terms.

$$\Delta G_{sol} = \Delta G_{ele} + \Delta G_{cav} + \Delta G_{vdW}$$

(4)

The cavitation term, which provides the work required to build the solute cavity, was determined using Pierotti´s scaled particle theory [23]. The van der Waals term was evaluated by means of an optimized linear relationship with the atomic surface area [20,21]. The electrostatic term, which represents the interaction between the charge distribution of the solute and the reaction field generated by the solute in the solvent, was computed using the MST-SCRF method.

The solute/solvent cavity was determined using a molecular shape algorithm [20,21]. In all calculations ab initio gas-phase geometries were used. Thus, the change in the molecular geometry upon solvation has a negligible effect on the thermodynamic parameters [24,25]. Calculations in solution were carried out using a modified version of the MOPAC program [26].

RESULTS AND DISCUSSION

Complexes constituted by acetate and tetramethylammonium ions in the gas-phase. The optimized structures and selected geometrical data of complexes **Ia**, **Ib**, **Ic** and **Id** are shown in Figure 2. As can be seen only a single minimum was found for complexes **Ib** and **Ic**. Thus, for each of these complexes geometry optimizations at the HF/6-31+G(d) level of the three starting arrangements displayed in Figure 1 converge to the same structure.

Minimum energy structures of complexes **Ia**, **Ib** and **Id** indicate that cations tend to form the maximum number of interactions with the surrounding anions. Moreover, in **Ib** and **Id** the anions are asymmetrically arranged with respect to the cations, which is mainly originated by a delicate balance between the repulsive and attractive interactions. Conversely, the minimum energy structure of complex **Ic** is almost symmetric. In this case the tetramethylammonium cations, which can be viewed as simple spheres, are located at the same distance of the acetate oxygen atoms and forming an angle of 132° with the carboxylate group. Interestingly, some trends are suggested by the present results for the electrostatic interactions involved in polypeptide-surfactant complexes: i) each surfactant is preferentially bounded to more than one carboxylate group; ii) the arrangement of the carboxylate groups along the polypeptide chain is not regular; and iii) the position of the surfactants when assemble with the polypeptide chain is strongly influenced by the repulsive interaction among ions of the same sing.

The quantum mechanical binding energies (eq 1) for complexes **Ia**, **Ib**, **Ic** and **Id** are given in Table 1. As expected, the strength of the binding increases with the number of molecular ions involved in the complex, the binding energy estimated at the MP2/6-31+G(d)//HF/6-31+G(d) level being favored for **Id** with respect to **Ib** and **Ic** by 75.9 and 77.4 kcal/mol,

8

respectively. It is worth noting that such difference drops to 31.9 and 30.4 kcal/mol when complex **Ia** is compared with **Ib** and **Ic**, respectively. Comparison between quantum mechanical binding energies estimated at the HF/6-31+G(d)//HF/6-31+G(d) and MP2/6-31+G(d)//HF/6-31+G(d) levels indicates that electron correlation contributions are non-negligible. The largest difference was obtained for complex **Id**, being 5.2 kcal/mol. It should be mentioned that in our previous work about ion-pairs [15], we found that the 6-31+G(d) is a suitable basis set to investigate the electrostatic interactions found in polyelectrolite-surfactant complexes.

The expected binding energies (eq 3) for complexes **Ib**, **Ic** and **Id** are listed in Table 2. It is worth noting that for the three complexes the $\Delta E_{b(E)}$ is more negative than the $\Delta E_{b(QM)}$. The difference between the two values, which provides an estimation of the cooperative effects in these complexes (eq 4), is also displayed in Table 2. The ΔE_{coop} values range from 9.5 to 10.7 kcal/mol at the MP2/6-31+G(d)//HF/6-31+G(d) level. As can be seen, HF and MP2 calculations provide similar ΔE_{coop} values, the difference between them being 0.4, 0.5 and 1.6 kcal/mol for complexes **Ib**, **Ic** and **Id**, respectively.

The values listed in Table 2 indicate that the binding provided by quantum mechanical calculations is weaker than that derived from the addition of intermolecular interactions. This means that the strength of the intermolecular electrostatic interactions is not enhanced upon increasing the number of ions in the complex. Thus, many body effects are clearly repulsive indicating that intermolecular electrostatic interactions are anticooperative. However, the magnitude of these destabilizing effects in polypeptide-surfactant complexes will be modulated by several factors like

the topology of the chains, the spatial arrangement of the charged groups and the influence of the immediate surrounding.

A comparison between many-body effects predicted for electrostatic and hydrogen bonding interactions from quantum mechanical calculations reveals a completely different behavior. Thus, formation of hydrogen bonding networks is more favorable than formation of isolated hydrogen bonds [16]. The ΔE_{coop} values predicted from DFT calculations for formate...(N-methylformamide)$_n$ model complexes, in which the monomers are linearly arranged, amount to -5.6, -9.5 and -12.5 for $n = 2$, 3 and 4, respectively [16]. These results clearly indicate that hydrogen bond is a cooperative interaction, this feature being indeed detected by experimental observations [27,28].

Complexes constituted by acetate and sodium ions in the gas-phase. The starting arrangements for geometry optimization of complexes **IIa-IId** were those displayed in Figure 1. The minimum energy structures obtained for the four complexes are shown in Figure 3. As was also found for complexes **Ib** and **Ic**, geometry optimizations of the three arrangements displayed in Figure 1 for complexes **IIb** and **IIc** converge to an unique minimum.

In all cases metal cations are symmetrically arranged with respect to the anions, the distance between the sodium cation and the oxygen atoms of the carboxylate group ranging from 2.052 to 2.408 Å. Furthermore, each cation tends to interact with the maximum number of oxygen atoms. This is especially remarkable in complexes **IIb** and **IId**, in which cations simultaneously interact with four and three oxygen atoms, respectively.

10

Table 1 lists the quantum mechanical binding energies for complexes **IIa**, **IIb**, **IIc** and **IId**. Results indicate that the binding is much more attractive (about 40-60%) for complexes involving metal cations than for those containing tetramethylammonium cations. Thus, the binding energy for complex **IIa** is 52.9 and 45.3 kcal/mol more favorable than for **Ia** at the HF/6-31+G(d)//HF/6-31+G(d) and MP2/6-31+G(d)//HF/6-31+G(d) levels, respectively. This difference is because the positive charge is more concentrated in the sodium cation than in the tetramethylammonium cation. On the other hand, the expected binding energies for complexes **IIb**, **IIc** and **IId** (Table 2) are more attractive than those predicted from quantum mechanical calculations. Thus, anticooperative energy effects are also obtained in the strong electrostatic interactions involved in such complexes.

Complexes constituted by acetate and tetramethylammonium ions in aqueous and chloroform solution. The free energies of solvation (ΔG_{sol}), the changes in the free energies of solvation upon complexation ($\Delta\Delta G_{sol}$) and the quantum mechanical binding energies in aqueous and chloroform solution for complexes **Ia-Id** are listed in Tables 3 and 4, respectively. As expected the $\Delta\Delta G_{sol}$ values are positive in all cases indicating that the complexes are less well solvated than their corresponding isolated monomers. Thus, the net charges are partially annihilated upon complexation. The destabilizaton of the complexes is larger in aqueous solution than in chloroform solution by about 40%. This is because the strength of the electrostatic interactions between the ions and the solvent increases very rapidly with the dielectric constant of the solvent.

The quantum mechanical binding energies in aqueous and chloroform solutions ($\Delta G_{b,aq(QM)}$ and ($\Delta G_{b,chl(QM)}$, respectively) for complexes **Ia-Id** were estimated by adding the quantum mechanical binding energies obtained in

11

the gas-phase at the MP2/6-31+G(d)//HF/6-31+G(d) level (Table 1) to the corresponding $\Delta\Delta G_{sol}$ values. Results have been included in Tables 3 and 4. As can be seen the environment plays a crucial role to the binding free energy of the four complexes. The complexation processes are favored in chloroform solution but the strength of the bindings is about 72-76% weaker than in the gas-phase. Moreover, the complexation process is destabilized in aqueous solution for complexes **Ia** and **Id** by 6.3 and 11.2 kcal/mol, respectively, being slightly favored for complexes **Ib** and **Ic** (0.6 and 6.0 kcal/mol, respectively). Thus, the large energy penalty arising upon desolvation of the interacting ions in aqueous solution is not compensated by the gas-phase contribution.

Unfortunately, SCRF calculations on complexes **IIa-IId** were not possible. This is because there are not suitable parameters to evaluate the van der Waals and cavitation contributions to ΔG_{sol} for sodium cation [20,21]. However, a more drastic influence of the environment is expected for these complexes. Thus, the energy penalty arising upon desolvation of the sodium cation is expected to be larger than that obtained for the tetramethylammonium cation since the charge is more localised in the former.

SUMMARY

Quantum mechanical calculations have been performed on eight complexes constituted by acetate anions and either tetramethylammonium or sodium cations. Results have allowed to characterize the effect of the number of molecular ions contained in the system on the complexation process considering different surrounding environments. As expected the binding

energy becomes more favorable when the number of molecular ions involved in the complex increases. However, such stabilization is lower than that predicted by the addition of the binding energies associated to all the pairs contained in the complexes. Thus, the intermolecular electrostatic interactions characteristic of complexes constituted by more than three molecular ions are clearly anticooperative. On the other hand, a comparison of the results obtained in gas-phase, chloroform solution and aqueous solution shows how the binding decreases with the dielectric constant of the environment.

ACKNOWLEDGEMENTS

REFERENCES

[1] D. J. Barlow, J. M. Thornton, J. Mol. Biol. 168 (1983) 867.

[2] X. Barril, C. Alemán, M. Orozco, F.J. Luque, Proteins 32 (1998) 67.

[3] J. Zuegg, J. E. Greedy, Biochemistry 38 (1999) 13862.

[4] P. Strop, S. L. Mayo, Biochemistry 39 (2000) 1251.

[5] W. J. Macknight, E. A. Ponomarenko, D. A. Tirrell, Acc. Chem. Res. 31 (1998) 781.

[6] G. Mao, T. Tsao, M. Tirrell, T.H. Davis, V. Hessel, H. Ringsdorf, Langmuir 9 (1993) 3461.

[7] S. Ujiie, K. Iimura, Macromolecules 25 (1992) 3174.

[8] C. G. Bazuin, F. A. Brandys, T.M. Eve, M. Plante, Macromol. Sym. 84 (1994) 183.

[9] A. Matsumoto, T. Odani, K. Sada, M. Miyata, K. Tashiro, Nature 405 (2000) 328.

[10] G. H. Fredickson, Macromolecules 26 (1993) 2825.

[11] Y. Cao; P. Smith, Polymer 34 (1993) 3139.

[12] E. A. Ponomarenko, A. J. Waddon, D. A. Tirrell, W.J. Macknight, Langmuir 12 (1996) 2169.

[13] E. A. Ponomarenko, A. J. Waddon, K. N Bakeev, D. A. Tirrell, W. J. MacKnight, Macromolecules 29 (1996) 4340.

[14] K. P. Pemawansa, A. Thakur, E. K. Karikari, I. M. Khan, Macromolecules 32 (1999) 1910.

[15] C. Alemán, D. Zanuy Chem. Phys. Lett. 319 (2000) 318.

[16] H. Guo; N. Gresh, B. P. Roques; D. R. Salahub J. Phys. Chem. B 104 (2000) 9746.

[17] Gaussian 98, Revision A.7, Frisch, M. J.; Trucks, G. W.; Schlegel, H. B.; Scuseria, G. E.; Robb, M. A.; Cheeseman, J. R.; Zakrzewski, V. G.; Montgomery, Jr.; Stratmann, R. E.; Burant, J. C.; Dapprich, S.; Millam, J.

M.; Daniels, A. D.; Kudin, K. N.; Strain, M. C.; Farkas, O.; Tomasi, J.; Barone, V.; Cossi, M.; Cammi, R.; Mennucci, B.; Pomelli, C.; Adamo, C.; Clifford, S.; Ochterski, J.; Petersson, G. A.; Ayala, P. Y.; Cui, Q.; Morokuma, K.; Malick, D. K.; Rabuck, A. D.; Raghavachari, K.; Foresman, J. B.; Cioslowski, J.; Ortiz, J. V.; Baboul, A. G.; Stefanov, B. B.; Liu, G.; Liashenko, A.; Piskorz, P.; Komaromi, I.; Gomperts, R.; Martin, R. L.; Fox, D. J.; Keith, T.; Al-Laham, M.A.; Peng, C. Y.; Nanayakkara, A.; Gonzalez, C.; Challacombe, M.; Gill, P. M. W.; Johnson, B.; Chen, W.; Wong, M. W.; Andres, J. L.; Gonzalez, C; Head-Gordon, M.; Replogle, E. S.; Pople, J. A., Gaussian, Inc., Pittsburgh PA, 1998.

[18] M. J. Frisch, J. A. Pople, J. S. Binkley, J. Chem. Phys. 80 (1984) 3265.

[19] S. F. Boys, F. Bernardi, Mol. Phys. 19 (1970) 553.

[20] M. Orozco, F. J. Luque, Chem. Phys. 182 (1994) 237.

[21] F. J. Luque, Y. Zhang, C. Alemán, M. Bach, J. Gao, M. Orozco, J. Phys. Chem. 100 (1996) 4269.

[22] S. Miertis, E. Scrocco, J. Tomasi, Chem. Phys. 55 (1981) 117.

[23] R. A. Pierotti, Chem. Rev. 76 (1976) 717.

[24] C. Alemán, E. Navarro, J. Puiggalí, J. Org. Chem. 60 (1995) 6135.

[25] G. D. Hawkins, C. J. Cramer, D. G. Truhlar, J. Phys. Chem. B 102 (1998) 3257.

[26] J. J. P. Stewart, MOPAC 93 Revision 2; Stewart Comp. Chem. 1994. Adapted to perform MST calculations by F. J. Luque and M. Orozco.

[27] I. M. Klotz, J. S. Franzen, J. Am. Chem. Soc. 84 (1962) 3461.

[28] B. W. Gung, Z. Zhu, B. Everingham, J. Am. Chem. Soc. 62 (1997) 3436.

Table 1

Energy (E; in a.u.) and quantum mechanical binding energy ($\Delta E_{b(QM)}$; in kcal/mol) calculated in the gas-phase for the investigated complexes[a].

Complex	E	$\Delta E_{b(QM)}$	E	$\Delta E_{b(QM)}$
	HF/6-31+G(d)	HF/6-31+G(d)	MP2/6-31+G(d)	MP2/6-31+G(d)
Ia	-440.086779	-95.6	-441.419566	-97.4
Ib	-667.385034	-126.0	-669.353042	-129.3
Ic	-652.820099	-124.8	-654.850602	-127.8
Id	-880.187835	-200.0	-882.858177	-205.2
IIa	-389.143463	-148.5	-389.768639	-142.7
IIb	-616.471906	-197.1	-617.726063	-188.6
IIc	-550.871669	-190.5	-551.491845	-182.4
IId	-778.357335	-340.6	-779.604549	-325.8

[a] Geometries calculated at the HF/6-31+G(d) level.

Table 2.

Expected binding energy ($\Delta E_{b(E)}$; in kcal/mol) and cooperative energies (ΔE_{coop}; in kcal/mol) calculated in the gas-phase for the investigated complexes[a]

Complex	$\Delta E_{b(E)}$ HF/6-31+G(d)	$\Delta E_{b(E)}$ MP2/6-31+G(d)	ΔE_{coop} HF/6-31+G(d)	ΔE_{coop} MP2/6-31+G(d)
Ib	-136.3	-140.0	10.3	10.7
Ic	-134.2	-137.6	9.3	9.8
Id	-211.1	-214.7	11.1	9.5
IIb	-211.1	-206.5	14.0	17.9
IIc	-199.2	-192.8	8.8	10.4
IId	-342.5	-332.8	1.9	7.0

[a] Geometries calculated at the HF/6-31+G(d) level.

Table 3

Free energy of solvation (ΔG_{sol}; in kcal/mol), change in the free energy of solvation upon complexation[a] ($\Delta\Delta G_{sol}$; in kcal/mol) and quantum mechanical binding energy[b] ($\Delta G_{b,aq(QM)}$; in kcal/mol) in aqueous solution for the complexes constituted by acetate and tetramethylammonium ions[c].

Complex	ΔG_{sol}	$\Delta\Delta G_{sol}$	$\Delta G_{b,aq(QM)}$
Ia	-31.2	103.7	6.3
Ib	-91.0	128.7	-0.6
Ic	-63.2	121.8	-6.0
Id	-53.4	216.4	11.2

[a] Determined as the difference between the free energy of solvation of the complex and the free energies of solvation of the corresponding monomers.

[b] Estimated from addition of the change in the free energy of solvation upon complexation to the quantum mechanical binding energy determined in the gas-phase at the MP2/6-31+G(d)//HF/6-31+G(d) level.

[c] Geometries calculated at the HF/6-31+G(d) level.

Table 4

Free energy of solvation (ΔG_{sol}; in kcal/mol), change in the free energy of solvation upon complexation[a] ($\Delta\Delta G_{sol}$; in kcal/mol) and quantum mechanical binding energy[b] ($\Delta G_{b,chl(QM)}$; in kcal/mol) in chloroform solution for the complexes constituted by acetate and tetramethylammonium ions[c].

Complex	ΔG_{sol}	$\Delta\Delta G_{sol}$	$\Delta G_{b,chl(QM)}$
Ia	-19.5	74.3	-23.1
Ib	-53.0	94.1	-35.2
Ic	-43.1	91.4	-36.4
Id	-35.4	152.2	-53.0

[a] Determined as the difference between the free energy of solvation of the complex and the free energies of solvation of the corresponding monomers.

[b] Estimated from addition of the change in the free energy of solvation upon complexation to the quantum mechanical binding energy determined in the gas-phase at the MP2/6-31+G(d)//HF/6-31+G(d) level.

[c] Geometries calculated at the HF/6-31+G(d) level.

CAPTIONS TO FIGURES

Figure 1. Starting points for geometry optimizations of complexes containing two, three and four molecular ions. Circles and cylinders represent molecular ions of different sign. Type **A** refer to the arrangements in which anions are placed at the positions expected for the carboxylate groups on the α-helix of polypeptide-surfactant complexes and cations are placed in front of the anions (see Scheme II). Type **B** refer to the arrangements in which the ions of different sign are aligned.

Figure 2. Optimized geometries for the complexes **Ia**, **Ib**, **Ic** and **Id**. Selected intermolecular parameters are displayed (in Å).

Figure 3. Optimized geometries for the complexes **IIa**, **IIb**, **IIc** and **IId**. Selected intermolecular parameters are displayed (in Å).

B

Ia, IIa

A   A   B

Ib, IIb,
IIc, IIc

A

Id, IId
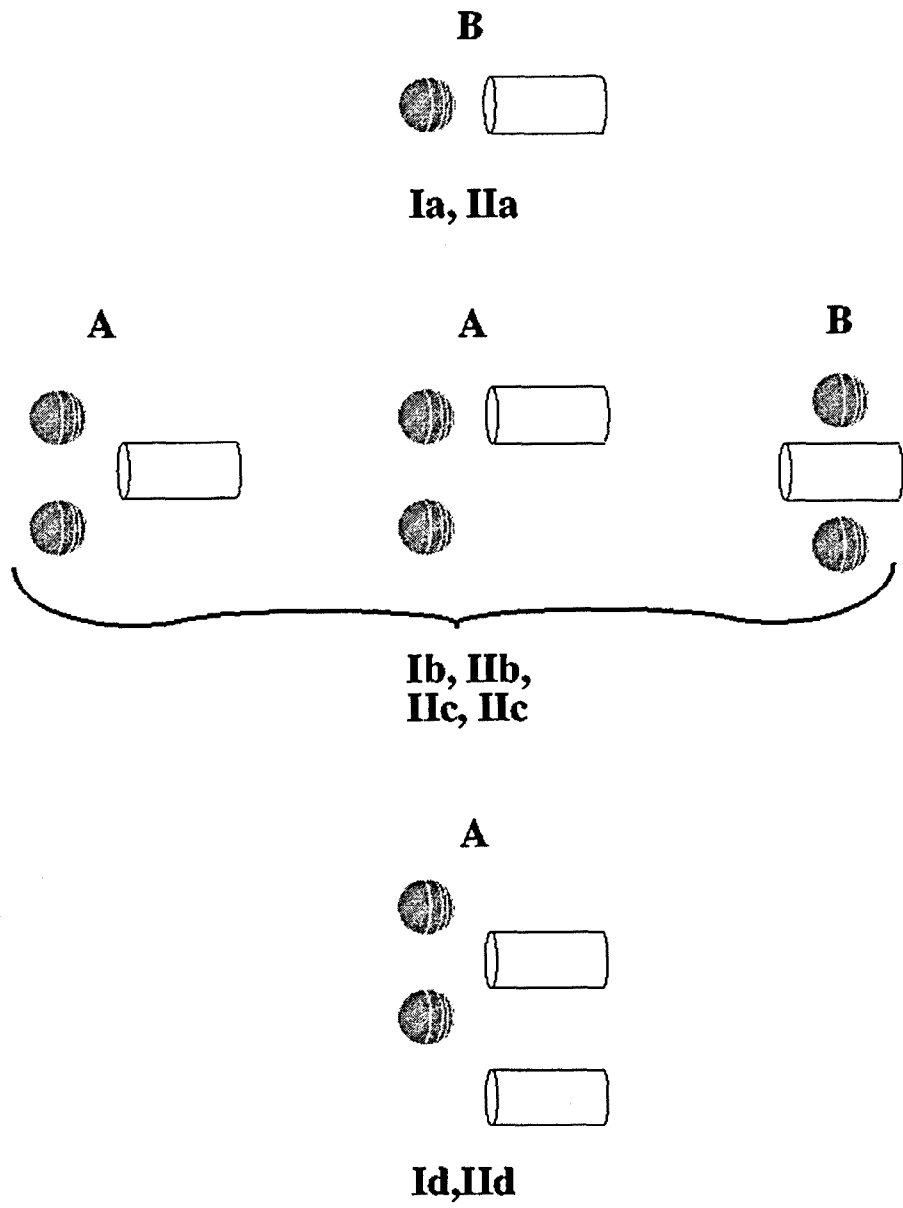
Fig.1. Alemán and Zanuy
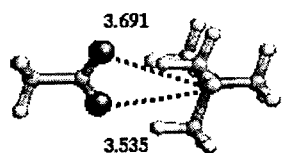
Ia
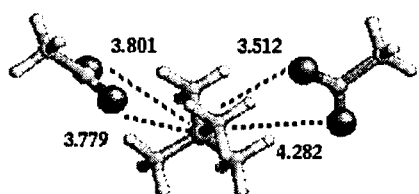
Ib
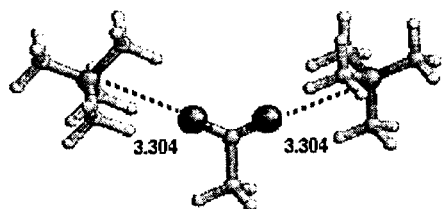
Ic
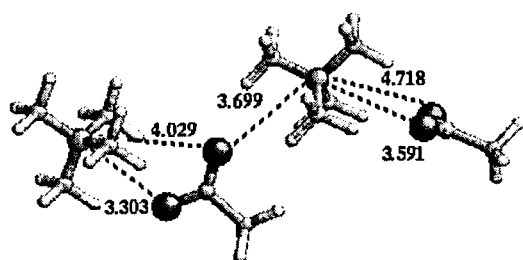
Id

Fig.2. Alemán and Zanuy

IIa
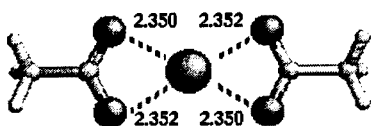
IIb
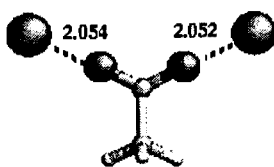
IIc
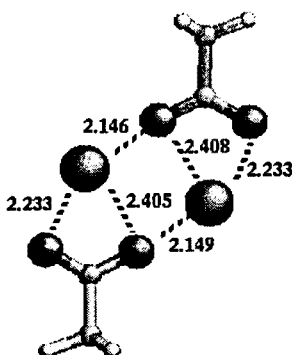
IId

Fig.3. Alemán and Zanuy

VI.7. "A Molecular Dynamics Study in Chloroform Solution of the Stoichiometric Complex Formed by Poly(α,L-glutamate) and Octyltrimethylammonium"

Zanuy D.; Alemán C.; Muñoz-Guerra, S. *Biopolymers*

A Molecular Dynamics Study in Chloroform Solution of the Stoichiometric Complex Formed by Poly(α,L-glutamate) and Octyltrimethylammonium Ions

David Zanuy, Carlos Alemán[*] and Sebastián Muñoz-Guerra

Departament d'Enginyeria Química, E. T. S. d'Enginyers Industrials de Barcelona, Universitat Politècnica de Catalunya, Diagonal 647, Barcelona E-08028, Spain

Corresponding author: aleman@eq.upc.es

1

ABSTRACT

We present a molecular dynamics simulation at 300 K in explicit solvent environment of chloroform of the stoichiometric complex formed by poly(α,L-glutamate) and octyltrimethylammonium ions. We observed that the α-helix conformation of the polypeptide chain remains stable during a 2-ns run. The surfactant ions predominantly adopted an extended conformation that is stabilized by favorable interactions with the organic solvent. Analysis of the organization of the surfactant with respect to the polypeptide chain indicated that each octyltrimethylammonium cation was preferentially bound to more than one carboxylate group. It was found that the most populated arrangement was that with the surfactant cations interacting with two carboxylate groups simultaneously.

INTRODUCTION

For the last decade complexes consisting of polyelectrolytes and oppositely charged surfactants have attracted considerable interest in polymer science.[1-3] Such complexes form spontaneously when dilute aqueous solutions of the two components are mixed.[1] The driving forces for the formation of such complexes are the electrostatic interactions between polyion chain units and oppositely charged surfactant ions and the hydrophobic interactions of the surfactant alkyl chains in water. If equimolar amounts of polyion chain units and surfactant molecules are mixed, stoichiometric complexes are formed. These complexes are insoluble in water but can be dissolved in some common organic solvents of low polarity without dissociation.[4-6] The simplicity of synthesis of stoichiometric polyelectrolyte-surfactant complexes as well as their solubility in nonaqueous solvents have increased the interest in this area.[1,7,8] As a consequence, the understanding of both the influence of the surfactant on the polyelectrolite conformation and the effect of the polyelectrolite chain on the organization of the surfactant is highly desirable.

Complexes consisting of poly(α,L-glutamate) and oppositely charged amphiphilic molecules bearing aliphatic chains (Scheme 1) are among the more interesting water-insoluble complexes.[1,5,7,9-12] This is because polymer-surfactant complexes derived from polypeptides may offer materials with very useful properties, especially those related with the secondary structure of the polypeptide. Poly(α,L-glutamic acid) adopts an

α-helix conformation stabilized by intramolecular hydrogen bonds between the CO of amide *i* and the NH of amide *i+3*.[13,14] This conformation seems to be retained by poly(α,L-glutamate) when complexed with surfactant cations.[1] Therefore, conformational changes, *i.e.* formation or disruption of intramolecular hydrogen bonds, induced by either solvent or temperature, may allow control of the related material properties.
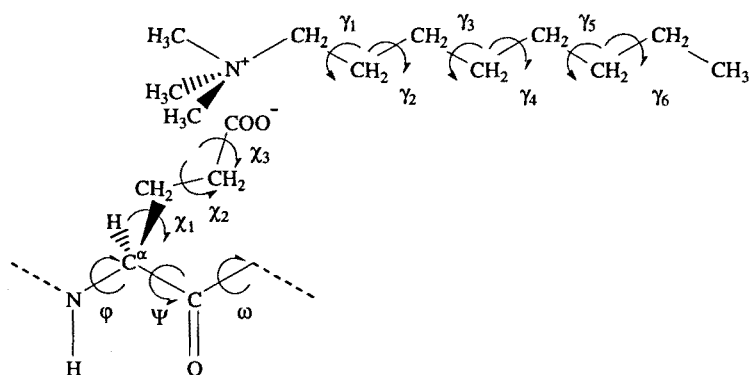
Scheme 1

The electrostatic interactions involved in poly(α,L-glutamate)-alkyltrimethylammonium complexes have been exhaustively investigated using sophisticated ab initio quantum mechanical calculations.[15,16] Thus, a wide number of small model systems were considered to analyze the more relevant features of this interaction. Results indicated that the strength of the electrostatic interaction slowly drops when the size of the alkyl group increases. On the other hand, calculations in small model systems consisting of more than two molecular ions, *i.e.* $N(CH_3)_4^+...CH3COO^-... N(CH_3)_4^+$,

4

CH3COO⁻...   N(CH₃)₄⁺...CH3COO⁻   and   N(CH₃)₄⁺...CH3COO⁻

...N(CH₃)₄... CH3COO⁻, revealed that the interaction characteristic of polypeptide-surfactant complexes is "*anticooperative*", *i.e.* the binding energy computed for a system containing n molecular ions is higher than that derived from the sum of the corresponding ion-pair binding energies.

An atomistic description of the structure of poly(α,L-glutamate)-alkyltrimethylammonium complexes has not been reported so far. In this work, we present a molecular dynamics (MD) simulation study on the structure of poly(α,L-glutamate)-octyltrimethylammonium complex, abbreviated 8ATMA·PAGA, in a dilute chloroform solution. By a computational efficiency reason we have concentrated our efforts on complexes formed with octyltrimethylammonium cations, even although complexes with longer surfactants (up to 18 carbon atoms[1]) have been reported. The simulation has provided structural information about both the *conformation of the polypeptide* and *the structure of the octyltrimethylammonium ions.*

METHODS

Molecular Model. MD simulations have been run on a stoichiometric complex of 8ATMA·PAGA. This is constituted by a polypeptide chain of 20 residues and blocked at the N-terminus with an acetyl group and at the C-terminus with a *N*-methylamide group. The initial set of atomic coordinates for 8ATMA·PAGA were generated according to our previous studies on

related systems. Thus, the α-helix conformation recently modeled for the poly(α,L-glutamic acid)[13] was assumed for the polyanion chain in the complex. The torsional angles used to generate such structure were $\varphi = -64.7°$, $\psi = -36.9°$, $\omega = 177.1°$ and $\chi_1 = -67.8°$. On the other hand, each surfactant molecule was initially arranged with the cation counterpart facing one carboxylate group. Finally, the octyl chains were arranged in all-*trans*. Figure 1 shows the molecular geometry of 8ATMA·PAGA used as starting point in MD simulations.

Electrostatic Interactions. In this study it is particularly relevant to assess the quality of the force-field used in MD simulations. Thus, such force-field should provide a good description of the electrostatic interactions between the surfactant cations and the polyanion, which have not been previously investigated using classical methods. For this purpose, we have computed the classical binding energies for a set of seven model complexes, the results being compared with those previously calculated using quantum mechanical methods at the HF/6-31+G(d) and MP2/6-31+G(d) levels.[15,16]

Classical energies have been computed with the Amber force-field[17] considering the molecular geometries obtained from HF/6-31+G(d) optimizations.[15,16] All the force-field parameters with exception of the atomic charges were taken from Amber libraries.[17] Clearly the value of the present study will depend upon the quality of the atomic charges used. The charges must give a description of the electrostatic properties of the system as accurate as is possible within a monopole approximation and they must

6

also be assigned in a manner compatible with the other elements of the force-field. In this work we have used molecular electrostatic potentials (MEPs) derived at the HF/6-31G(d)[18] level for the generation of atom-centered charges.

The seven complexes considered in the analysis are displayed in Table 1, which also lists the classical and quantum mechanical binding energies for each complex. Results show that force-field calculations work very well for the electrostatic interactions found in polypeptide-surfactant complexes. Thus, the quantum mechanical energies are reproduced not only from a qualitative point of view but also from a quantitative one. Thus, excellent correlation coefficients ($r = 0.999$ and 0.996 for HF/6-31+G(d) and MP2/6-31+G(d), respectively) and scaling coefficients close to one ($c = 1.01$ and 1.10 for HF/6-31+G(d) and MP2/6-31+G(d), respectively) were obtained from the regression analyses ($y = cx$) between classical and quantum mechanical energies. It should be noted that classical calculations of $CH_3COO^-...^+NR(CH_3)$ complexes, where R is an alkyl chain, are able to capture the effect of the size of R in the binding energy. Thus, the binding energy slowly drops when the size of the alkyl group R increases.

Electrostatic parameters for 8ATMA·PAGA were derived using the same strategy (Figure 2). These atomic charges together with the force-field parameters included in the Amber libraries for the van der Waals and bonded terms were used in MD simulations.

Computational Details. All simulations were performed with the Amber 4.1 simulation package.[19] Bond lengths were constrained to their standard values using the SHAKE algorithm.[20] A cubic solvent box (cell-axis = 56.32 Å) of 1332 chloroform molecules (density = 1.46 g/mL) was created and equilibrated. The 8ATMA·PAGA complex was centered in the solvent box and the overlapping chloroform molecules were removed. The resulting system contains 1165 chloroform molecules and 5732 explicit atoms. The OPLS model was used to describe the solvent molecules.[21] The temperature of the system was brought to 300 K by 30 ps of NVT (constant volume and temperature)-MD (P = 1 atm) with the solvent molecules fixed. After this, the energy of the system was equilibrated by performing 60 ps of NVT-MD in which both the solvent molecules and the 8ATMA·PAGA complex were allowed to move freely. The resulting structure was the starting point of 2 ns NVT-MD at 300 K. During equilibration and subsequent MD run, periodic boundary conditions were applied using the nearest image convention.

Residue-based cutoffs were applied at 12 Å, *i.e.* if two residues or a residue and a chloroform molecule have any atom within 12 Å, the interaction between the entire pair is evaluated. A numerical integration time step of 2 fs was used for all the calculations. The nonbonded pair list was updated every 25 MD steps. The MD trajectories were saved every 500 steps (1 ps interval) for subsequent analysis of the peptide conformation and surfactant organization.

RESULTS AND DISCUSSION

Conformation of the Polypeptide Chain. The progress of the polypeptide conformation can be followed by the atom-positional root mean square deviation (rmsd) of the polyion atoms from the initial α-helix conformation. Figure 3a plots the rmsd deviations of the main chain atoms (N, C^{α} and C) involved in both all the residues and the 10 central residues as a function of the simulation time. As can be seen the structures of the poly(α,L-glutamate) chain are close to the initial model conformation, the average rmsd being 1.81 ± 1.38 Å. Moreover, such value decreases to 0.74 ± 0.50 Å when only the atoms involved in the central residues are considered. Thus, the central part of the helix presents very small fluctuations whereas larger movements are located at the tails, especially at the C-terminus side. This is consistent with the evolution of the radius of gyration (R_G) along the simulation, which is provided in Figure 3b. The R_G provides a measure of the size and compactness of the molecule. Note that the R_G grows from 9.22 Å to 10.5 Å, this elongation being consistent with the fraying of the C-terminus side.

Figure 4a shows the trajectory of the fraction of hydrogen bonds between the CO of amide i and the NH of amide $i+3$, which is relative to 18 initial hydrogen bonds for the model α-helix. The criterion used to define a hydrogen bond were that the O...H distance was less than 2.5 Å and the $<$N-H...O angle was larger than 135°. It is worth noting that more than 70% of the initial hydrogen bonds remain essentially intact after 2 ns of simulation.

Inspection to the spatio-temporal evolution of the hydrogen bonds (Figure 4b) confirms that the broken hydrogen bonds are essentially located at the C-terminus side of the helix. Figure 5 provides an atomistic picture of the structures of the polypeptide extracted at times 0, 0.5, 1.0, 1.5 and 2 ns.

In order to get a deeper insight into the structure of the polyanion, the dihedral angles χ_1, χ_2, and χ_3 were analyzed. For this purpose a population analysis was performed considering all the structures recorded along the MD simulation, the conformations being grouped in six categories: *trans* ($150° \leq \chi_i < 210°$), *skew*$^+$ ($90° \leq \chi_i < 150°$), *gauche*$^+$ ($30° \leq \chi_i < 90°$), *cis* ($-30° \leq \chi_i < 30°$), *gauche*$^-$ ($-90° \leq \chi_i < -30°$) and *skew*$^-$ ($-150° \leq \chi_i < -90°$). The *trans* clearly was the most favored rotamer for both χ_1 and χ_2, the population being 79.0% and 68.7 %, respectively. Conversely, a large conformational flexibility was detected for χ_3, which is illustrated by the temporal evolution of this dihedral angle (Figure 6). This distribution was obtained by averaging the stored structures in blocks of 100 ps. It is worth noting that all the folded rotamers present a considerable population whereas the planar conformations, *i.e.* *trans* and *cis*, are the least populated.

In summary, these results point out that the conformation of the polypeptide in the complex is very similar to the α-helix of poly(α,L-glutamic acid). Thus, electrostatic interactions with the surfactant molecules are not able to induce significant conformational changes in the polypeptide. The stability of this ordered secondary structure is in excellent agreement with the interpretation of both circular dichroism and FTIR data.[1,22] Table 2

compares the most relevant parameters for the α-helices of poly(α,L-glutamate) in 8ATMA·PAGA and poly(α,L-glutamic acid).

Conformation of the Surfactant Ions. The following variables have been measured to characterize the conformation of the surfactant ions: (a) the end-to-end distance, which corresponds to the distance between the nitrogen atom and the methyl carbon atom of the octyl chain, and (b) the six dihedral angles of the octyl chain.

Figure 7 plots the evolution of the end-to-end distance averaged for the 20 surfactant ions during the MD process. This distance is shorter than 10.06 Å, which corresponds to the all-*trans* conformation considered in the initial structure. The average value is 9.00±0.08 Å indicating a contraction of about 1 Å. Test calculations revealed that the end-to-end distance decreases about 0.8-1.0 Å when one dihedral angle of the eight carbon linear chain changes from *trans* to either *gauche*$^+$ or *gauche*$^-$. These results suggest that for each surfactant ion only one dihedral angle adopt a folded conformation along the MD simulation, whereas the remaining dihedral angles retain the *trans* conformation. Furthermore, the small standard deviations displayed in Figure 6 point out that all the surfactant ions present a similar conformational pattern.

Table 3 shows the dihedral angle distribution for the 20 surfactant ions contained in the complex under study, the conformations being grouped in four categories: *trans*, *gauche*$^+$, *gauche*$^-$ and the remaining conformers. The

intervals used to define the conformations were those listed in the previous section. As it can be seen, in all cases the *trans* is the predominant conformation. This preference is strongest for the dihedral angles γ_1 and γ_2, in which the population of *trans* conformation is 96% and 81%, respectively. The population of folded conformations in the remainining dihedral angles is about 20-30%, the amount of *gauche*$^+$ and *gauche*$^-$ being very similar. These results are consistent with the trajectory of the end-to-end distance (Figure 7).

The conformational preferences of the surfactant ions are explained considering the favorable interactions between the octyl groups and the explicit solvent molecules. Thus, the largest solvent-exposed surface area of the hydrophobic methylene groups is achieved when the surfactant ions adopt an extended conformation. For instance, the solvent-exposed surface area of the octyltrimethylammonium chain in all-*trans* conformation, which amounts to 340 Å^2, decreases by about 10 Å^2 when one dihedral angle changes from *trans* to either *gauche*$^+$ or *gauche*$^-$. The greater solvent-accessibility of the hydrophobic octyl group in the extended conformation increases the favorable van der Waals interactions between the surfactant ions and the organic solvent.

Organization of the Surfactants Ions with Respect to the Polypeptide Chain. Figure 8a displays a distribution of the number of carboxylate groups that interact with each surfactant ion during the trajectory. The

criterion used to define the electrostatic interaction was that the distance between the nitrogen atom of the surfactant ion and the carbon atom of the carboxylate group was less that 5.50 Å. This distance is about 1.5 Å larger than that the optimum value predicted by quantum mechanical calculations for $N(CH_3)_4^+...CH_3COO^-$ (4.01 Å) complex.[15] Single point calculations indicate that the binding energy only decreases about 30% when this distance increases from 4.01 to 5.50 Å. Accordingly, 5.50 Å seems to be a reasonable value to define a specific electrostatic interaction between a carboxylate group and a surfactant ion.

As can be seen the surfactant ions are preferentially bound to more than one carboxylate group. Thus, the most populated arrangement corresponds to that in which the surfactant ion interacts with two carboxylate groups simultaneously, being followed by that in which the interaction occurs with three carboxylate groups at the same time. The situation in which a surfactant cation simultaneously interacts with four carboxylate groups is the least frequent. Indeed, although the 20 surfactant ions present this multiple interaction several times during the trajectory, they are short-lived in all cases. Furthermore, Figure 8a reveals that the arrangement in which the surfactant ion only interacts with one carboxylate group is not very common.

The multiple interactions displayed by the carboxylate groups reveal a movement of the surfactant ions with respect to the initial structure, in which each surfactant was directly arranged in front of a carboxylate group.

These results are in good agreement with quantum mechanical calculations of complexes containing two acetate anions and one tetramethylammonium cation (data not shown). Geometry optimizations at the HF/6-31+G(d) level of such complex were performed using as starting points different arrangements of the molecular ions, including those in which the cation is directly confronted to only one anion. In all cases the system evolved towards an arrangement in which the cation similarly interacts with the two anions, *i.e.* the geometric parameters of the two possible electrostatic interactions were optimized.

Figure 9a shows a representative snapshot of 8ATMA·PAGA complex, in which surfactant ions predominantly form multiple interactions with the polyelectrolite chain. A detailed picture of the four types of arrangements found for the octyltrimethylammonium cations is displayed in Figure 9b: a surfactant ion interacting with one, two, three and four carboxylate groups. The parameters d_1, d_2, d_3 and d_4 correspond to the distances between the nitrogen atom of the surfactant ion and the carbon atom of the interacting carboxylate groups, where $d_1 < d_2 < d_3 < d_4$. Figure 8b shows the evolution of d_1, d_2 and d_3 along the simulation. It was not possible to follow the trajectory of d_4 because the population of surfactant ions interacting with four carboxylate groups at the same time was very low. As can be seen, d_2 and d_3 are about 0.4 and 0.7 Å larger than d_1, respectively, pointing out that the surfactant ions are asymmetrically arranged with respect to the carboxylate groups. This asymmetric arrangement was also predicted from quantum mechanical calculations on model compounds, being attributed to

14

the repulsive interactions among ions of the same sign. Table 3 lists the averaged intermolecular parameters for the four types of interactions displayed in Figure 9.

In Figure 8a it can be seen that the last surfactant ion, *i.e.* number 20, presents an anomalous behavior. In this case the most populated arrangement corresponds to that in which the cation only interacts with one carboxylate group. However, a detailed inspection to the structures stored along the simulation indicates that this surfactant ion also interacts with the oxygen atoms of the two last amide groups (Figure 10). This is consistent with the results displayed in Figure 4b according to which the helix conformation disrupts at the C-terminus side.

CONCLUSIONS

In this work we have carried out a MD simulation of poly(α,L-glutamate)-octyltrimethylammonium complex in chloroform solution. The results have allowed to rationalize the structural tendencies of both surfactant and polypeptide chains in the complex. Furthermore, a detailed view of the interaction between the octyltrimethylammonium ions and the carboxylate groups of the polypeptide chain has been provided. Thus, it has been found that the situation in which a surfactant cation interacts with several carboxylate groups at the same time is the most frequent. This is an interesting result since it provides an atomistic picture of this interaction. It should be noted that the experimental study of the conformational

15

preferences of polypeptide-surfactant complexes at the atomic level is very difficult. We hope with this contribution to add some insight into the understanding of these interesting complexes.

ACKNOWLEDGEMENTS

REFERENCES

1. MacKnight, W. L.; Ponomarenko, E. A.; Tirrell, D. A. Acc. Chem. Res. 1998, 31, 781.

2. Okuzaki, H.; Osada, Y. Macromolecules 1995, 28, 380.

3. Antonietti, M.; Conrad, J. Angew. Chem., Int. Ed. Enl. 1994, 33, 1869.

4. Seki, M.; Morishima, Y.; Kamachi, M. Macromolecules 1992, 25, 6540.

5. Bakeev, K. N.; Yang, M. S.; MacKnight, W. J.; Zezin, A. B.; Kabanov, V. A. Macromolecules 1994, 27, 300.

6. Kabanov, A. V.; Sergeev, V. G.; Foster, M.; Kasaikin, V. A.; Levashov, A. V.; Kavanov, V. A. Macromolecules 1995, 28, 3657.

7. Antonietti, M.; Conrad, J.; Thünemann, A. Macromolecules 1994, 27, 6007.

8. Morishima, Y.; Seki, M.; Tominaga, Y.; Kamachi, M. J. Polym. Sci. A 1992, 30, 2099.

9. Ponomarenko, E. A.; Tirell, D. A.; MacKnight, W. J. Macromolecules 1996, 29, 8751.

10. Ponomarenko, E. A.; Waddon, A. J.; Tirell, D. A.; MacKnight, W. J. Langmuir 1996, 12, 2169.

11. Liu, J.; Takisawa, N.; Kodama, H.; Shirahama, K. Langmuir 1998, 14, 4489.

12. Liu, J.; Takisawa, N.; Shirahama, K. J. Phys. Chem. B 1998, 102, 6696.

13. Zanuy, D.; Alemán, C. Biopolymers 1999, 49, 497.

14. Holtzer, A.; Hawkins, R. B. J. Am. Chem. Soc. 1996, 118, 4220.

15. Alemán, C.; Zanuy, D. Chem. Phys. Lett. 2000, 319, 318.

16. Alemán, C.; Zanuy, D. Submitted work.

17. Cornell, W. D.; Cieplak, P.; Bayly, C. I.; Gould, I. R.; Merz Jr., K. M.; Ferguson, D. M.; Spellmeyer, T.; Fox, J.; Caldwell, J. W.; Kollman, P.A. J. Am. Chem. Soc. 1995, 117, 5179.

18. Hariharan, P. C.; Pople, J. A. Theor. Chim. Acta 1973, 28, 213.

19. Pearlman, D. A.; Case, D. A.; Caldwell, J. W.; Ross, W. S.; Cheatham III, T. E.; Ferguson, D. M.; Seibel, G. L.; Singh, C.; Weiner, P. K.; Kollman, P. A. Amber 4.1., University of California, San Francisco (1995).

20. Ryckaert, J.-P.; Ciccotti, G.; Berendsen, H. J. C. J. Comp. Phys. 1977, 23, 327.

21. Jorgensen, W. L.; Briggs, J. M.; Contreras, M. L. J. Phys. Chem. 1990, 94, 1683.

22. Ponomarenko, E. A.; Waddon, A. J.; Bakeev, K. N.; Tirell, D. A.; MacKnight, W. J. Macromolecules 1996, 29, 4340.

CAPTIONS TO FIGURES

Figure 1. Equatorial and axial projections of the molecular geometry used as starting point in MD simulation of 8ATMA·PAGA.

Figure 2. Partial atomic charges derived from ab initio quantum mechanical calculations for 8ATMA·PAGA.

Figure 3. (a) Backbone atom-positional root-mean square deviation (rmsd) from the initial α-helix conformation of the polypeptide chain as a function of the simulation time. Plots with dashed and solid lines correspond to all the residues and the 10 central residues, respectively. (b) Radius of gyration (R_G) for the polypeptide chain as a function of the simulation time.

Figure 4. (a) Trajetory of the fraction of $i,i+3$ type hydrogen bonds in the polypeptide chain. (b) Spatio-temporal evolution of $i,i+3$ type hydrogen bonds. Note that the residue number, i, denotes the ith residue with the acceptor oxygen.

Figure 5. Ribbon snapshots of the polypeptide chain representing equally spaced intervals over the 2 ns of MD simulation.

Figure 6. Temporal evolution of the conformational distribution for the torsional angle χ_3 during the MD simulation. The population analyses were performed considering blocks of 100 ps.

19

Figure 7. Evolution of the end-to-end distance for the octyltrimethylammonium ions. The average for the 20 surfactant ions is represented, the standard deviation being indicated by horizontal bars.

Figure 8. (a) Distribution of the number of carboxylate groups that simultaneously interact with each of the 20 surfactant ions. From left to right: interactions with only one carboxylate group (black), two carboxylate groups at the same time (light gray), three carboxylate groups at the same time (medium gray) and four carboxylate groups at the same time (dark gray). (b) Evolution of the distance between the nitrogen atom of the surfactant ion and the carbon atom of the carboxylate group. The meaning of d_1, d_2 and d_3 is indicated in Figure 9b (see text). The average for the 20 surfactant ions is represented, the standard deviation being indicated by horizontal bars at intervals of 20 ps.

Figure 9. (a) Equatorial and axial projections of a representative snapshot for the 8ATMA·PAGA complex. (b) The four types of arrangements found for the surfactant ions with respect to the carboxylate groups are indicated: interaction with one, two, three and four carboxylate groups. It should be noted that in all cases $d_i < d_{i+1}$.

Figure 10. Detailed view of the interaction between the last surfactant ions and the amide groups of the polypeptide. The side chains in which the

carboxylate group does not interact with the surfactant, have not been

represented for clarification.

Table 1. Classical and Quantum mechanical[a] binding energies (in kcal/mol) for seven model systems mimicking the electrostatic interactions involved in polypeptide-surfactant complexes.

Complex[b]	Classical	HF/6-31+G(d)	MP2/6-31G(d)
$CH_3COO^-...^+N(CH_3)_4$	-95.6	-95.6	-98.3
$CH_3COO^-...^+NR(CH_3)$; R=-CH_2CH_3	-94.0	-94.2	-97.4
$CH_3COO^-...^+NR(CH_3)$; R=-$(CH_2)_2CH_3$	-92.7	-93.5	-96.9
$CH_3COO^-...^+NR(CH_3)$; R=-$(CH_2)_3CH_3$	-91.8	-93.1	-95.4
$(CH_3)_4N^+...CH_3COO^-...^+N(CH_3)_4$	-129.0	-124.8	-127.8
$CH_3COO^-...^+N(CH_3)_4^+...CH_3COO^-$	-128.3	-126.0	-129.3
$(CH_3)_4N^+...CH_3COO^-...^+N(CH_3)_4...CH_3COO^-$	-202.1	-200.0	-205.2

a) Quantum mechanical calculations from references 15 and 16. The molecular geometries correspond to those obtained at the HF/6-31+G(d) level.

Table 2. Structural parameters for the α-helices of poly(α,L-glutamate) in 8ATMA·PAGA and poly(α,L-glutamic acid).

Parameter	8ATMA·PAGA	Poly(α,L-glutamic acid)
φ^a	-71.6°	-64.7°
ψ	-58.9°	-36.9°
ω	179.1°	177.1°
χ_1^b	-152.4°	-67.8°
χ_2	148.7°	-
$d(H...O)^c$	1.81 Å	2.15 Å
<N-H...O	149.7 Å	153.1°±8.4°
h^d	1.57	1.61 Å
υ^e	3.64	3.54

a) The φ, ψ and ω are the backbone dihedral angles.

b) The χ_1 and χ_2 are the side chain dihedral angles. χ_3 has not been included in the Table due to its large conformational flexibility (see Figure 6).

c) d(H...O) and <N-H...O are the hydrogen bonding parameters.

d) The h is the rise per residue.

e) The υ is the number of amino acids per turn.

Table 3. Dihedral angle distribution for the 20 surfactant ions considered in the 8ATMA·PAGA complex. The population analysis (in %) of the dihedral angles associated to each bond in the octyl chain is specified.

#	trans	gauche$^+$	gauche$^-$	other
γ_1	96	0.2	0.2	3.6
γ_2	81.6	6.5	7.6	4.3
γ_3	71.3	10.2	13.4	5.1
γ_4	71.6	12.9	10.7	4.8
γ_5	66.4	14.4	14.4	4.8
γ_6	63.0	17.1	15.2	4.7

Table 4. Averaged intermolecular parameters[a] for the four types of interactions displayed in Figure 9[b].

Parameter	d_1	d_2	d_3	d_4
N...C_1 (in Å)	4.50±0.25	4.87±0.24	5.15±0.19	5.30±0.03
C_2-N...C_1 (in °)	111.2±30.7	111.8±29.4	107.1±24.8	100.6±6.4
N...O_1-C_1-O_2 (in °)	66.2±37.7	86.3±51.1	99.3±45.9	98.9±10.4

a) The distance N...C_1, the angle C_2-N...C_1 and the dihedral N...O_1-C_1-O_2 correspond to the following scheme:
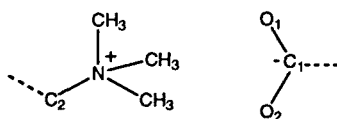
b) The parameters d_1, d_2, d_3 and d_4 refer to those displayed in Figure 9b.
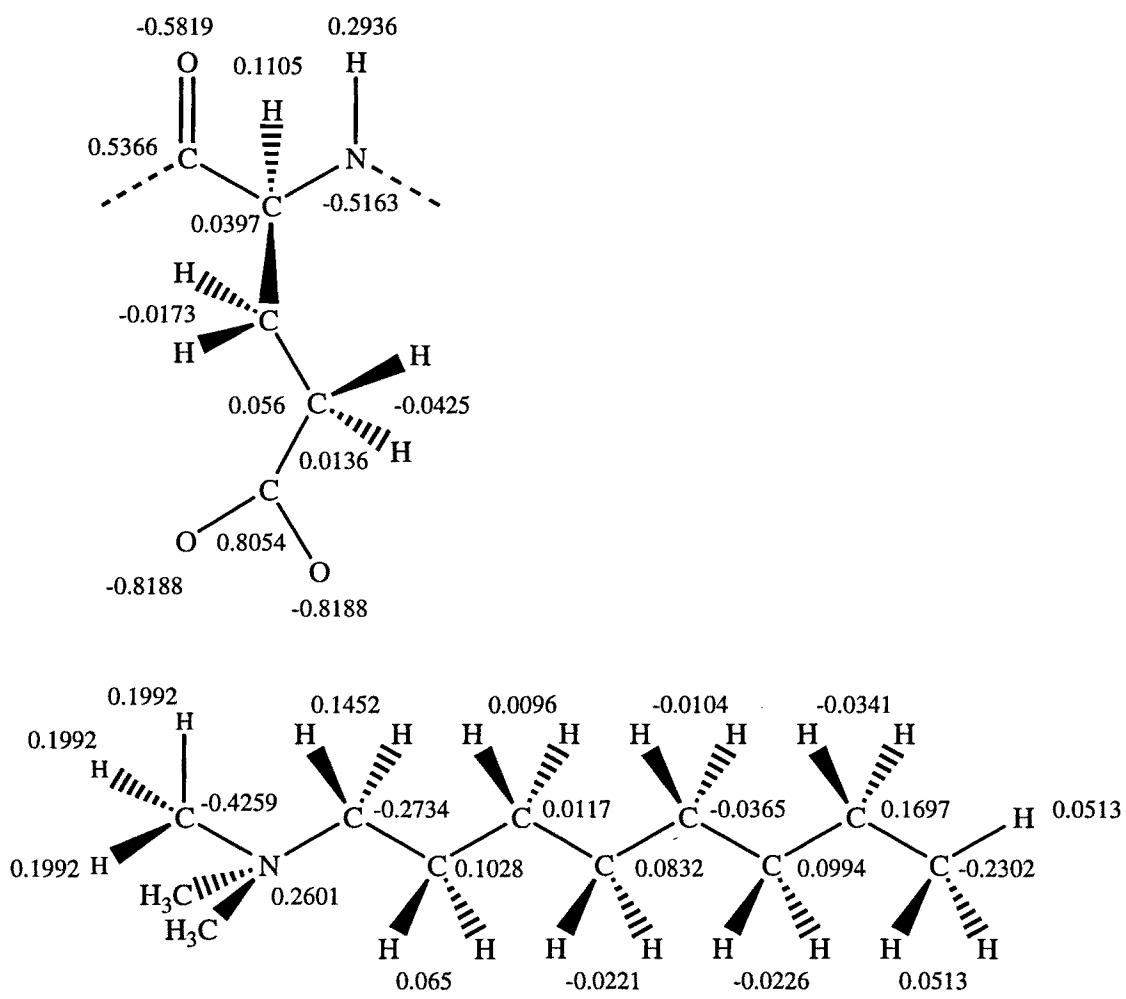
Fig.2. Zanuy et al.
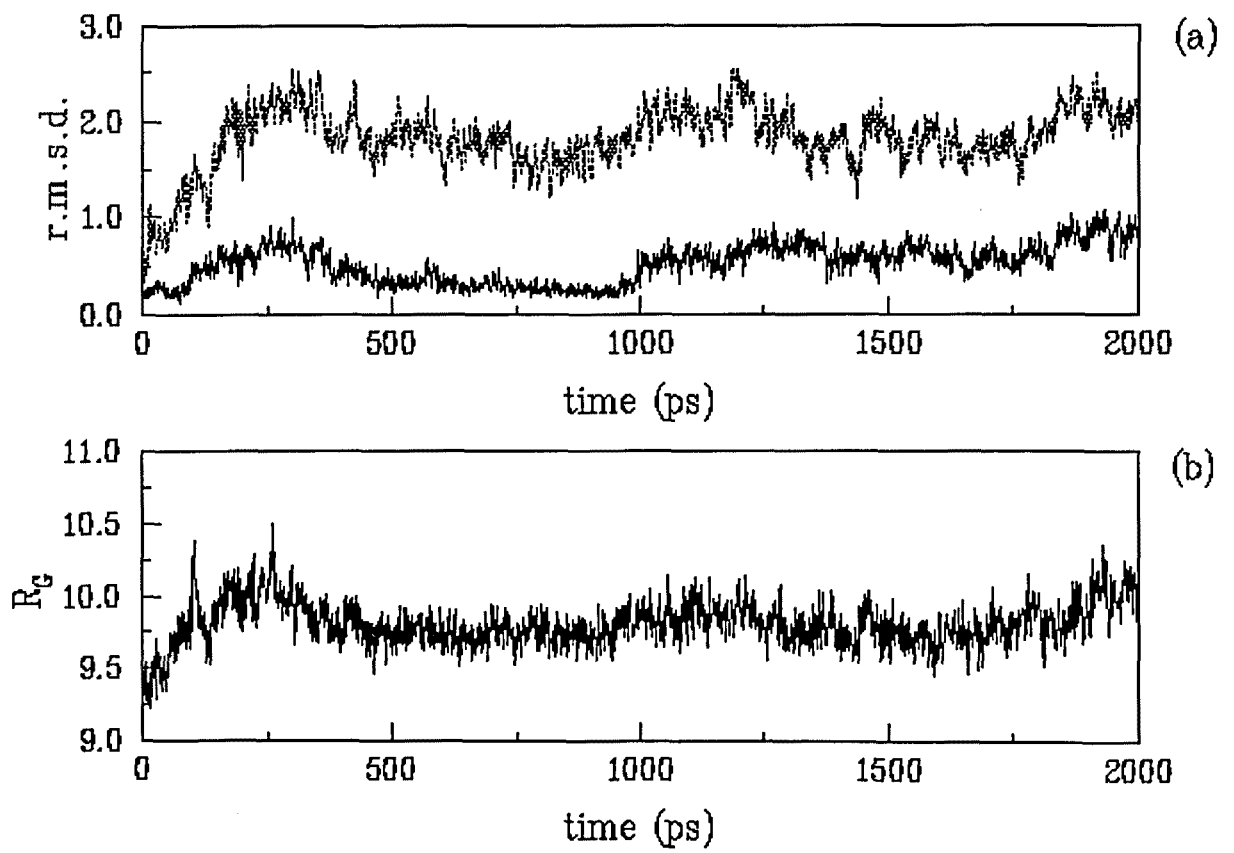
Fig.3. Zanuy et al.
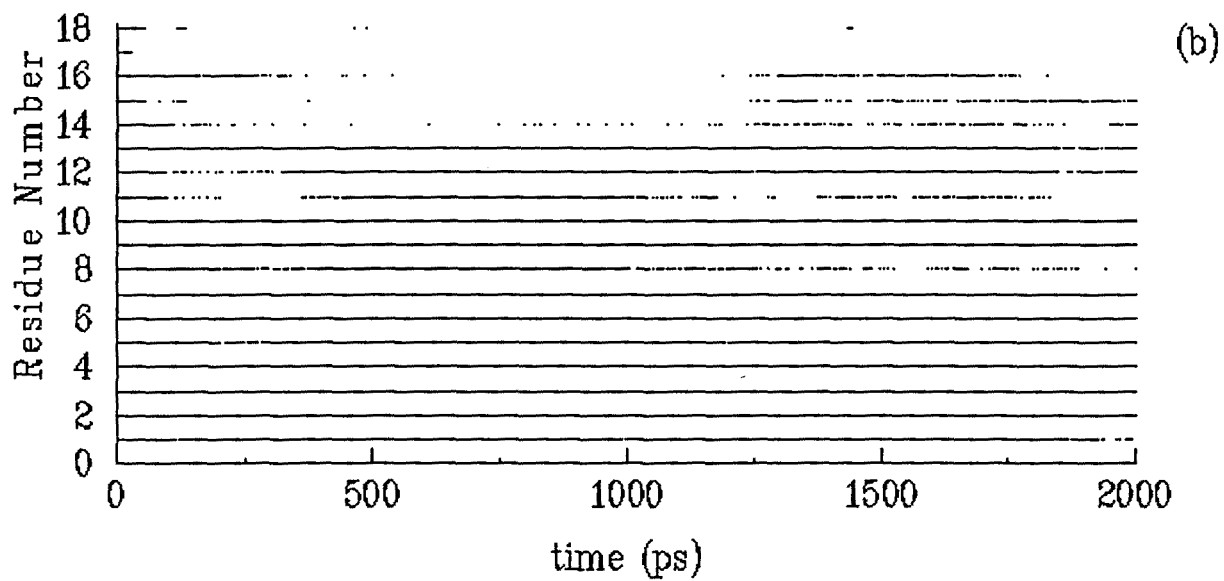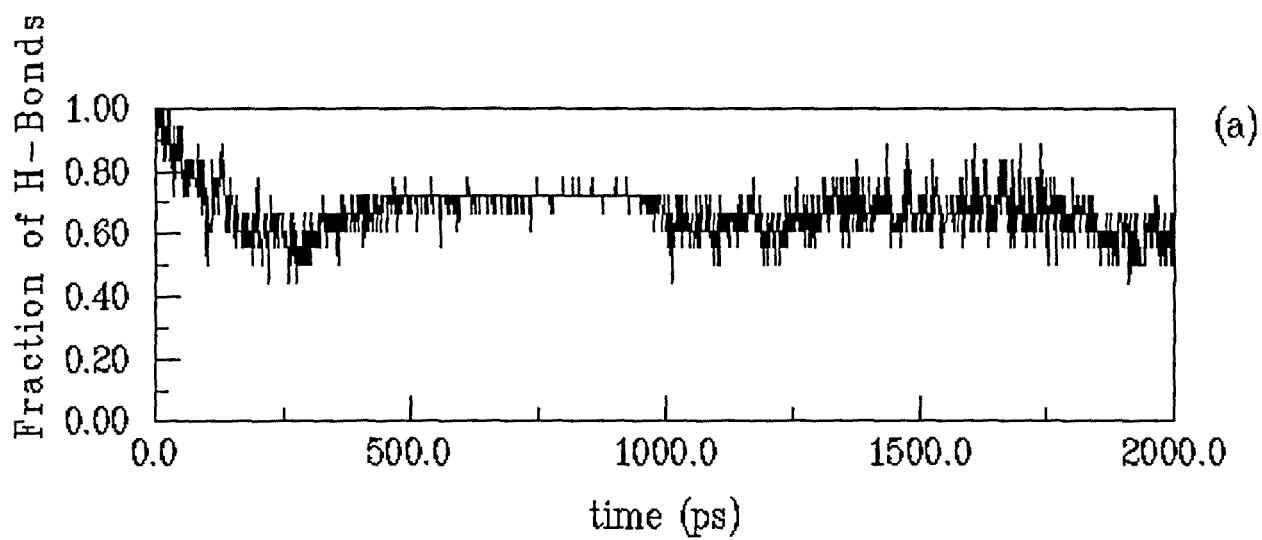
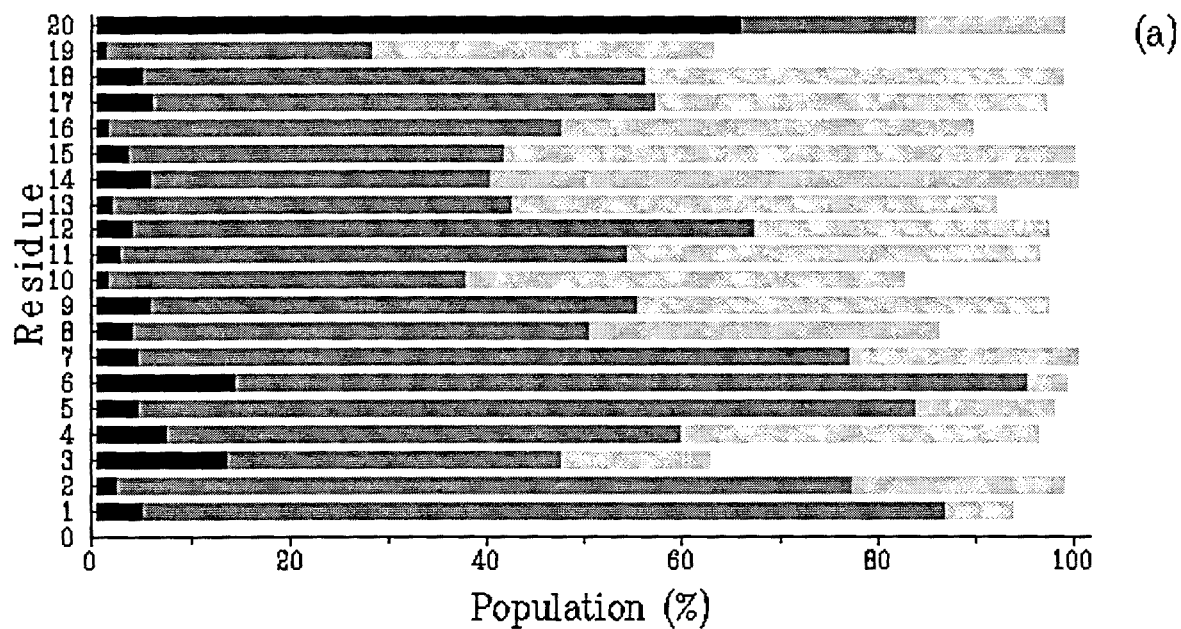Fig.4. Zanuy et al.
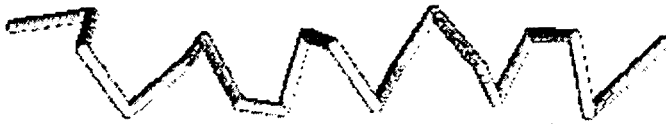
Fig.5. Zanuy et al.
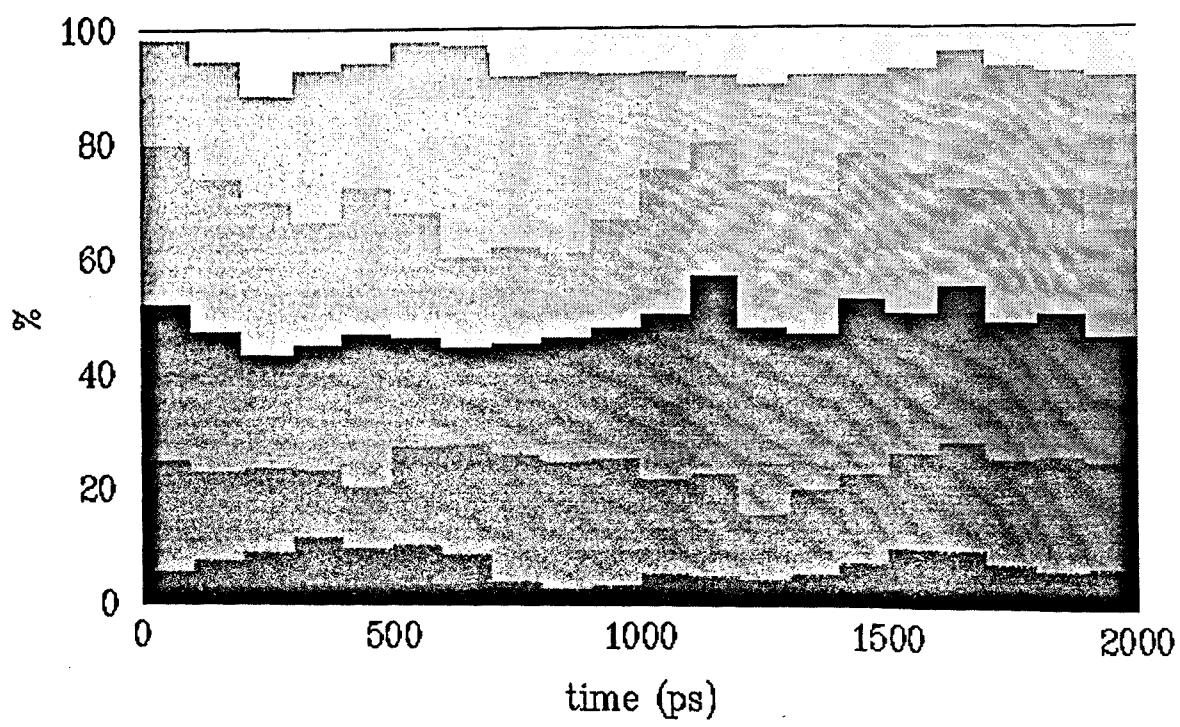
Fig.6. Zanuy et al.
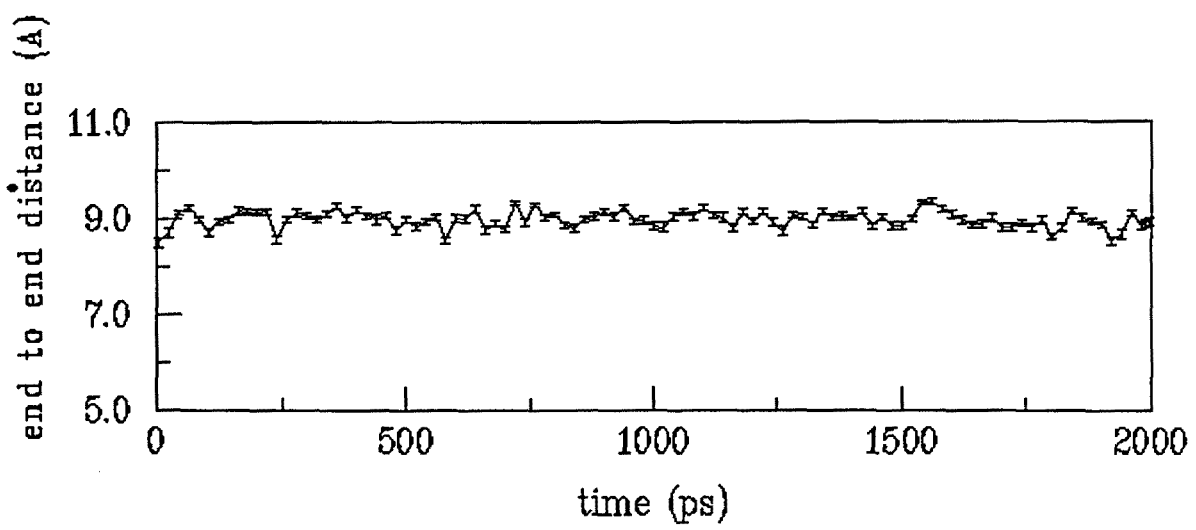
Fig.7. Zanuy et al.
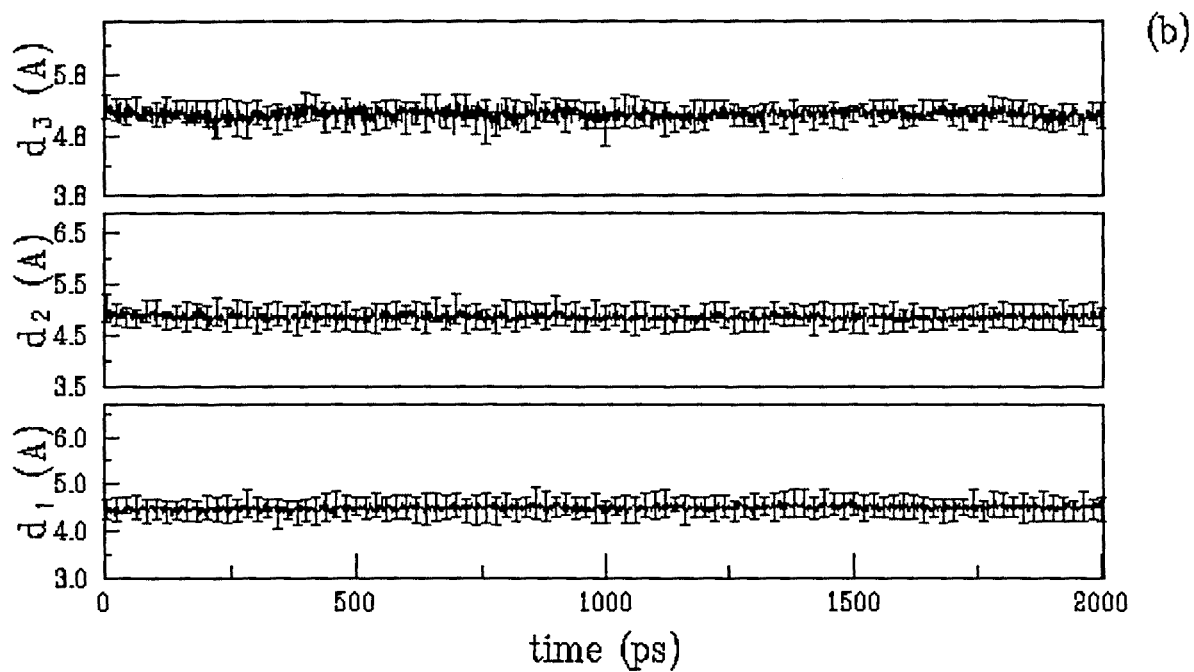
Fig.8. Zanuy et al.
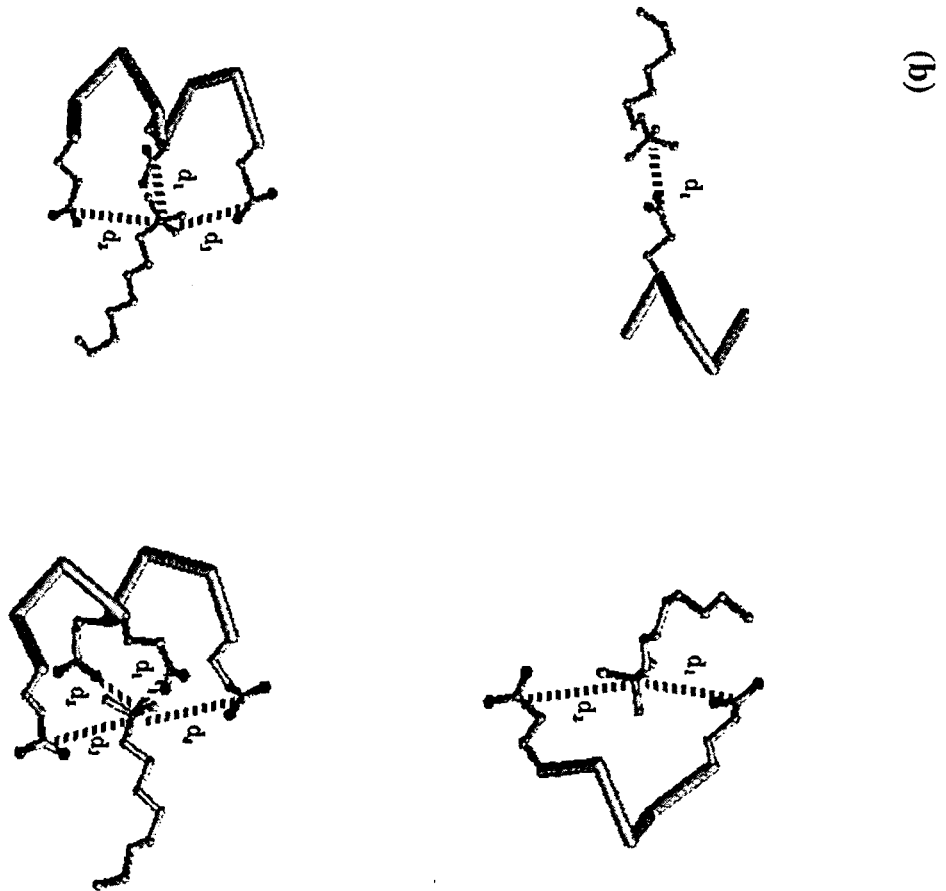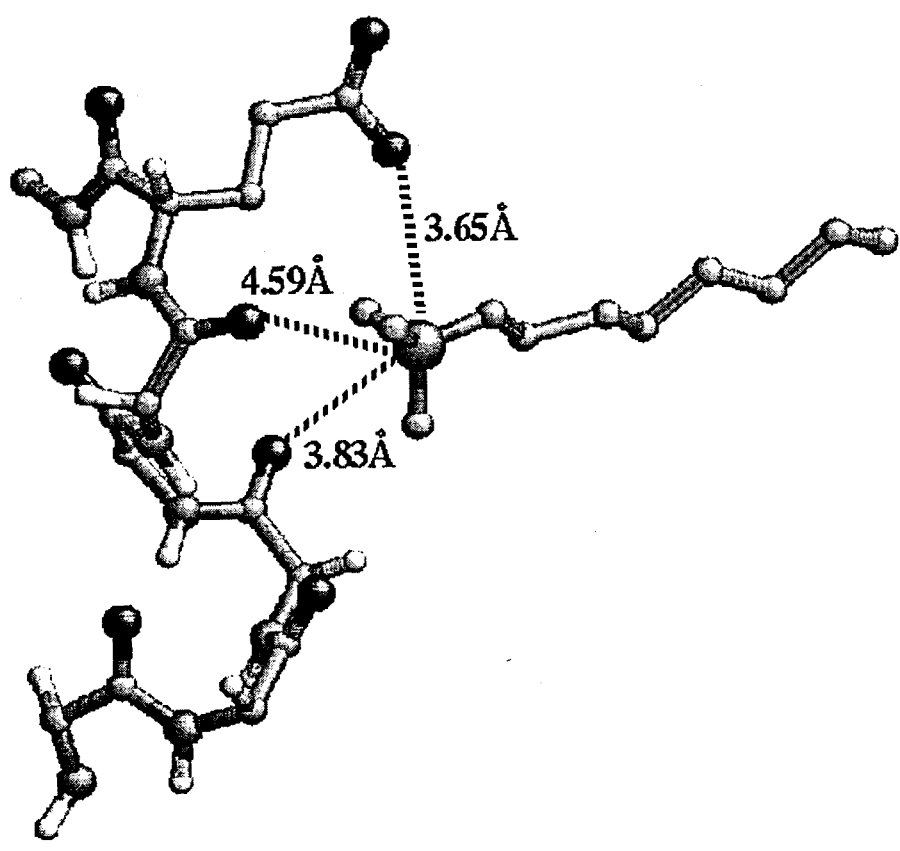
Fig.9. Zanuy et al.

Fig.10. Zanuy et al.

VI.8. Complejos autoasociados derivados del PGGA

En este capítulo se presentan los estudios realizados acerca de las propiedades estructurales de los complejos nATMA·PGGA. Para comparar los resultados obtenidos con los presentados en el punto anterior, se usó el mismo catión molecular que para los complejos derivados del PAGA. En este caso fue necesario determinar la conformación que adopta la cadena de polianión, debido a que, como ya ha sido comentado anteriormente, los datos experimentales disponibles son muy poco concluyentes.

Para poder establecer dicha conformación se realizaron diversas simulaciones partiendo de 3 posibles conformaciones iniciales para el anión molecular. Por analogía con el comportamiento de los complejos estequiométricos derivados del PAGA, dónde la conformación del anión molecular es la adoptada por el poliácido y por los ésteres alquílicos, dichas conformaciones correspondieron a las dos más características de los poli(α-alquil-γ-glutamato)s (hélices 5/2 y 2/1, de las formas II y III, respectivamente) y la hélice 17/5 del PGGA (figura VI.6.). En todas las estructuras de partida los cationes moleculares se ubicaron enfrentando cada molécula de tensioactivo a un único grupo carboxilato, al igual que en el complejo 8ATMA·PAGA. De esta forma será posible comparar las características estructurales de los complejos formados a partir de PGGA y de PAGA.

VI.8.1. Métodos

Se realizaron tres simulaciones de dinámica molecular en disolución de cloroformo para cada una de las conformaciones consideradas. En la primera dinámica se partió de una hélice 17/5 (MD1), en la segunda de una hélice 5/2 (MD2) y en la tercera de una hélice 2/1 (MD3). La energía del sistema se calculó mediante los parámetros del campo de fuerzas de AMBER (Cornell et al., 1995) a excepción de las cargas atómicas, las cuales se parametrizaron a partir del ajuste del MEP cuántico a nivel HF/6-31G(d) al MEP clásico. Todas las distancias de enlace fueron constreñidas a sus valores de equilibrio usando el algoritmo *SHAKE* (Rycaert et al., 1977).
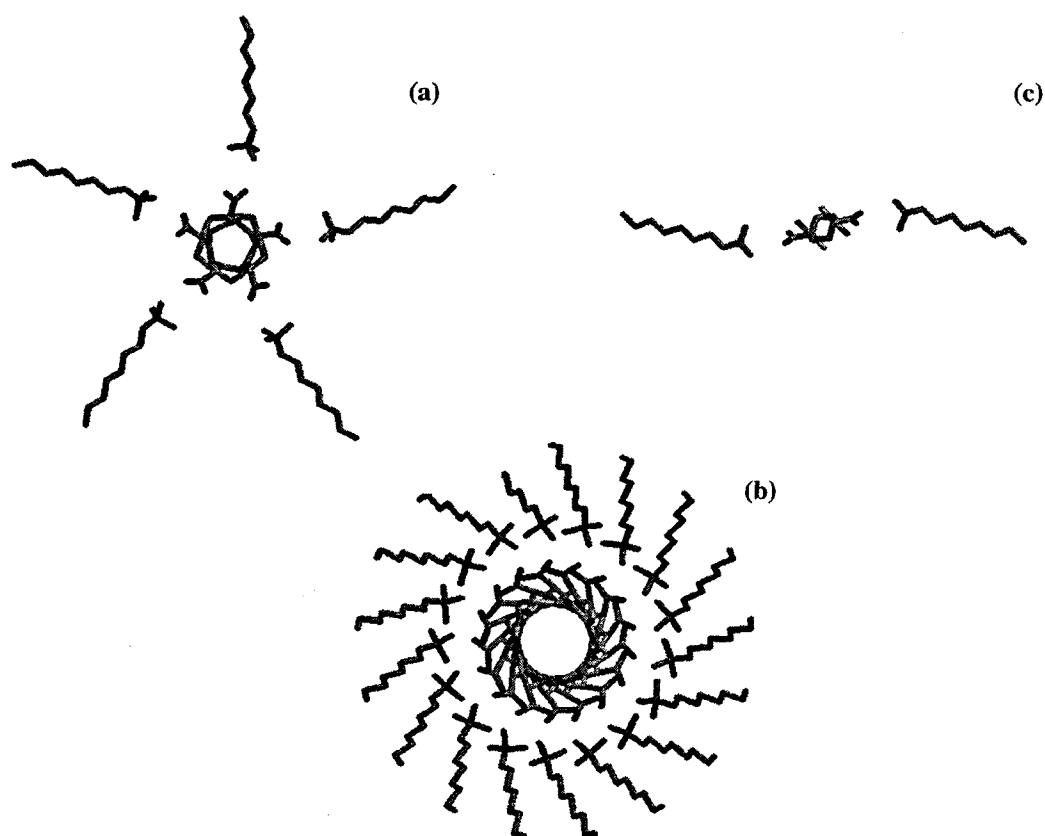
Figura VI.6. Proyección ecuatorial de los sistemas empleados como punto de partida en las simulaciones de dinámica molecular. Las conformaciones del anión molecular corresponden a hélices 5/2 (a), 17/5 (b) y 2/1 (c).

Se construyeron dos cajas de simulación, una cúbica para las simulaciones MD1 y MD2 (x = 56.32 Å), y una rómbica (x = 46.08 Å, y = 46.08 Å, z = 92.16 Å) para la MD3, en las que se incluyeron 1331 y 1458 moléculas de cloroformo respectivamente (densidad = 1.46 g/mL). Las moléculas de cloroformo se representaron mediante el modelo OPLS (Jorgensen et al., 1990). Ambos sistemas fueron equilibrados energéticamente a una temperatura de 300 K. El cambio de forma y tamaño de la caja en la simulación MD3 es consecuencia de la longitud que presenta la cadena de polímero en conformación 2/1, 4.6Å por residuo.

El modelo empleado para el polianión en MD1 y MD2 consistió en una cadena de 20 residuos, mientras que dicho número disminuyó a 18 residuos para la simulación MD3. Cada cadena de polianión se bloqueó con un grupo acetilo y un grupo N-metil

amida en los extremos *N-terminal* y *C-terminal*, respectivamente. A su vez, en cada caso se incluyó un número de cationes moleculares igual al número de residuos de la cadena de polianión. Cada complejo 8ATMA·PGGA se centró en su correspondiente caja de simulación y las moléculas de cloroformo que se solapaban con las posiciones de los átomos del complejo fueron eliminadas. De esta forma, el número total de moléculas de cloroformo en los sistemas simulados fue de 1191 para MD1 y MD2, y de 1223 para MD3.

Las tres dinámicas realizadas se equilibraron energéticamente en dos pasos. Primero se aumentó la temperatura desde 0 a 300 K a lo largo de 30 ps, manteniendo fijos los átomos de cloroformo. A continuación, se dejó que todas las especies moleculares evolucionaran libremente hasta que la energía del sistema se equilibró (60 ps). La estructura resultante fue el punto de inicio de 200 ps de simulación, para cada una de las conformaciones iniciales. Este corto intervalo de tiempo fue suficiente para proporcionar resultados representativos del sistema objeto de estudio.

Todas las simulaciones se llevaron a cabo a volumen y temperatura constante, y aplicando condiciones periódicas de contorno. Se empleó un tiempo de integración de 2 fs y un *cutoff* de 12Å para las interacciones no - enlazantes. La trayectoria de cada simulación se obtuvo guardando una estructura cada 2 ps.

VI.8.2. Resultados

VI.8.2.1. *Conformación del anión molecular*

La evolución de la conformación de la cadena de polímero fue seguida mediante la desviación de la distancia cuadrática media, rmsd (*root mean square deviation*), y el radio de giro (R_G). La evolución del rmsd permitió evaluar como se desviaba la conformación de la cadena polimérica con respecto a la estructura inicial, mientras que el radio de giro proporcionó una estimación del tamaño y la compactación de cada una de las conformaciones.

En las tres simulaciones puede observarse como las conformaciones iniciales se pierden rápidamente, tal y como muestra el brusco aumento del rmsd en los primeros ps de simulación (figura **VI.7a**).
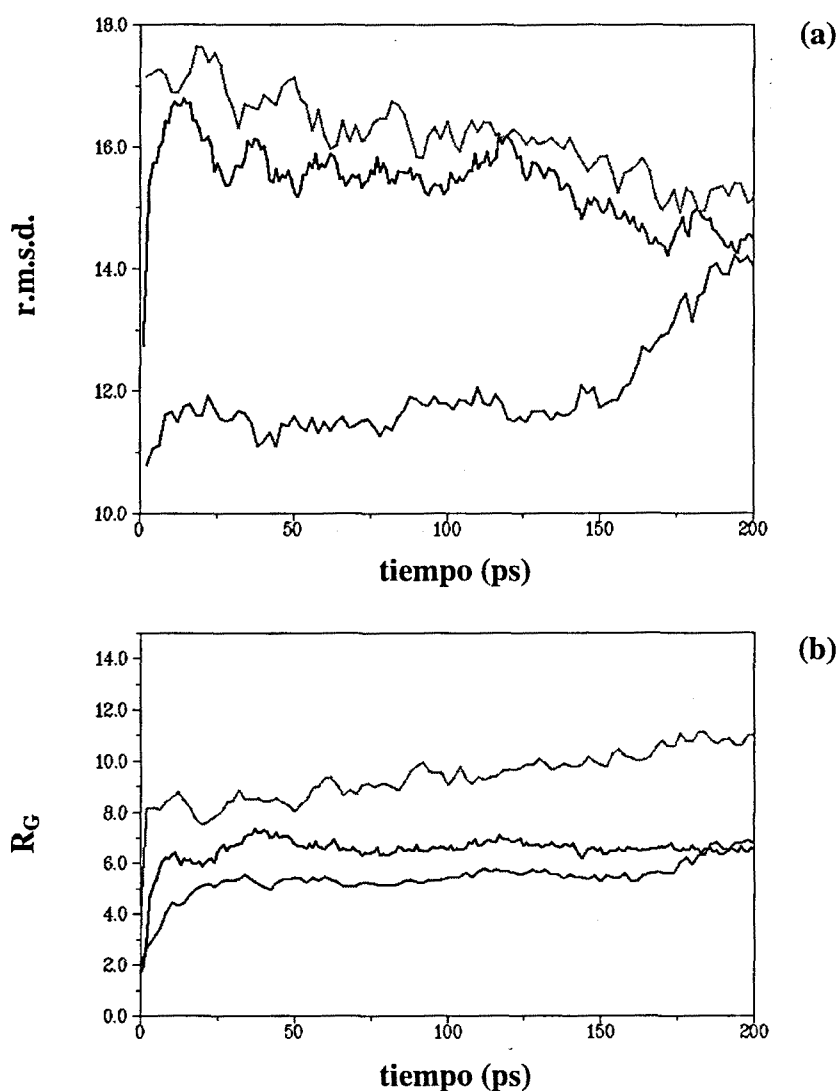

Figura VI.7. Evolución del (**a**) rmsd (en Å) de la cadena polimérica y del (**b**) R_G (en Å) a lo largo del tiempo. En ambas representaciones la línea negra representa MD1, la roja MD2 y la verde MD3.

En los tres casos se obtienen estructuras irregulares pero parcialmente extendidas. Este hecho queda reflejado en la evolución del radio de giro para cada una de las simulaciones (figura **VI.7b**). Las dos conformaciones helicoidales, más compactas, tienden rápidamente a sufrir una clara elongación (tabla **VI.2**). Así, el valor de la R_G para la hélice 5/2 evoluciona desde 12.73 a 14.50Å, mientras que para la hélice 17/5 se pasa de 10.78Å a 14.04Å. En el caso de la hélice 2/1 puede observarse una

ligera compactación de la estructura. Su R_G evoluciona de 17.15 a 15.18Å, tendiendo hacia valores cercanos a los obtenidos en MD1 y MD2.

Tabla VI.2. Valores iniciales (R_{G_i}) y finales (R_{G_f}) del R_G para las tres conformaciones consideradas. Todos los valores se dan en Å.

Conformación inicial	R_{G_i}	R_{G_f}
5/2	12.73	15.50
17/5	10.78	14.04
2/1	17.15	15.18

Por último, en aquellas conformaciones de partida que presentaban puentes de hidrógeno intramoleculares se siguió su presencia a lo largo de la trayectoria (figura **VI.8**) y de su posición en la cadena polimérica (figura **VI.9**). Puede verse como esta interacción se pierde en los primeros pasos de la simulación en consonancia con lo ya observado en la figura **VI.7**. En el caso de la hélice 5/2 esta pérdida resulta dramática, desapareciendo en los primeros picosegundos de simulación prácticamente todos los puentes de hidrógeno (figura **VI.9b**).
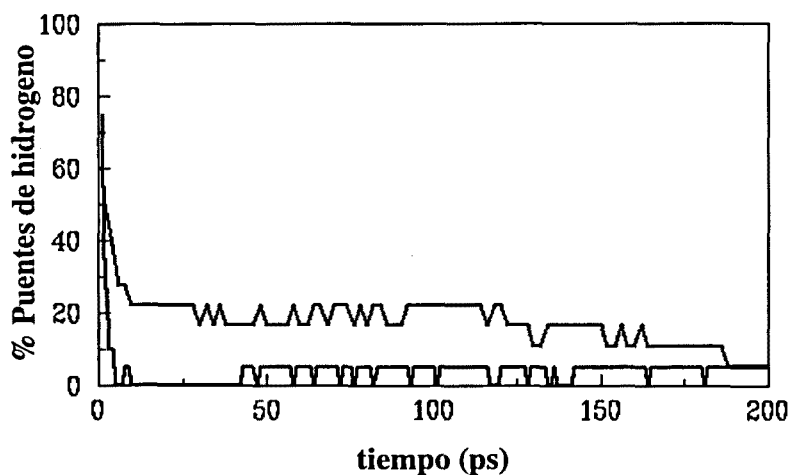

Figura VI.8. Evolución del tanto por ciento de puentes de hidrógeno a lo largo del tiempo. La línea roja corresponde a la hélice 17/5 y la negra a la 5/2.

La hélice 17/5, en cambio, tiende a mantener algunas características estructurales de la conformación inicial. Tal como se ve en la figura **VI.9a**, los puentes de hidrógeno de los residuos 2,3 y 4 se mantienen estables durante más de 100 ps. Este hecho nos puede explicar, en parte, los resultados de CD obtenidos para estos sistemas. En disoluciones de cloroformo, se observa cierto comportamiento dicroico pero con una intensidad muy baja. Podría interpretarse que el sistema mayoritariamente presenta una conformación irregular, pero se conservaría parte de la conformación del PGGA en algunos pequeños segmentos de la cadena.
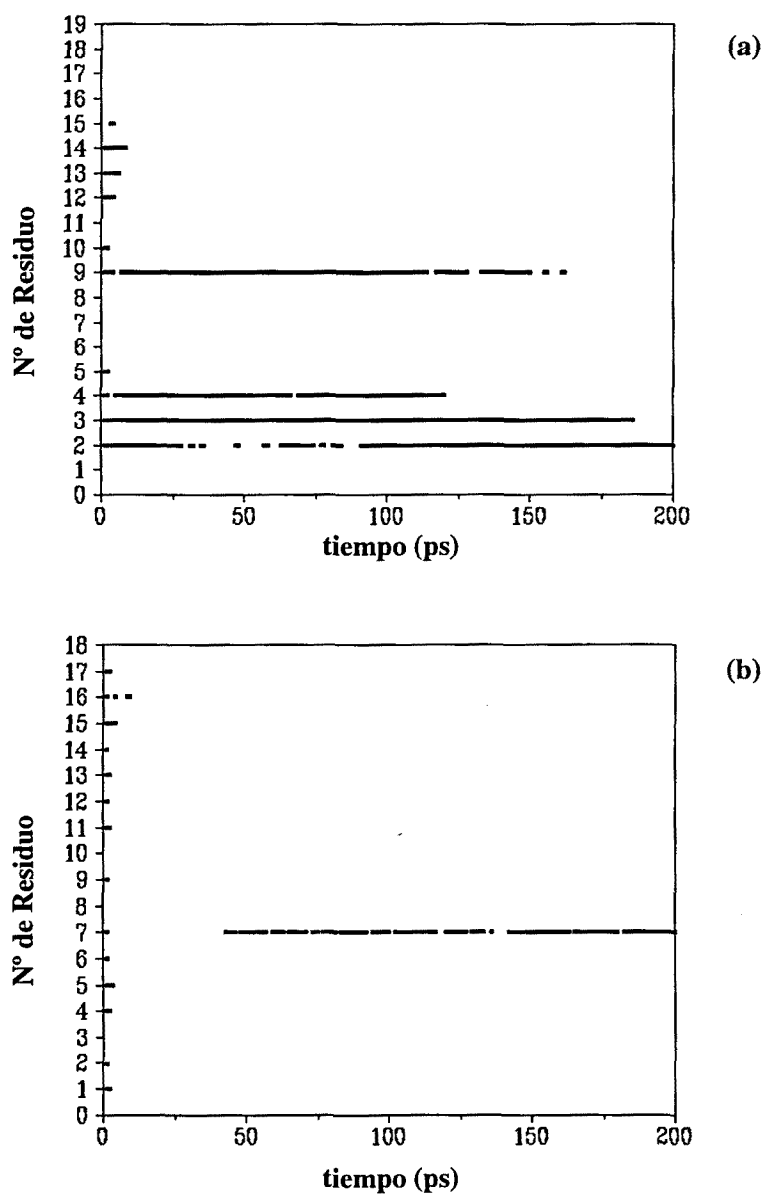
Figura VI.9. Evolución temporal y posicional de los puentes de hidrógeno. En las dos figuras se indica explícitamente la posición del aceptor de puente de hidrógeno para el esquema particular de cada conformación. La hélice 17/5 (a), con un esquema i, i+3, y la hélice 5/2, con un esquema i, i+2 (b).

A pesar de esta última conclusión debe destacarse que en general las tres trayectorias tienden a dar conformaciones de polímero irregulares, tal como se puede apreciar claramente en la figura **VI.10**. Al mismo tiempo, es revelador que partiendo de tres conformaciones muy diferentes en trayectorias tan cortas se obtengan estructuras relativamente parecidas, lo cual parece indicar que la conformación más favorecida es la irregular.
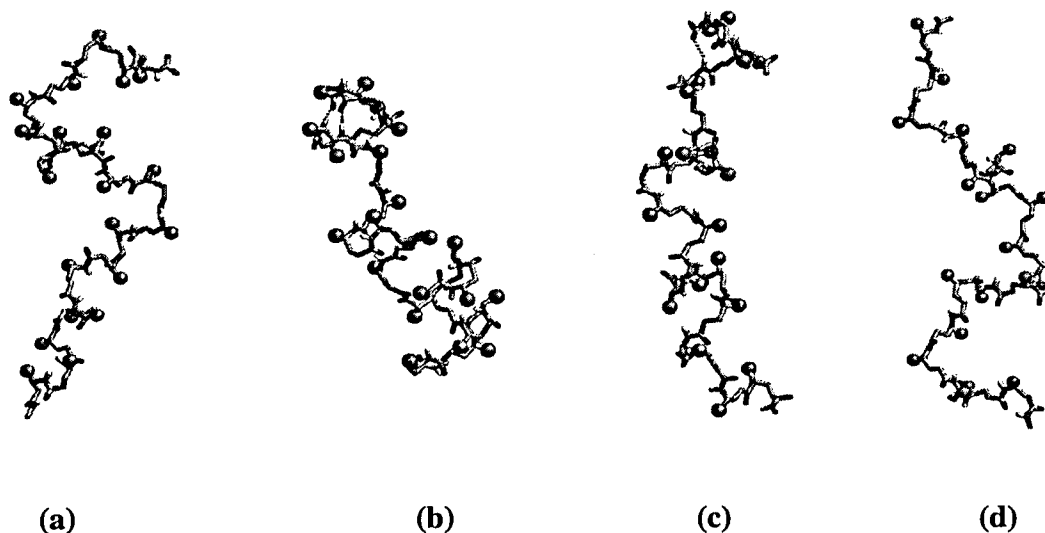

(a)   (b)   (c)   (d)

Figura VI.10. Visión axial de las conformaciones obtenidas en MD1 después de 200 ps (a), en MD2 después de 100 ps (b) y 200 ps (c) y en MD3 después de 200 ps (d). En todas las estructuras los grupos carboxilo de las cadenas laterales se representan mediante esferas verdes y las líneas discontinuas representan los puentes de hidrógeno del esquema original que se mantienen.

VI.8.2.2. Conformación del tensioactivo

La conformación adoptada por la cadena lateral del catión molecular presenta un comportamiento muy parecido al descrito en el complejo 8ATMA·PAGA. Todos los ángulos diedros de ésta tienden a mantenerse preferentemente en conformación *trans*. Este comportamiento se repite en las tres simulaciones realizadas y queda reflejado en la tabla **VI.3**. Es destacable como la primera torsión ($\gamma 1$, en el esquema adjunto a la tabla **VI.3**) tiene una mayor tendencia a presentar una conformación extendida que el resto de los ángulos diedros, tal como se observaba en el complejo 8ATMA·PAGA. Cabe destacar que en la simulación MD3 todas las torsiones muestran una mayor predisposición a adoptar conformaciones en *skew* en detrimento de las conformaciones *gauche*. Sin embargo, la tendencia general es parecida en los tres sistemas.

Tabla VI.3. Distribución conformacional para los 20 cationes moleculares en la simulación MD1 (negrita), MD2 (cursiva) y MD3 (texto plano). El análisis de población (%) corresponde las torsiones asociadas a cada enlace de la cadena de octilo (véase el esquema adjunto).
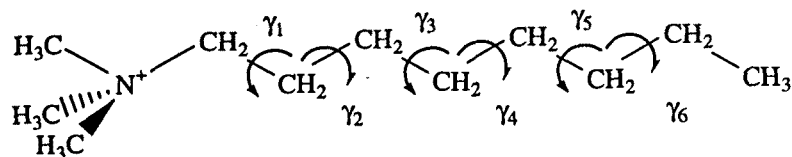
Angulo diedro	trans	gauche +	gauche -	otras
γ_1	**94.0** *94.4* 84.8	**0.8** *0.3* 0.1	**0.1** *0.1* 02	**5.1** *5.1* 15.0
γ_2	**72.9** *74.1* 72.4	**16.0** *8.0* 3.1	**5.7** *12.0* 9.2	**5.3** *5.8* 14.5
γ_3	**72.8** *66.6* 58.9	**10.8** *8.6* 9.6	**9.8** *18.8* 15.5	**6.5** *6.1* 16.0
γ_4	**68.7** *68.0* 65.0	**13.6** *12.2* 11.7	**11.0** *13.4* 8.2	**6.6** *6.4* 15.0
γ_5	**60.8** *65.7* 52.7	**19.6** *14.4* 10.8	**13.1** *13.2* 20.1	**6.5** *6.6* 16.3
γ_6	**60.7** *67.4* 54.6	**18.5** *11.1* 9.8	**14.5** *15.8* 19.6	**6.3** *5.6* 16.0

Estos resultados parecen indicar que la conformación de la cadena alquílica del catión molecular es independiente de la constitución del polianión. Este comportamiento es coherente con la manera en que se estructuran los complejos poliectrolito - tensioactivo en fase sólida, donde se observa como las cadenas alquílicas del tensioactivo se organizan en una fase distinta a la que lo hacen las cadenas de polianión. Al mismo tiempo, está en consonancia con las propiedades del medio en que se encuentran los complejos. Las cadenas alquílicas tienden a extenderse para aumentar la superficie accesible al disolvente orgánico, tal como ya se mostraba en los complejos de PAGA estudiados en el apartado anterior.

VI.8.2.3. Interacción tensioactivo - anión molecular

Para caracterizar la interacción de los tensioactivos con la cadena principal se empleó el mismo criterio que en el apartado anterior. Es decir, se considera que un catión molecular interacciona con algún grupo del polipéptido, si la distancia entre el nitrógeno de catión y el carbono de dicho grupo es inferior a 5.5 Å.

La figura **VI.11** representa el promedio a lo largo del tiempo de simulación del número de grupos carboxilato que interaccionan con un determinado catión molecular. Al igual que ocurría en los complejos 8ATMA·PAGA en todas las simulaciones las moléculas de tensioactivo tienden a interaccionar con más de un grupo carboxilato. Sin embargo, en el caso de los complejos formados por PGGA, la cantidad de moléculas que interaccionan con tres o más grupos carboxilato se reduce notablemente. En estos sistemas el número de aniones que interaccionan con una molécula de tensioactivo tiende a ser dos. Es destacable, a su vez, que en dos de las tres simulaciones aparezca más de un tensioactivo que preferentemente interacciona con un único grupo carboxilato. En la dinámica MD2 los tensioactivos que inicialmente estaban encarados a los residuos 6 y 15 mantienen únicamente la interacción con sendos carboxilatos durante más del 90% del tiempo. Un resultado análogo se observa en la dinámica MD3, donde los tensioactivos 1, 2, 12 y 14 interaccionan durante los 200 ps de simulación con un solo grupo carboxilato.

La geometría de las interacciones entre los cationes moleculares y los grupos carboxilato, en las tres simulaciones, son análogas a las que se obtenían en los complejos 8ATMA·PAGA. Los valores promedio de los parámetros analizados, distancias y ángulos de interacción (tabla **VI.4**) son muy similares en ambos sistemas. Al igual que las interacciones que se daban con el anión molecular derivado del PAGA, estas son asimétricas. Es decir, cuando un tensioactivo interacciona con dos o más grupos carboxilato, las distancias de un catión molecular a cada grupo aniónico no son las mismas, sino que existe una jerarquía ascendente en el valor de cada distancia catión - carboxilato. Cada carboxilato adicional se encuentra a una distancia superior a la descrita para la interacción entre un tensioactivo y un sólo carboxilato. Tal como se introdujo en el apartado anterior, este comportamiento característico puede expresarse de la siguiente forma: $d_1 < d_2 < d_3 < d_4$, dónde el subíndice indica el número de interacciones que presenta cada tensioactivo.

Si se hace una análisis de otras posibles interacciones entre tensioactivos y grupos polares de la cadena polimérica, se observa como en los sistemas constituidos por PGGA los carbonilos de los grupos amida interaccionan muy frecuentemente con los cationes moleculares (figura **VI.12**). Es destacable que para los tres sistemas estudiados siempre existe esta interacción, siendo a su vez relativamente frecuente la

interacción de un tensioactivo con más de un grupo carbonilo. Estos resultados están de acuerdo con los obtenidos para los complejos 8ATMA·PAGA, donde los cationes moleculares únicamente podían interaccionar con los grupos amida cuando se perdía su conformación helicoidal.

Tabla VI.4. Resumen los principales parámetros geométricos que caracterizan la interacción entre las moléculas de tensioactivo y los grupos carboxilato del polianión de PGGA (las poblaciones relativas de cada tipo de interacción se muestran en las figuras VI.11). En dicha tabla se muestran los valores promedio a lo largo de los 200 ps de trayectoria para las tres simulaciones.
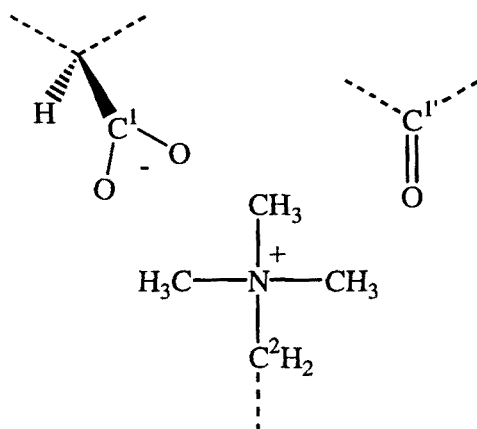
Parámetro [a]	[b]d_1	d_2	d_3[c]	d_4[c]
MD1 $N...C^1$ (en Å)	4.50 ± 0.29	4.87 ± 0.31	5.18 ± 0.19	5.21 ± 0.04
$N...C^1...C^2$ (en °)	112.0 ± 36.4	108.6 ± 33.0	107.8 ± 28.1	90.6 ± 2.5
MD2 $N...C^1$ (en Å)	4.50 ± 0.30	4.90 ± 0.29	5.17 ± 0.20	5.32 ± 0.03
$N...C^1...C^2$ (en °)	118..7 ± 34.5	110.4 ± 31.8	107.5 ± 25.7	105.7 ± 3.2
MD3 $N...C^1$ (en Å)	4.50 ± 0.27	4.85 ± 0.30	5.20 ± 0.18	5.42 ± 0.01
$N...C^1...C^2$ (en °)	114.1 ± 35.4	103.1 ± 29.9	107.8 ± 12.6	90.2 ± 0.5

[a] Según el esquema mostrado en la parte superior

[b] d_n corresponden a las distancias entre un tensioactivo y los diferentes grupos carboxilato con los que interacciona según el mismo criterio y la misma nomenclatura utilizada en el estudio de los complejos 8ATMA·PAGA.

[c] Aquellos parámetros geométricos que presentan una desviación estándar muy baja es debido a que dicha interacción aparece con muy poca frecuencia.
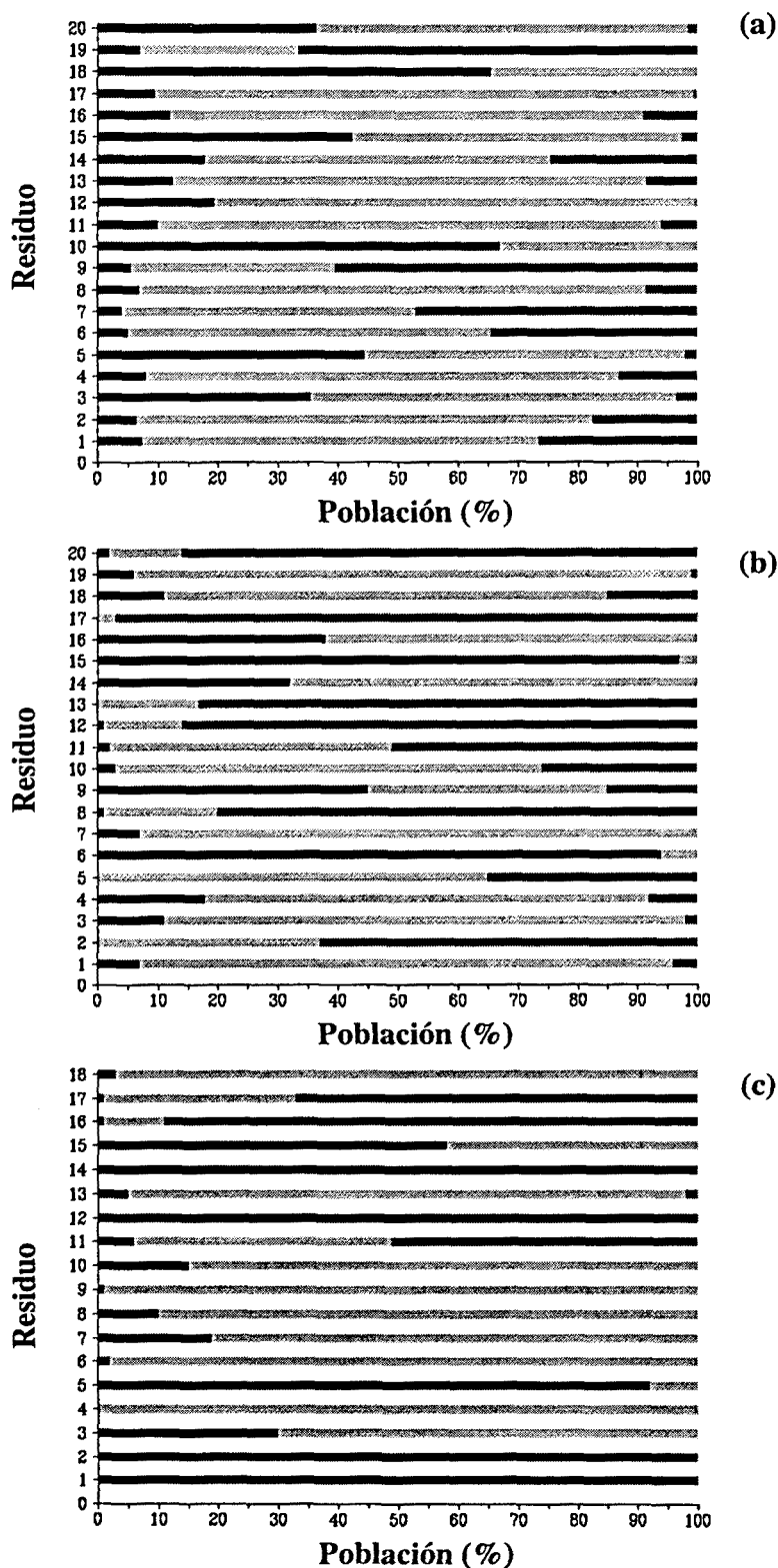
Figura VI.11. Representación de la distribución del número de grupos carboxilato que interaccionan simultáneamente con cada uno de los cationes moleculares en MD1 **(a)**, MD2 **(b)** y MD3 **(c)**. De izquierda a derecha se representa carboxilato (en rojo), dos (amarillo), tres (verde) y cuatro (azul).

Es destacable que la geometría de estas últimas interacciones es igualmente asimétrica y que sigue la misma tendencia observada en las interacciones carboxilato - tensioactivo. Es decir, $d_1 < d_2 < d_3 < d_4$, tal como puede verse en la tabla **VI.5**. Como ocurría en la interacción con los grupos carboxilato, el patrón de interacción que predomina es un tensioactivo interaccionando con uno o dos grupos carbonilo. A pesar de la diferente naturaleza química de los grupos, el número total de interacciones que cada catión presenta con la cadena de PGGA es a la postre muy parecido al descrito en el complejo formado por PAGA.

Tabla VI.5. Resumen los principales parámetros geométricos que caracterizan la interacción entre las moléculas de tensioactivo y los grupos amida del polianión de PGGA (las poblaciones relativas de cada tipo de interacción se muestran en las figuras **VI.12**). En dicha tabla se muestran los valores promedio a lo largo de los 200 ps de trayectoria para las tres simulaciones.

Parámetro [a]	[b]d_1	d_2	d_3[c]	d_4[c]
N...$C^{1'}$ (en Å)	4.90 ± 0.29	5.20 ± 0.16	5.31 ± 0.05	5.45 ± 0.01
N...$C^{1'}$...C^2 (en °)	116.0 ± 32.8	111.1 ± 25.8	107.2 ± 4.4	68.8 ± 0.01
N...$C^{1'}$ (en Å)	4.87 ± 0.28	5.10 ± 0.20	5.28 ± 0.07	5.43 ± 0.02
N...$C^{1'}$...C^2 (en °)	124.6 ± 32.2	119.7 ± 30.5	114.4 ± 5.3	114.2 ± 0.01
N...$C^{1'}$ (en Å)	4.85 ± 0.32	5.12 ± 0.16	5.36 ± 0.05	------------[d]
N...$C^{1'}$...C^2 (en °)	120.2 ± 34.4	125.2 ± 23.2	118.0 ± 0.02	----------

[a] Según el esquema incluido en la tabla **IV.4**
[b] d_n corresponden a las distancias de interacción entre un tensioactivo y los grupos amida con los que interacciona. La nomenclatura es coincidente con la presentada en la tabla **IV.4**
[c] Aquellos parámetros geométricos que presentan una desviación estándar muy baja (<0.1Å y 6°) es debido a que dicha interacción aparece con muy poca frecuencia.
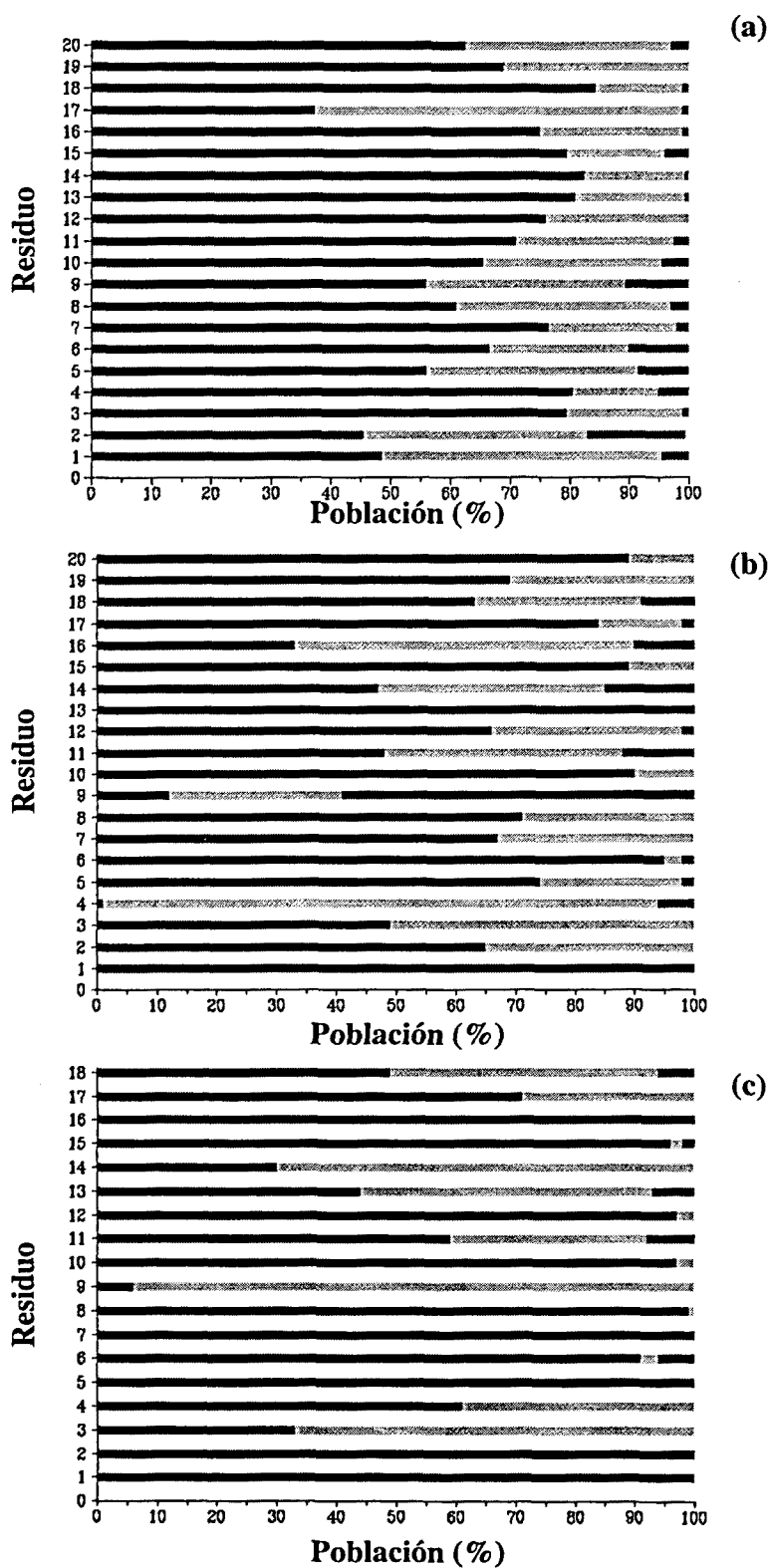[d] interacción no detectada a lo largo de los 200 ps de simulación

Figura VI.12 . Representación de la distribución del número de grupos carbonilo que interaccionan simultáneamente con cada uno de los cationes moleculares para MD1 (a), MD2 (b) y MD3 (c). De izquierda a derecha se representa un carboxilato (en rojo), dos (en amarillo), tres (verde) y cuatro (azul).

Tal como se ha expuesto, la pérdida de la conformación es un factor común en las tres simulaciones realizadas para los complejos 8ATMA·PGGA. Esta desestructuración parece estar relacionada con la accesibilidad de los grupos amida a los cationes moleculares. En el PAGA en conformación de hélice α, los grupos amida están mucho menos accesibles puesto que la cadena lateral del polímero presenta dos grupos metilo. Sin embargo, en el PGGA, independientemente de la conformación que pueda adoptar, el grupo carboxilato se encuentra unido directamente a la cadena de polímero. De este modo cuando los cationes moleculares interaccionan con los aniones del polímero, se acercan lo suficientemente a la cadena principal como para interaccionar también con sus grupos amida. Este factor tiene consecuencias dramáticas en la estructuración de la cadena polimérica, especialmente en las conformaciones estabilizadas por puentes de hidrógeno intramoleculares, puesto que los cationes inducen a la rotura de los mismos. (figura **VI.13**).
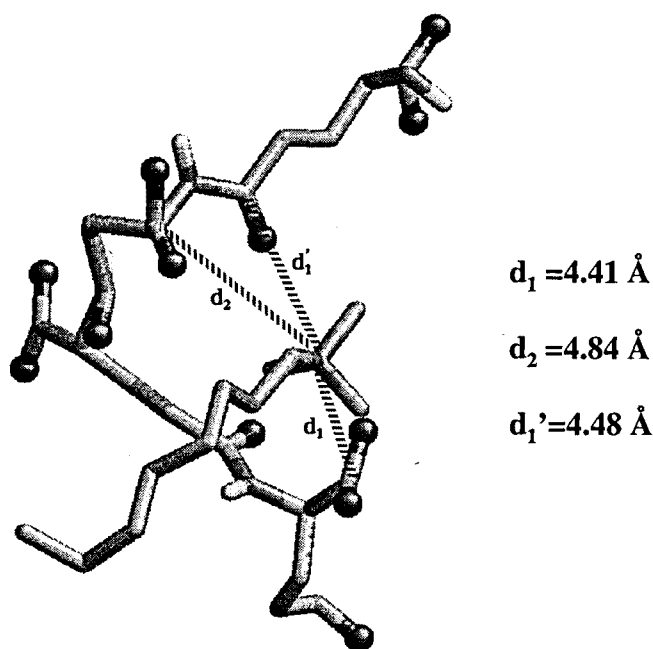

$d_1 = 4.41$ Å

$d_2 = 4.84$ Å

$d_1' = 4.48$ Å

Figura VI.13 Detalle de la interacción entre un catión molecular y la cadena de polipéptido. d_1 y d_2 corresponden a las distancias entre el nitrógeno del catión molecular y el carbono de los grupos carboxilato. d_1' corresponde a la distancia entre el catión molecular y el carbono del grupo amida con el que interacciona. Nótese como la interacción tensioactivo - amida impide que los grupos amida cercanos interaccionen entre sí, desestabilizando las conformaciones helicoidales con puentes de hidrógeno intramoleculares.

VI.9. Conclusiones parciales

1) La energía libre de interacción de los complejos formados por el anión acetato y el catión alquiltrimetilamonio es estabilizante para todos los sistemas investigados. Sin embargo dicha interacción se hace más débil cuanto más larga es la cadena alquílica del catión molecular. La formación de estos complejos en disolución acuosa se encuentra desfavorecida debido al gran coste energético que implica la desolvatación de los iones moleculares no acomplejados. Este coste energético es menor en disolventes orgánicos como el cloroformo, siendo parcialmente compensado por la fuerte interacción electrostática entre los iones moleculares.

2) La geometría de la interacción en complejos iónicos formados por más de dos iones moleculares del tipo anión acetato y catión alquiltrimetilamonio se caracteriza por ser asimétrica. Independientemente de la proporción relativa anión/catión molecular, cada especie iónica tiende a interaccionar con el mayor número posible de especies con carga opuesta. Como es de esperar, la energía libre de interacción se vuelve más favorable cuando el número de iones moleculares involucrados en el complejo aumenta. Sin embargo dicha estabilización es inferior a lo esperado, indicando que las interacciones electrostáticas características de estos complejos presentan un comportamiento anticooperativo.

3) Una de las principales características de los complejos estequimétricos nATMA·PAGA en disolución de cloroformo es la gran estabilidad conformacional de hélice α formada por la cadena polipeptídica. Esto es debido a que la cadena lateral de los tensioactivos impiden al disolvente interaccionar con la cadena de polipéptido. A su vez, los grupos aniónicos del polipéptido no pueden interaccionar con los grupos polares de la cadena principal puesto que están continuamente interaccionando con el tensioactivo. La interacción entre los cationes moleculares y los grupos aniónicos del polipéptido es marcadamente asimétrica y presenta muy frecuentemente una estequiometría diferente a 1:1. Así, cada catión molecular tiende a rodearse del número más elevado posible de grupos carboxilato.

4) En los complejos *n*ATMA·PGGA la cadena de polímero no presenta ninguna conformación regular preferente debido a las interacciones que se establecen entre los grupos amida de dicha cadena y los cationes moleculares. Esta interacción, y a diferencia de los complejos *n*ATMA·PAGA, es posible ya que la cadena principal presenta una mayor accesibilidad a los tensioactivos. Así, la interacción de los cationes moleculares con los grupos carboxilato del PGGA facilita el acercamiento de los primeros a la cadena principal del polipéptido.

VII. RESULTADOS:

ESTRUCTURA DE LOS POLI(α-ALQUIL-β-L-ASPARTATO)S CON GRUPOS ALQUILO LARGOS

VII. ESTRUCTURA DE LOS POLI(α-ALQUIL-β-L-ASPARTATO)S CON GRUPOS ALQUILO LARGOS

VII.1. Polímeros tipo peine

Los polímeros tipo peine (*Comb-like polymers*) son macromoléculas que se caracterizan por contener cadenas laterales relativamente largas que se disponen con cierta regularidad a lo largo de la cadena principal. Estos polímeros pueden ser considerados como un caso especial de polímeros ramificados (Platé y Shibaev, 1987), debido a su particular constitución: la longitud de sus cadenas laterales es igual o superior a la sección transversal de la macromolécula. Este factor, junto con el efecto producido por la proximidad de las cadenas laterales, y las propiedades inherentes a la cadena principal, son responsables de las características físico - químicas específicas de estos sistemas poliméricos (figura **VII.1**).
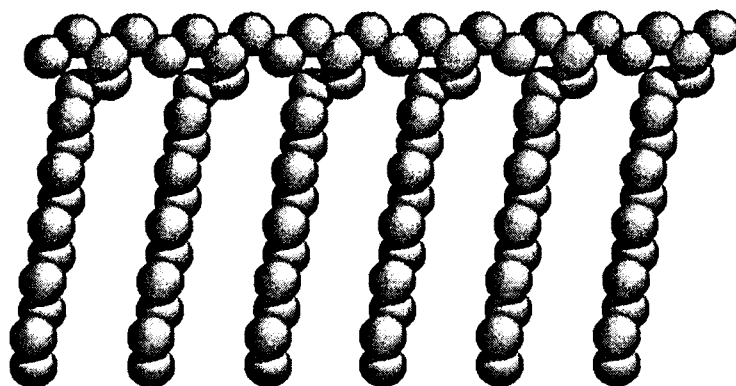

Figura VII.1. Representación esquemática de la constitución de un polímero tipo peine. En azul se representa la cadena principal del polímero y en verde las cadenas laterales.

La característica más destacable de estos polímeros es su marcada tendencia al empaquetamiento bifásico, es decir, a presentar una estructuración diferencial entre las cadenas laterales y las cadenas principales del polímero. Este empaquetamiento les confiere propiedades térmicas muy particulares que se manifiestan en forma de

transiciones de fase. Dichas transiciones corresponden a alteraciones de los parámetros estructurales de alguna de las dos fases en que se organiza el polímero, las cuales se comportan como sistemas independientes. Este comportamiento aparentemente "dual" es especialmente extremado cuando las cadenas laterales son lineales y alifáticas. (Daly et al.,1994).

VII.2. Polímeros tipo peine derivados de polipéptidos con cadenas laterales alquílicas

Analizar las propiedades estructurales de los polímeros tipo peine implica determinar cual es el factor que determina su ordenación bifásica. El uso de polímeros derivados de amino ácidos ha sido de gran utilidad para estudiar este tipo de sistemas, debido a que los polipéptidos presentan una marcada tendencia a dar por sí mismos conformaciones regulares.

De esta forma, el estudio de polímeros tipo peine basados en derivados alquílicos de la poli(α-L-Lisina) permitió identificar el factor predominante que inducía la formación de estructuras bifásicas. Platé y Shibaev (1987) estudiaron sistemáticamente la estructura de esta familia de polímeros en función de la longitud de la cadena alquílica. Dichos autores describieron como para longitudes inferiores a 9 átomos de carbono la estructuración del sistema se caracterizaba por presentar un empaquetamiento óptimo de las cadenas de polipéptido. Es decir, estas cadenas adoptaban una conformación de hélice α, empaquetándose en una red hexagonal, mientras que las cadenas laterales optimizaban su ordenación adaptándose a la organización de las cadenas polipéptídicas.

Sin embargo, a partir de ese tamaño de cadena lateral y a medida que ésta aumentaba en longitud, se vio como la conformación helicoidal de la cadena polipeptídica se iba distorsionando. Así, a partir de una longitud de 17 o más de átomos de carbono en la cadena alquílica, se observó un cambio conformacional drástico en la cadena polipeptídica, llegándose a una conformación de hoja β.

Este hecho se interpretó como el efecto de las cadenas laterales sobre la estructuración del sistema. Las cadenas alifáticas presentan una tendencia tan marcada a estructurarse entre ellas, que inducen cambios dramáticos en las propiedades conformacionales del polipéptido. De esta forma se concluyó que la estructuración de los polímeros peine con cadenas laterales alquílicas estaba guiada por la estructura que pueden adoptar estas últimas.

VII.2.1. Poli(γ-alquil-α-L-glutamato)s

Una de las familias de polipéptidos tipo peine más estudiada ha sido la de los ésteres alquílicos derivados del PAGA (figura VII.2). Estos polímeros se caracterizan por presentar propiedades estructurales marcadamente dependientes de la longitud de la cadena alifática.
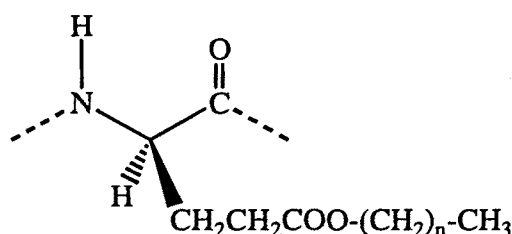

$$CH_2CH_2COO\text{-}(CH_2)_n\text{-}CH_3$$

Figura VII.2. Representación esquemática de los Poli(γ-alquil-α-L-glutamato)s con cadenas alquílicas lineales, dónde *n+1* corresponde al número de átomos de carbono de la cadena alquílica del éster.

Así, cuando las cadenas alquílicas presentan una longitud igual o inferior a 8 átomos de carbono, los polímeros se ordenan en una sola fase, tal como muestran diversos estudios realizados mediante difracción de rayos X (Watanabe et. al.,1977; Sasaki et. al., 1978; Sasaki et. al., 1979). Las cadenas polipeptídicas adoptan una conformación de hélice α y se empaquetan en una celdilla hexagonal, optimizando la ocupación del espacio (figura VII.3a). A su vez, las propiedades térmicas de este tipo de poli(α-glutamato)s de alquilo son análogas a las descritas para cualquier polímero semicristalino no ramificado (Watanabe et al., 1985).

Sin embargo, cuando el número de átomos de carbono es igual o superior a 10 las propiedades estructurales de los polímeros de esta familia cambian radicalmente: Watanabe et al. (1985) observaron, mediante el uso difracción de rayos X, como estos

sistemas tendían a formar estructuras laminares. Las cadenas de polipéptido conservaban su conformación helicoidal, pero ya no se empaquetaban en una red hexagonal sino que se agrupaban en láminas separadas por zonas ocupadas por las cadenas laterales. Éstas, a su vez, se distribuían en dirección perpendicular a la superficie de la lámina (figura **VII.3b**). La manera en que las cadenas alquílicas se ordenan es de nuevo la clave que determina este nuevo patrón de estructuración. Así, las cadenas laterales tienden a ordenarse de forma similar a como lo hacen los alcanos cristalizados, en una red de tipo hexagonal.
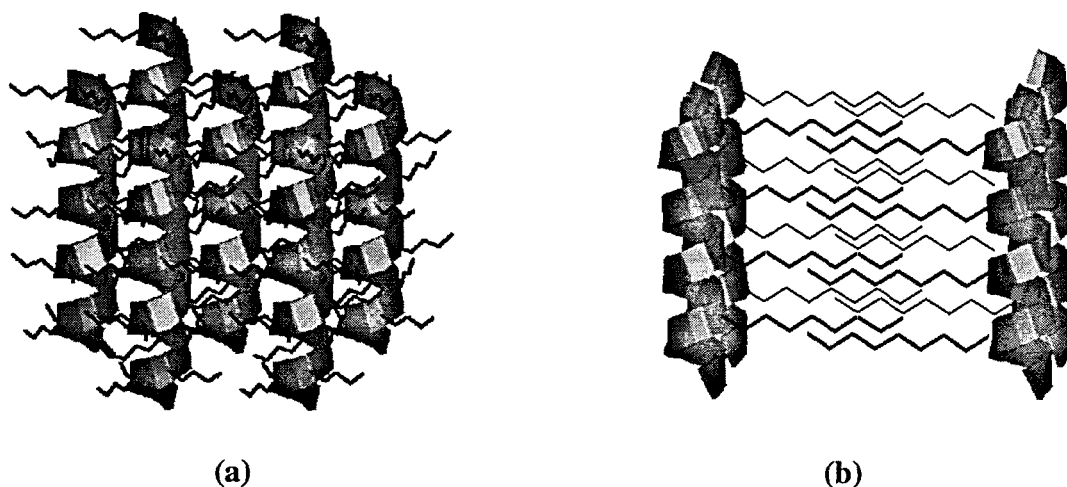

(a)   **(b)**

Figura VII.3. Representación esquemática de los dos tipos de empaquetamiento de las cadenas polipeptídicas para los poli(γ-alquil-α-L-glutamato)s en función de la longitud de la cadena lateral: un empaquetamiento hexagonal para un número de átomos de carbono en la cadena lateral igual o inferior a 8 (a) y un empaquetamiento laminar para un número superior a 10 (b).

VII.2.2. Transiciones de fase de los Poli(γ-alquil-α-L-glutamato)s con una longitud de cadena alifática igual o superior a 10 átomos de carbono

Una consecuencia directa de la particular ordenación que presentan estos polímeros es la aparición de transiciones de fase como respuesta al calentamiento. Los estudios realizados mediante DSC por Watanabe et al. (1985) mostraron dos transiciones fase distintas características de estos polímeros. A su vez, los cambios estructurales que se producen durante estos procesos térmicos fueron caracterizados mediante difracción de rayos X por el mismo grupo de investigación.

La primera transición de fase se daba por encima de una temperatura T_1, característica para cada tipo de sistema, y correspondía a la fusión de la fase cristalina en que se ordenaban las cadenas laterales. Si se seguían calentando estos sistemas se llegaba a una segunda transición de fase, a partir de una temperatura T_2, que correspondía a la pérdida de la ordenación en el empaquetamiento de las cadenas polipeptídicas, sin que por ello se perdiera la conformación de hélice α. Esta última transición de fase conducía a la aparición de una estructura de cristal líquido uniaxial, dónde las cadenas de polímero se orientaban a lo largo del eje z.

VII.3. Poli (α-alquil-β-L-aspartato)s

VII.3.1 Estructura de los poli(α-alquil-β-L-aspartato)s con grupos alquilo lineales

Los poli(α-alquil-β-L-aspartato)s, abreviados PAALA-n, dónde n indica el número de átomos de carbono de la cadena alquílica, son otro ejemplo de polímeros cuya estructura se ve altamente influenciada por la longitud de la cadena lateral (figura **VII.4**). El empaquetamiento cristalino más corriente de los PAALA-n con $n \leq 6$ es de tipo pseudohexagonal, con las cadenas de polipéptido adoptando una conformación de hélice 13/4, similar a la hélice α de los polipéptidos derivados de α-amino ácidos (López-Carrasquero et al., 1996; Navas et. al, 1997).

El PAALA-8 ya presenta un cambio en el patrón de empaquetamiento, dando lugar a una estructura tridimensional en la cual las hélices se empaquetan en láminas y las cadenas laterales ocupan los espacios interlaminares (López-Carrasquero et al. 1995; Navas et. al, 1997).
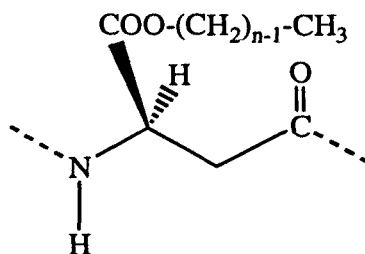
$$COO\text{-}(CH_2)_{n-1}\text{-}CH_3$$

Figura VII.4. Representación esquemática de los PAALA-n. En el esquema la cadena alifática está constituida por n átomos de carbono.

Cuando el número de átomos de carbono es superior a 8, estos polímeros adoptan estructuras bifásicas similares a las descritas para los poli(γ-alquil-α-L-glutamato)s de cadena lateral larga. López-Carrasquero et al. (1995) estudiaron la estructura para los derivados con $n=12$, 18 y 22 mediante difracción de rayos X. Se observó como estos polímeros se caracterizaban por presentar dos fases cristalinas separadas, que podían describirse como una estructura formada por láminas de hélices que están inmersas en una matriz cristalina parafínica.

VII.3.2. Transiciones de fase en los PAALA-*n* con n ≥ 12

Los poli(α-alquil-β-L-aspartato)s con cadena lateral alquílica larga se caracterizan por presentar dos transiciones de fase cuando aumenta la temperatura, tal como se muestra en la tabla **VII.1**. Estas transiciones separan tres fases estructuralmente distintas, que fueron designadas A, B y C (López-Carrasquero et al., 1995).

Tabla VII.1. Temperaturas (en °C) observadas para las dos transiciones de fase en los poli(α-alquil-β-L-aspartato)s con cadena lateral larga.

Polímero	Transición A → B (T_1)	Transición B → C (T_2)
PAALA-12	-15	50
PAALA-18	54-64	117
PAALA-22	60-75	129

La caracterización de estas dos transiciones fue realizada mediante DSC y difracción de rayos X. Los datos obtenidos sugirieron un comportamiento similar al descrito anteriormente para los poli(γ-alquil-α-glutamato)s. Por analogía con estos polímeros, se interpretó que la fase A estaba constituida por láminas de hélices 13/4 con las cadenas laterales cristalizadas en un dominio hexagonal diferenciado. La fase B es similar a la fase A, pero en este caso las cadenas laterales se encuentran en un estado fundido. Finalmente, la fase C estaría constituida por un conjunto de hélices independientes en disposición uniaxial, dentro de una matriz amorfa de cadenas laterales (figura **VII.5**).
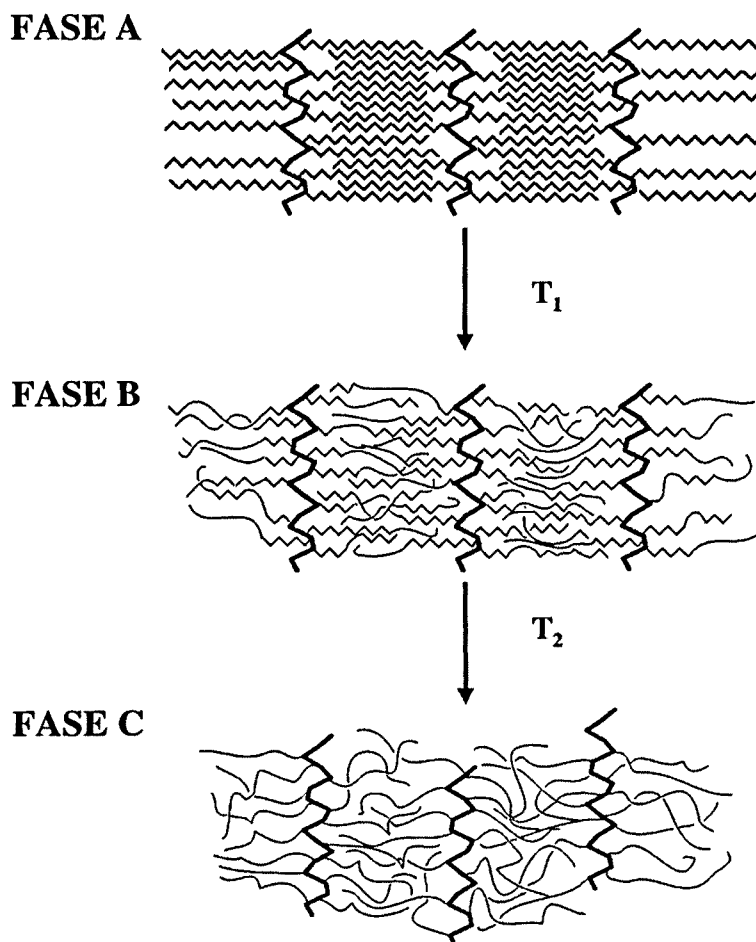
FASE A

T_1

FASE B

T_2

FASE C

Figura VII.5. Representación esquemática de las transiciones de fase en los PAALA-n con n ≥ 12. En la primera fase (A) se ven las cadenas alifáticas cristalizadas y las cadenas de polímero empaquetadas en forma laminar. Cuando se calienta el sistema hasta una temperatura T_1 la fase parafínica funde (fase B). Si se sigue calentando el polímero hasta una temperatura T_2 se pierde el empaquetamiento laminar de las cadenas polipeptídicas (fase C)

VII.3.3. Microestructura de la fase B en PAALA-*n* con n ≥ 12

A partir de los datos obtenidos mediante difracción de rayos X y DSC, se había presupuesto que la fase B debía presentar un importante grado de desorden en la fase parafínica.

Recientemente, mediante el uso de herramientas avanzadas de simulación molecular, León et al. (2000c) investigaron las características conformacionales y estructurales de la fase B para los PAALA-*n* con 12, 16 y 18 átomos de carbono en la

cadena lateral. Estas simulaciones permitieron describir con precisión la organización de las cadenas laterales en la fase B.

Un análisis detallado de la distribución conformacional de las cadenas laterales en las microestructuras resultantes de las simulaciones de MC indicó la ausencia de estructuración en la fase parafínica. Así la distribución de los átomos de las cadenas laterales se asimiló, de forma aproximada, a la organización de un líquido parafínico atrapado entre láminas de polímero. No obstante se detectó una cierta orientación preferencial de las cadenas alquílicas, las cuales tendían a disponerse perpendicularmente a las láminas de hélices.

Por otro lado los resultados obtenidos a partir de dicho análisis pusieron de manifiesto que a lo largo de la cadena lateral, en función de la posición del enlace, existía una diferenciación en el tipo de conformación adoptada. Además, se advirtió la existencia de un cambio abrupto en la distribución de conformaciones. Partiendo de la cadena principal, se pudo distinguir un segmento de cadena alifática donde la conformación predominante venía determinada por la tendencia de las cadenas alifáticas a situarse en la región interlaminar. Este segmento estaba constituido aproximadamente por los 5 primeros metilenos. Al alejarse de este punto se advertía un incremento brusco en la tendencia a presentar conformaciones extendidas.

Estos resultados llevaron a dos conclusiones de considerable relevancia: existe una zona interfásica, constituida por los átomos de la cadena lateral más cercanos a la principal, que determina la estructuración interlaminar de la fase parafínica. A su vez, y a pesar de perderse la ordenación global en dicha fase, las cadenas laterales tienden a presentar un orden parcial, alineándose preferentemente en la dirección perpendicular a las láminas del polímero. Este hecho es consecuencia de que se tiende a mantener la conformación característica de una fase ordenada en los extremos de las cadenas laterales (figura **VII.6**).
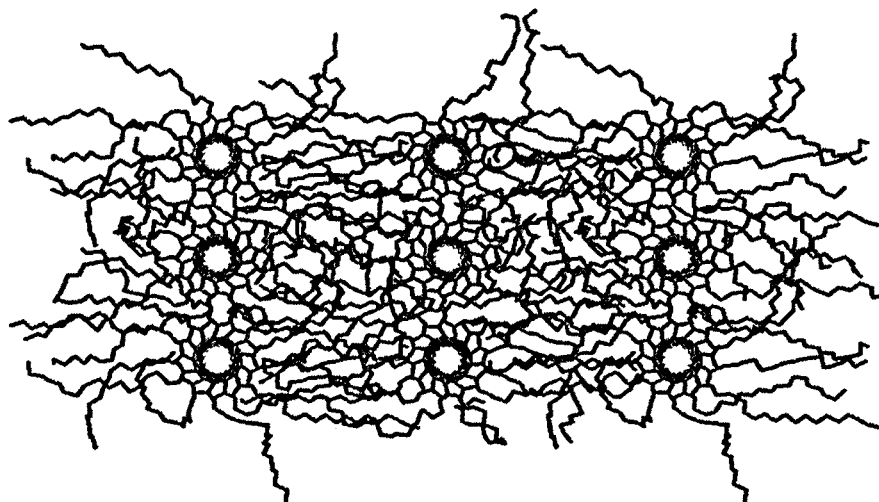
Figura VII.6. Vista superior de la estructura obtenida por Leon et al (2000) mediante simulaciones de MC para el PAALA-18. Nótese el desorden de la fase parafínica y, a su vez, la tendencia de las cadenas laterales a orientarse en la dirección perpendicular a la lámina. A su vez, queda muy bien reflejado como la estructuración de la zona interlaminar induce a los segmentos de cadena alquílica cercanos a la interfase péptido - parafina a adoptar conformaciones no extendidas.

VII.4. Objetivos

El objetivo general de este capítulo es estudiar las características estructurales de las fases A y C de los PAALA-n tipo peine (n≥ 12), complementado el trabajo iniciado por León et al. (2000b) acerca de las transiciones de fase en esta familia de polímeros. Este objetivo general puede desglosarse en los siguientes objetivos específicos:

1) Estudiar las características estructurales de la fase A en el PAALA-18 mediante simulaciones de MC-CB, analizando en detalle el comportamiento conformacional de las cadenas parafínicas cristalizadas y comparando los resultados con los obtenidos para la fase B del mismo polímero.

2) Estudiar la transición de la fase B a la fase C en el PAALA-18 mediante simulaciones de MC-CB, analizando los principales cambios estructurales y conformacionales involucrados en dicha transición. Caracterizar la fase C del PAALA-18, comparando los parámetros estructurales más relevantes con los obtenidos para las fases A y B.